Some Studies on the Prospect of Finding New Physics Beyond the Standard Model at the LHC

Thesis Submitted to
The University of Calcutta
for The Degree of
Doctor of Philosophy (Science)

By
Subhadeep Mondal

Department of Theoretical Physics
Indian Association for the Cultivation of Science
2A & 2B, Raja S.C.Mullick Road, Jadavpur
Kolkata - 700 032, India

September, 2014

Abstract

After the discovery of a ~ 125 GeV Higgs boson at the Large Hadron Collider (LHC), now the Standard Model (SM) of particle physics is complete although there are still some doubts over the fact that this can be a beyond the Standard Model (BSM) Higgs boson. More updated data on Higgs boson coupling measurements will reveal its true identity. Meanwhile, we need to go beyond the SM to address some vital experimental findings. One of them is the neutrino oscillation data that indicates at least two neutrinos have tiny but non-zero masses. The other one is the existence of Dark Matter (DM) revealed from cosmological data. Weak scale supersymmetry (SUSY) is the most popular choice for explaining these new physics phenomena beyond the SM. However, even Minimal Supersymmetric Standard Model (MSSM) itself is not sufficient to explain the neutrino oscillation data under R-parity conserving scenario. In this thesis, we, therefore, attempt to explore a SUSY model with added singlets that can account for small neutrino masses by means of inverse seesaw mechanism. As a consequence, we can have a mixed sneutrino lightest SUSY particle (LSP) that may be as light as ~ 50 GeV. Within R-parity conserving scenario, this LSP can serve as a very good DM candidate satisfying all existing constraints arising from collider, DM and low energy experiments. This model can have enhanced same-sign dilepton final states with large missing energy coming from gluino and squark pair as well as squark-gluino associated productions and their cascade decays through charginos. The two body decays of the lighter chargino into a charged lepton and a singlet sneutrino has a characteristic decay pattern which is correlated with the observed large atmospheric neutrino mixing angle. This feature can be probed at the LHC through trilepton channel. Moreover, the ~ 125 GeV Higgs boson now have a new decay channel into a pair of LSP sneutrinos that is completely invisible. Most recent data published by ATLAS and CMS collaborations at the LHC in different Higgs boson decay channels constrain this sort of non-standard decays. We perform a two parameter global analysis of the available experimental data to date to determine the optimal invisible Higgs boson branching fraction in this scenario. This new decay provides us a new missing energy channel that can be probed at the LHC. We present detailed cut-based analyses for these different proposed signals at the LHC to test the viability of such a scenario.

To my parents who have simply let me be.

Acknowledgement

I am grateful to the Department of Science and Technology, Government of India for providing me the financial assistance for the completion of my thesis work.

I have no words to express my gratitude to the members of the Department of Theoretical Physics of IACS, particularly Prof. Sourov Roy. It is his ever extended guiding hand that has led me this far. I have lost count how many times I have played with his patience and yet after each of these encounters I was greeted with a smile and a pat on the back. He always had some words of encouragements even in my worst times that kept me going. I am grateful to Prof. Dilip Kumar Ghosh, Prof. Utpal Chattopadhyay, Dr. Pushan Majumdar, Prof. Koushik Ray, Prof. Soumitra SenGupta, Prof. Shudhanshu Sekhar Mandal, Prof. Krishnendu Sengupta, Dr. Arnab Sen and Dr. Arnab Das for their constant encouragement and valuable assistance . I am also thankful to all the non-teaching staff members of my department (Mr. Subrata Balti, Mr. Bikash Darjee, Mr. Bhudeb Ghosh, Mr. Tapan Moulik and Mr. Suresh Mandal) who were always there to assist us.

I shall remain indebted to my ex professors of Jadavpur University Physics department, specially Prof. Ranjan Bhattacharyya, Prof Dhiranjan Roy, Prof. Narayan Banerjee, Prof. Amitava Datta and Prof. Soumen Kumar Roy whose incredible teaching skills and patient guidance laid the foundation of my fondness of the subject.

I would like to thank my collaborators Prof. Biswarup Mokhopadhyaya, Dr. Sanjoy Biswas, Dr. P. S. Bhupal Dev, Shankha Banerjee and Dr. Pradipta Ghosh. I was privileged enough to have Dr. Pradipta Ghosh as my departmental senior. He has always been like my elder brother away from home and till date remains one of my inspirations. I should also mention the names of Dr. Debottam Das, Dr. Joydip Mitra, Dr. Dwipesh Majumdar, Dr. Soumya Prasad Mukherjee and Dr. Sudipta Palchowdhury from whom I continue to learn a lot. The long journey from my masters to completion of this thesis was made easier by the ever cheerful presence and support of my colleagues Dr. Kush Saha, Dr. Sanhita Modak, Ashmita Das, Amit chakraborty, Sourav Mondal, Sabyasachi Chakraborty, Manimala chakraborty, Ipsita Saha, Dr. soumya Rao, Dr. Swapan Majhi, Sutirtha Mukherjee, Anirban Datta, Sanjib Ghosh, Sangita Dey, Abhishek Dey, Dr. Shreyoshi Mondal, Bhaskar Mukherjee, Sourav Nandy, Asmi Haldar and Tanmoy Pal.

The acknowledgement page will remain incomplete without the mention of my band of brothers, Sumit, Sunando, Debmalya, Anirban, Saikat, Arunava, Arnab and Nirmalya, who have always been there since my college days to pick me up at the end of a disastrous day and somehow managed to inject enough energy into me to head out

for another days' work. A vote of thanks will be an injustice to the whirlwind journey we have had and so will it be to just acknowledge my family. Without these people, I would cease to exist.

Subhadeep Mondal

List of Publications

1. **Invisible Higgs Decay in a Supersymmetric Inverse Seesaw Model with Light Sneutrino Dark Matter.**
   Shankha Banerjee, *P. S. Bhupal Dev*, *Subhadeep Mondal*, *Biswarup Mukhopadhyaya*, *Sourov Roy*.
   JHEP **10 (2013) 221 [arXiv: 1306.2143].**

2. **Phenomenology of Light Sneutrino Dark Matter in cMSSM/mSUGRA with Inverse Seesaw.**
   P. S. Bhupal Dev, *Subhadeep Mondal*, *Biswarup Mukhopadhyaya Sourov Roy.*
   JHEP **09 (2012) 110 [Erratum-ibid. 11, 169 (2013)] [arXiv:1207.6542].**

3. **Exploring novel correlations in trilepton channels at the LHC for the minimal supersymmetric inverse seesaw model**
   Subhadeep Mondal, *Sanjoy Biswas*, *Pradipta Ghosh*, *Sourov Roy.*
   JHEP **05 (2012) 134 [arXiv:1201.1556].**

Contents

1 Introduction **1**

1.1 The Standard Model . . . 1

1.1.1 Particle Content . . . 1

1.1.2 Spontaneous Symmetry Breaking and Mass Generation . . . 3

1.2 Supersymmetry . . . 8

1.2.1 Supersymmetric Transformation and Superfields . . . 9

1.2.2 Supersymmetric Lagrangian . . . 14

1.2.3 The Scalar Potential . . . 16

1.2.4 Supersymmetry Breaking . . . 17

1.2.5 Minimal Supersymmetric Standard Model: Particle content . . . 21

1.2.6 The superpotential and SUSY breaking Lagrangian . . . 21

1.2.7 Particle masses in MSSM . . . 23

1.2.8 R-parity in Supersymmetry . . . 26

1.3 Neutrino Physics . . . 28

1.3.1 Neutrino mass . . . 31

1.4 Dark Matter . . . 35

1.4.1 Relic Density . . . 36

1.4.2 Detection of the DM . . . 37

1.4.3 DM candidates . . . 40

2 Supersymmetric Inverse Seesaw **53**

2.1 Minimal Supersymmetric Inverse Seesaw Model . . . 57

2.1.1 Phenomenological aspects . . . 58

3 Exploring novel correlations in trilepton channels in MSISM **63**

3.1 Decays of chargino and neutralino . . . 65

3.1.1 Chargino decay . . . 65

3.1.2 Neutralino decay . . . 67

3.1.3 Trilepton signal and the benchmark points . . . 68

3.2 Event generation and background analysis 71
3.3 Results 75
3.4 Summary 83

4 Light sneutrino Dark Matter in SISM 90
4.1 Searching for a light DM 91
4.2 Some Benchmark Points 93
4.3 Collider Signatures 100
4.4 Event Generation, Background Simulation and Results 103
4.5 Summary 107

5 Invisible Higgs Decay in SISM 114
5.1 Invisible Higgs Decay Width and Current Data 115
5.1.1 Constraining model parameters 120
5.1.2 Some benchmark points 122
5.2 Collider Analysis 123
5.2.1 Event generation 124
5.2.2 The VBF channel 125
5.2.3 The Zh channel 127
5.3 Results in the light of updated LHC data 129
5.4 Summary 130

6 Conclusion 135

Chapter 1

Introduction

1.1 The Standard Model

All the matter forms in our Universe can be traced back to a few fundamental building blocks of nature interacting by four fundamental forces: strong, weak, electromagnetic and gravitational. The Standard Model (SM) of fundamental interactions is a mathematical framework that explains strong, weak and electromagnetic interactions of elementary particles [1, 2]. It is based on gauge principle, which states that all the forces of nature are mediated by exchange of the gauge fields of the corresponding gauge group. The symmetry group of the SM is $SU(3)_C \times SU(2)_L \times U(1)_Y$. $SU(3)_C$ governs the strong interaction [3, 4] while $SU(2)_L \times U(1)_Y$ describes the unified description of electroweak forces [5,6]. The interactions are associated with gauge fields with coupling coefficients g_s , g and g' corresponding to $SU(3)_C$, $SU(2)_L$ and $U(1)_Y$ gauge subgroups respectively. The SM contains elementary particles which are the basic ingredients of all the matter surrounding us.

1.1.1 Particle Content

The elementary building blocks of matter are spin-half particles (fermions), called quarks and leptons. These fermions come in three generations with identical quantum numbers and different masses. The heavier fermions are unstable and decay into lighter particles belonging to other generations. These light fermions make up most of the ordinary matter. The four fermions in each family are distinguished by their charges under strong and electromagnetic interactions. Two of them are quarks, which are charged under the strong interactions, and two are leptons, which are not. The two quarks have electromagnetic charges 2/3 (up quarks) and $-1/3$ (down quarks) respectively, and the two leptons have charges -1 (charged leptons) and 0 (neutrinos),

in units in which the electron charge is -1. Each fermion is associated with two chiralities. Chirality is conserved for massless fermions, in which case the chirality coincides with the helicity. The two possible chiralities are called left-handed (denoted by "L") and right-handed (denoted by "R"). Massive charged fermions are described by two components of different chiralities combined into a Dirac spinor. For the neutrinos, on the other hand, only the left-handed chirality has been observed so far.

The SM interactions are associated with the exchange of four vector bosons (spin = 1). The photon mediates electromagnetic interactions, the gluon mediates strong interactions, the Z and W mediate weak interactions. Among these the photons and the gluons are massless, while the Z and the W are massive. Putting all these together, the assignments into doublets and into singlets with the corresponding gauge transformation properties are given in the Table 1.1. Above the electroweak scale ($\approx$ 174 GeV),

Particles	$SU(3)_c$	$SU(2)_L$	$U(1)_Y$
$L_{i_L} = \begin{pmatrix} \nu_{\ell_i} \\ \ell_i \end{pmatrix}$	1	2	-1
ℓ_{i_R}	1	1	-2
$Q_{i_L} = \begin{pmatrix} u_i \\ d_i \end{pmatrix}$	3	2	1/3
u_{i_R}	3	1	4/3
d_{i_R}	3	1	-2/3
W^a_μ	1	3	0
B_μ	1	1	0
G^A	8	1	0

Table 1.1: Gauge quantum numbers of the SM fermions and gauge bosons. Here $\ell_i = e, \mu, \tau$, $u_i = u, c, t$ and $d_i = d, s, b$. The singlet representation is given by 1. "μ" is the Lorentz index that runs from 1 to 4. "A" appears for the non-Abelian gauge group $SU(3)_C$ and can take values 1,....,8, whereas, "a" appears for $SU(2)_L$ and can take values 1,..,3.

the electromagnetic and weak interactions become indistinguishable and are unified under the "electroweak" interaction. The left chiral components of up and down type fermions are unified in electroweak doublets. The electroweak scale is where such an "electroweak" symmetry breaks. It is one of the fundamental scales of the nature known at present. The mechanism through which the electroweak symmetry breaks is called spontaneous symmetry breaking. It is through such a mechanism that the fermions and the massive gauge bosons acquire a mass proportional to the electroweak

scale. There have been doubts over the years about the mechanism triggering this spontaneous breaking. Within the framework of the SM this mechanism is known as the Higgs mechanism. This mechanism postulated the existence of a spin "zero" field, known as the Higgs field. The SM massive particles acquire their masses through their interactions with the Higgs field and the masses are proportional to their couplings to the Higgs field. In the next subsection we discuss the mass generation mechanism in SM in brief.

1.1.2 Spontaneous Symmetry Breaking and Mass Generation

Fermions and gauge bosons in the SM are forced to be massless in the presence of an exact $SU(2)_L \times U(1)_Y$ symmetry. This gauge symmetry, therefore, must be broken, in order to assign masses to both the gauge bosons and the fermions. This can be done through the mechanism of spontaneous symmetry breaking (SSB).

To understand the concept of SSB, let us consider a real scalar field $\phi(x)$ and a potential,

$$V(\phi) = \frac{1}{2}\mu^2\phi^2 + \frac{1}{4}\lambda\phi^4 \tag{1.1}$$

Here we assume a discrete symmetry $\phi \leftrightarrow -\phi$ that prevents terms with odd powers of ϕ in the potential. The minimum of the potential occurs at $\phi = 0$. Since $V'(\phi)|_{\phi=0} = 0$, it implies that $\phi = 0$ is an extremum. However, if $\mu^2 < 0$, $V''(\phi)|_{\phi=0} = \mu^2$ means that $\phi = 0$ is a maximum rather than a minimum. The stable minima in that case occur at the points, $\phi = \pm v$, where, $v = \pm\sqrt{-\mu^2/\lambda}$. $v \equiv \langle 0|\phi|0\rangle$ is called the vacuum expectation value (VEV). The parameters μ and λ determine the vacuum structure. The condition, $\lambda > 0$ has to be obeyed so that the potential is bounded from below. In fig. 1.1 we show the structures of the potential for different signs of μ^2 and a positive λ. Now if we expand around the classical minimum $\phi = v$,

$$\phi(x) = v + \eta(x), \tag{1.2}$$

where $\eta(x)$ represents the quantum fluctuations about the minimum, substituting Eq. 1.2 in Eq. 1.1, we obtain,

$$V'(\eta) = \lambda v^2\eta^2 + \lambda v\eta^3 + \frac{1}{4}\lambda\eta^4 + \text{const.} \tag{1.3}$$

Since $V'(\eta)$ consists of terms with odd powers of η, it is no more symmetric under the reflection symmetry and the symmetry is said to be broken spontaneously.

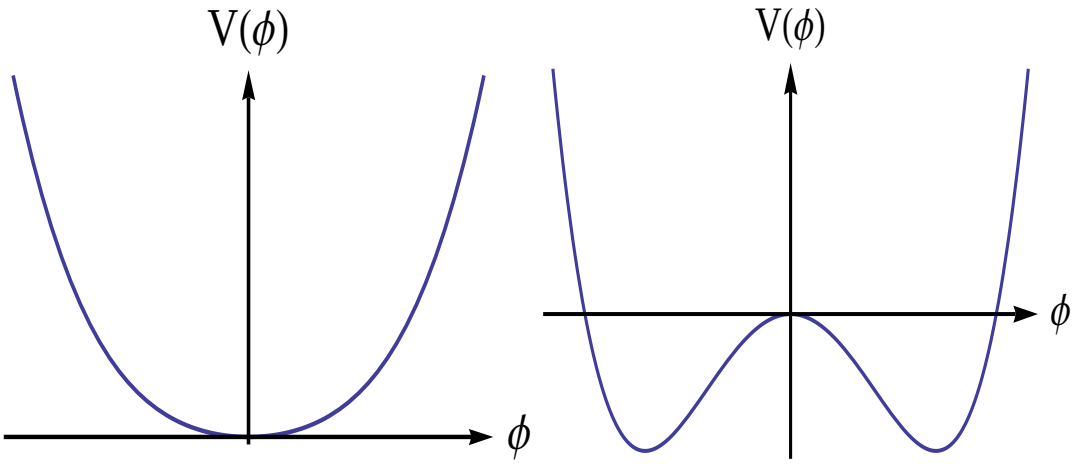

Figure 1.1: The figure on the left panel shows the structure of the potential with $\mu^2 > 0,\ \lambda > 0$, whereas the right panel shows the same with $\mu^2 < 0,\ \lambda > 0$.

In SM, the scalar field appears in a doublet structure and the vacuum expectation value of the neutral component acquires a non-zero vacuum expectation value,

$$\langle \Phi \rangle = \frac{1}{\sqrt{2}} \begin{pmatrix} 0 \\ v \end{pmatrix} \tag{1.4}$$

that breaks the gauge symmetry,

$$SU(3)_c \times SU(2)_L \times U(1)_Y \rightarrow SU(3)_c \times U(1)_{em}.$$

In the process three of the four degrees of freedom of the doublet scalar field are absorbed by three linear combination of the electroweak gauge fields to form their longitudinal polarization and acquire masses, whereas the fourth linear combination, corresponding to the unbroken $U(1)$ symmetry still remains massless. This massless mode is the photon (A) which is the mediator of the long-range electro-magnetic interaction and the three massive modes are the $W^{\pm}$ and Z vector bosons which mediate the short-range weak interaction. In terms of the original fields W^a_μ, B_μ:

$$W^{\pm}_\mu = \frac{1}{\sqrt{2}}(W^1_\mu \mp i W^2_\mu), \quad Z_\mu = W^3_\mu \cos\theta_W - B_\mu \sin\theta_W, \quad A_\mu = W^3_\mu \sin\theta_W + B_\mu \cos\theta_W \tag{1.5}$$

and the corresponding masses are

$$m_W = \frac{1}{2} v g, \quad m_Z = \frac{1}{2} v \sqrt{g^2 + g'^2}, \quad m_A = 0. \tag{1.6}$$

The fermion masses can also be generated with the same scalar field Φ and its conjugate, $\widetilde{\Phi} = -i\tau_2 \Phi^*$ by introducing the following Yukawa terms in the Lagrangian:

$$-\mathcal{L}_{Yukawa} = y_{e_{ij}} \bar{L}_i \Phi e_{R_j} + y_{d_{ij}} \bar{Q}_i \Phi d_{R_j} + y_{u_{ij}} \bar{Q}_i \widetilde{\Phi} u_{R_j} + h.c. \tag{1.7}$$

After Φ obtains a vev, corresponding fermion masses are given by

$$M_e = \frac{vy_e}{\sqrt{2}}, \quad M_d = \frac{vy_d}{\sqrt{2}}, \quad M_u = \frac{vy_u}{\sqrt{2}}. \tag{1.8}$$

Note that, since there are no right-handed components of neutrinos in SM, they remain massless.

After three of the four degrees of freedom of the scalar field Φ are absorbed by the gauge fields, the remaining one is called the Higgs boson (h). In the unitary gauge the neutral component of Φ is given by

$$\Phi(x) = \frac{1}{\sqrt{2}} \begin{pmatrix} 0 \\ v + h(x) \end{pmatrix}. \tag{1.9}$$

Replacing Φ in Eq. 1.1 one can obtain the Higgs boson mass (m_h) from the expansion as in Eq. 1.3

$$m_h = \sqrt{2\lambda v^2} = \sqrt{-2\mu^2}. \tag{1.10}$$

The SM has been extremely successful in explaining the particle masses and interactions known to us so far. All the parameters of the SM have been determined experimentally to an extremely high degree of accuracy over the past three decades or so, in the precision measurements at the Large Electron-Positron (LEP) collider, the proton-anti proton collider (Tevatron) and most recently at the proton-proton Large Hadron Collider(LHC). Until the last couple of years, the only missing block in the puzzle was the elusive Higgs boson.

With the recent discovery of the Higgs boson at the LHC [7, 8], now the SM is complete. However, there still exist some doubts over the fact that this may also be a new scalar coming from the existence of some new physics. More precise measurement of the couplings of the discovered scalar will tell us in future if it is indeed the coveted SM Higgs boson. Despite of its stupendous success, the SM still has some shortcomings that forces us to look beyond.

- The SM Higgs boson mass has been found to be $m_h \approx 125$ GeV [9,10]. However, m_h^2 receives large quantum corrections in the theory coming from all the particles which couples directly or indirectly with the Higgs boson. For example, say we have a correction to m_h^2 coming from a loop containing a Dirac fermion, f with mass m_f as shown in Fig. 1.2. If the coupling is given by the parameter λ_f, then the correction factor is given by

$$\Delta m_h^2 = \frac{|\lambda_f|^2}{16\pi^2} \left[-2\Lambda_{UV}^2 + 6m_f^2 \ln(\Lambda_{UV}/m_f) + ... \right]. \tag{1.11}$$

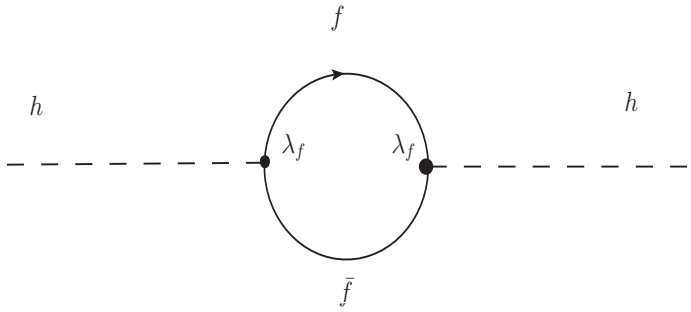

Figure 1.2: Higgs boson mass correction coming from fermions at 1-loop level.

Here Λ_{UV} is an ultraviolet momentum cutoff used to regulate the loop integral. Now if Λ_{UV} is of Planck mass (M_P) order, then this quantum correction is 30 orders larger than the desired value. Then the tree level mass parameter has to be highly fine-tuned in order to cancel the radiative correction to yield a physical Higgs boson mass at the weak scale. This scenario is not theoretically impossible but it is technically unnatural. Hence this is known as the "naturalness problem" [11,12] in the SM. One can solve this problem by taking a much smaller cut-off scale.

- Data obtained from neutrino oscillation experiments confirm neutrino flavor oscillation [13,14]. The existing data allows us to determine two mass square differences, the solar and atmospheric neutrino mixing angles (θ_{12} and θ_{23} respectively) and the reactor neutrino mixing angle (θ_{13}). This set of data indicates at least two neutrinos have non-zero masses and there exists significant mixing among the neutrino states. An explanation of this phenomena requires the existence of physics beyond the SM.

- Astrophysical experiments over the years have confirmed the existence of a new kind of matter, that does not absorb, reflect or emit light, making it extremely hard to detect. Unlike normal matter it does not take part in electromagnetic interaction. This matter is known as the Dark Matter (DM). The DM make up about 26% of all the matter in the universe and the researchers are able to infer its existence only from the gravitational effect it has on the visible matter. The most recent measurement from PLANCK satellite data provides the best fit value of DM relic density [15]:

$$\Omega_{DM}h^2 = 0.1199 \pm 0.0027, \tag{1.12}$$

where h is the Hubble constant in units of 100 km.s^{-1}.Mpc^{-1}. A DM candidate must be stable over the cosmological time scale ($\gtrsim 10^{18}$ sec.). It must be electri-

cally neutral and interact weakly with the ordinary matter particles. Moreover, analyses of structure formation in the universe indicate that most of the DM should be non-relativistic. All these arguments rule out the only viable DM candidate in the SM, i.e, neutrinos. Hence we must look beyond the SM to find a suitable DM candidate.

The discovery of accelerated expansion of the universe [16] suggest that the bulk (70%) of the energy density of the universe is in the form of dark energy. It is distributed evenly throughout the universe. Its exotic physical properties cannot be accounted for in the SM. The latest PLANCK data gives an estimate of the dark energy of the universe [17]

$$\Omega_\Lambda = 0.693 \pm 0.019. \tag{1.13}$$

A theoretical explanation for the dark energy should come from some beyond the SM physics involving gravity [19].

- Our universe appears to be consisting of only matter and no anti-matter. The asymmetry between matter and anti-matter can be characterized in terms of the ratio $\eta_B = \frac{n_B - n_{\bar{B}}}{n_\gamma}$, where n_B, $n_{\bar{B}}$ and n_γ denote number density of baryons, anti-baryons and photons respectively in the universe. WMAP has provided the most accurate measurement of η_B so far [18]:

$$\eta_B = (6.19 \pm 0.15) \times 10^{-10} \quad (68\%\ C.L.\ value). \tag{1.14}$$

The mechanism that can produce this non-zero baryon asymmetry dynamically starting from a baryon-symmetric universe is known as "baryogenesis" [20]. It is possible within the framework of SM to produce baryogenesis. However, detail analysis reveal that it is not possible to produce the desired value of η_B because CP violation in CKM matrix is too small ($\sim 10^{-20}$) and the electroweak phase transition is not sufficiently strong unless the SM higgs boson mass, $m_h < 80$ GeV, which is already excluded. Hence one must have additional sources of CP violation to explain this asymmetry [20].

- There are some experimental anomalies that do not agree with the SM predictions. The measured value of muon anomalous magnetic moment shows a 3.4σ excess [21] over the SM predicted value. The top quark forward-backward asymmetry also shows a 3σ deviation from the SM expected value in the large $t\bar{t}$ invariant mass region [22].

- The SM cannot account for the most familiar force in our everyday lives, i.e, gravitational force. However, this force becomes dominating only at the Planck scale. Hence the SM cannot be a valid theory for all the energy scales.

All these problems suggest that we need to look beyond the SM (BSM) scenario. Different BSM scenario looks into these problems in different ways. In this thesis, however, we only concentrate on one of these various scenarios, namely, Supersymmetry (SUSY). In the next section, we give a brief introduction to the minimal version of SUSY.

1.2 Supersymmetry

Supersymmetry is a general term for a symmetry that relates bosons and fermions. Over the years, SUSY has remained the most popular candidate for BSM physics. It has a very natural way of solving the hierarchy problem. If SUSY were exact, radiative corrections to the scalar mass squared appearing in the SM theory would be absent because the contribution of fermion loops exactly cancels against the boson loops. The additional loops arising in a SUSY theory against the usual fermionic loop are shown in Fig. 1.3. This has been one of the main reasons behind all the phenomenological

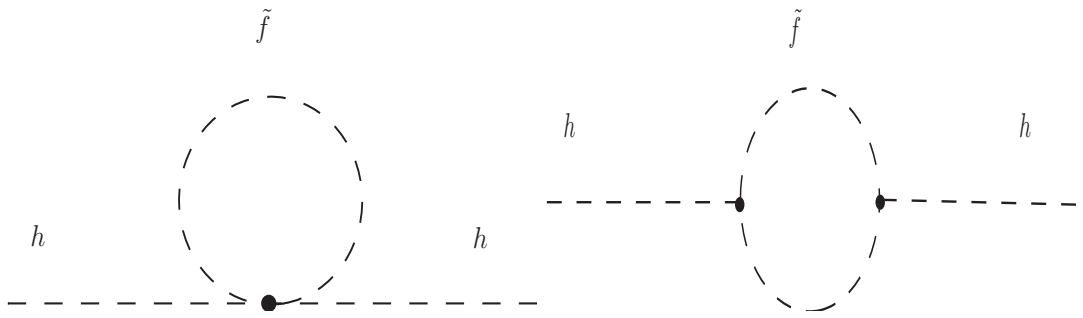

Figure 1.3: Higgs boson mass correction coming from scalar counterparts of fermions at 1-loop level.

interests in SUSY. Its minimal version also leads to a number of new phenomena which are being probed at the LHC and will be probed at any future collider experiments. We briefly introduce SUSY algebra and its general framework before discussing the minimal supersymmetric standard model.

1.2.1 Supersymmetric Transformation and Superfields

A symmetry transformation turning a bosonic state into a fermionic state and vice versa is known as supersymmetry [23–36]. The SUSY generator (Q) satisfies:

$$Q|boson\rangle = |fermion\rangle, \quad Q|fermion\rangle = |boson\rangle \tag{1.15}$$

Every SM particles are accompanied by its supersymmetric partners, called superpartners. In a SUSY theory every SM fermion has a bosonic superpartner and every boson has a fermionic superpartner.

For SUSY, generators required are the Poincaré generators P^μ and $M^{\mu\nu}$ and the spinor generators Q^A_α, $\bar{Q}^A_{\dot{\alpha}}$, where $A = 1, ..., N$. Here we discuss only about the simple $N = 1$ SUSY scenario.

Poincaré symmetry:

The Poincaré group corresponds to the basic symmetries of special relativity. It acts on the space time coordinates x^μ as

$$x^\mu \to x'^\mu = \Lambda^\mu_\nu x^\nu + a^\mu, \tag{1.16}$$

where Λ^μ_ν represents Lorentz transformation that leaves the metric tensor $\eta_{\mu\nu} = diag(1, -1, -1, -1)$ invariant

$$\Lambda^T \eta \Lambda = \eta \tag{1.17}$$

and a^μ represents translation. Generators of the Poincaré group follow the following algebra:

$$[P^\mu, P^\nu] = 0 \tag{1.18}$$

$$[M^{\mu\nu}, P^\sigma] = i\left(P^\mu \eta^{\nu\sigma} - P^\nu \eta^{\mu\sigma}\right) \tag{1.19}$$

$$[M^{\mu\nu}, M^{\rho\sigma}] = i\left(M^{\mu\sigma}\eta^{\nu\rho} + M^{\nu\rho}\eta^{\mu\sigma} - M^{\mu\rho}\eta^{\nu\sigma} - M^{\nu\sigma}\eta^{\mu\rho}\right). \tag{1.20}$$

$M^{\mu\nu}$ has a matrix representation

$$(M^{\rho\sigma})^\mu_\nu = i\left(\eta^{\mu\nu}\delta^\rho_\nu - \eta^{\rho\mu}\delta^\sigma_\nu\right). \tag{1.21}$$

Supersymmetric algebra:

The anti-commutation relations obeyed by the SUSY generators are the following

$$\{Q_\alpha, Q_\beta\} = 0 \tag{1.22}$$

$$\{\bar{Q}_{\dot{\alpha}}, \bar{Q}_{\dot{\beta}}\} = 0 \tag{1.23}$$

$$\{Q_\alpha, \bar{Q}_{\dot{\beta}}\} = 2(\sigma^\mu_{\alpha\dot{\beta}})P_\mu \tag{1.24}$$

where,

$$\sigma^\mu \equiv (1, \sigma_i); \quad \bar{\sigma}^\mu \equiv (1, -\sigma^i) \tag{1.25}$$

and $\alpha, \beta, \dot{\alpha}, \dot{\beta} = 1, 2, \dot{1}, \dot{2}$ (Weyl 2-component spinor notation). Here σ_i are the usual 2×2 Pauli matrices. The commutation relations with the generators of the Poincaré group are:

$$[P^\mu, Q_\alpha] = 0 \tag{1.26}$$

$$[P^\mu, P^\nu] = 0 \tag{1.27}$$

$$[M^{\mu\nu}, Q_\alpha] = -i\,(\sigma^{\mu\nu})^\beta_\alpha\, Q_\beta \tag{1.28}$$

$$\left[M^{\mu\nu}, \bar{Q}^{\dot{\alpha}}\right] = -i\,(\bar{\sigma}^{\mu\nu})^{\dot{\alpha}}_{\dot{\beta}}\, \bar{Q}^{\dot{\beta}}. \tag{1.29}$$

From these relations one can derive the two invariants of the Poincaré group:

$$P^2 = P_\alpha P^\alpha, \quad W^2 = W_\mu W^\mu \tag{1.30}$$

where,

$$W_\mu = -\frac{i}{2}\epsilon_{\mu\nu\rho\sigma} M^{\nu\rho} P^\sigma. \tag{1.31}$$

Now one can verify that

$$[Q_\alpha, P^2] = 0, \quad [Q_\alpha, W^2] \neq 0, \tag{1.32}$$

which implies that the irreducible multiplets will have particles with same mass but different spin.

Grassmann variables:

SUSY transformations and invariants can be formulated in an efficient way in the framework of superspace [37]. The superspace differs from the usual Minkowsky space-time by the addition of two new coordinates, θ_α and $\bar{\theta}_{\dot{\alpha}}$, which are called Grassmann variables.

$$\{\theta_\alpha\}_{\alpha=1,2} \text{ and } \{\bar{\theta}_{\dot{\alpha}}\}_{\dot{\alpha}=\dot{1},\dot{2}}. \tag{1.33}$$

These are discretely varying variables and they anticommute with each other:

$$\{\theta_\alpha, \theta_\beta\} = \{\theta_\alpha, \bar{\theta}_{\dot{\beta}}\} = \{\bar{\theta}_{\dot{\alpha}}, \bar{\theta}_{\dot{\beta}}\} = 0. \tag{1.34}$$

Thus we go from space to superspace

$$\begin{array}{c} Space \Rightarrow Superspace \\ (x_\mu) \qquad (x_\mu, \theta_\alpha, \bar{\theta}_{\dot{\alpha}}) \end{array}$$

Superfield and SUSY transformation:

A finite SUSY transformation can be written as $exp\left[i(\theta Q + \bar{Q}\bar{\theta} - x_\mu P^\mu)\right]$. The objects on which the SUSY transformation acts must also be functions of θ, $\bar{\theta}$, which requires the introduction of the superfields. Using the properties of the Grassmann variables, a general superfield can be written as

$$\begin{aligned}\Phi(x,\theta,\bar{\theta}) = f(x) + \theta^A\phi_A(x) + \bar{\theta}_{\dot{A}}\bar{\chi}^{\dot{A}}(x) + (\theta\theta)m(x) + (\bar{\theta}\bar{\theta})n(x) + \\ (\theta\sigma^\mu\bar{\theta})V_\mu(x) + (\theta\theta)\bar{\theta}_{\dot{A}}\bar{\lambda}^{\dot{A}}(x) + (\bar{\theta}\bar{\theta})\theta^A\psi_A(x) + (\theta\theta)(\bar{\theta}\bar{\theta})d(x),\end{aligned} \tag{1.35}$$

where, $f(x)$, $\phi(x)$, $\bar{\chi}(x)$, $m(x)$, $n(x)$, $V_\mu(x)$, $\bar{\lambda}(x)$, $\psi(x)$ and $d(x)$ are called component fields.

An infinitesimal SUSY transformation on a superfield can be written as

$$\delta_S(\alpha,\bar{\alpha})\Phi(x,\theta,\bar{\theta}) = \left[\alpha\frac{\partial}{\partial\theta} + \bar{\alpha}\frac{\partial}{\partial\bar{\theta}} - i(\alpha\sigma_\mu\bar{\theta} - \theta\sigma_\mu\bar{\alpha})\frac{\partial}{\partial x_\mu}\right]\Phi(x,\theta,\bar{\theta}), \tag{1.36}$$

where, α, $\bar{\alpha}$ are the Grassmann variables and Φ is a superfield. The SUSY generators look like

$$Q_\alpha = \frac{\partial}{\partial\theta^\alpha} - i\sigma^\mu_{\alpha\dot{\beta}}\bar{\theta}^{\dot{\theta}}\partial_\mu; \quad \bar{Q}_{\dot{\alpha}} = -\frac{\partial}{\partial\bar{\theta}^{\dot{\alpha}}} + i\theta^\beta\sigma^\mu_{\beta\dot{\alpha}}\partial_\mu. \tag{1.37}$$

The SUSY-covariant derivatives anti-commute with the SUSY transformations:

$$D_\alpha = \frac{\partial}{\partial\theta^\alpha} + i\sigma^\mu_{\alpha\dot{\beta}}\bar{\theta}^{\dot{\theta}}\partial_\mu; \quad \bar{D}_{\dot{\alpha}} = -\frac{\partial}{\partial\bar{\theta}^{\dot{\alpha}}} - i\theta^\beta\sigma^\mu_{\beta\dot{\alpha}}\partial_\mu. \tag{1.38}$$

Note that, α and θ have a mass dimension $-1/2$ while Q and D have mass dimension $+1/2$. In SUSY it is often more convenient to work in chiral representation. In this representation, θ and $\bar{\theta}$ are treated in slightly different ways. The SUSY transformations and the covariant derivatives for left chiral fields (Φ_L) are given by:

$$\begin{aligned}\delta_S\Phi_L = \left(\alpha\frac{\partial}{\partial\theta} + \bar{\alpha}\frac{\partial}{\partial\bar{\theta}} + 2i\theta\sigma^\mu\bar{\alpha}\partial_\mu\right)\Phi_L; \\ D_L = \frac{\partial}{\partial\theta} + 2i\sigma^\mu\bar{\theta}\partial_\mu \;\;\&\;\; \bar{D}_L = -\frac{\partial}{\partial\bar{\theta}}\end{aligned} \tag{1.39}$$

and those for the right chiral fields (Φ_R) are:

$$\begin{aligned}\delta_S\Phi_R = \left(\alpha\frac{\partial}{\partial\theta} + \bar{\alpha}\frac{\partial}{\partial\bar{\theta}} - 2i\alpha\sigma^\mu\bar{\theta}\partial_\mu\right)\Phi_R; \\ \bar{D}_R = -\frac{\partial}{\partial\bar{\theta}} - 2i\theta\sigma^\mu\partial_\mu \;\;\&\;\; D_R = \frac{\partial}{\partial\theta}.\end{aligned} \tag{1.40}$$

As evident from Eq. 1.39 and 1.40, $\bar{D}(D)$ has particularly simple form in the $L(R)$ representation. To switch between these two representations, one can use the identity:

$$\Phi(x,\theta,\bar{\theta}) = \Phi_L(x_\mu + i\theta\sigma_\mu\bar{\theta},\theta,\bar{\theta}) = \Phi_R(x_\mu - i\theta\sigma_\mu\bar{\theta},\theta,\bar{\theta}). \tag{1.41}$$

To describe the SUSY formalism, we need two kinds of superfields, which are irreducible representations of SUSY algebra. The are called chiral and vector superfields.

Chiral superfields:

The name "chiral superfield" is derived from the fact that the SM fermions are chiral. The left-handed (LH) and right-handed (RH) components transform differently under $SU(2)_L \times U(1)_Y$. Hence the superfield should have only two physical fermionic degrees of freedom. Apart from that the superfields also contain their bosonic superpartners, called sfermions.

To construct the superfield we demand in chiral representation,

$$\bar{D}\Phi_L = 0, \tag{1.42}$$

i.e, Φ_L is independent of $\bar{\theta}$, or

$$D\Phi_R = 0, \tag{1.43}$$

i.e, Φ_R is independent of θ. For example, let us consider the LH-superfield expansion:

$$\Phi_L(x,\theta) = \phi(x) + \sqrt{2}\theta^\alpha\psi_\alpha(x) + \theta^\alpha\theta^\beta\epsilon_{\alpha\beta}F(x), \tag{1.44}$$

where, $\epsilon_{\alpha\beta}$ is the anti-symmetric tensor in two dimensions. The properties of Grassmann variables do not allow any terms with three or more factors of θ. The fields ϕ and F are complex scalars whereas ψ is a Weyl spinor. The Φ_R can be expanded similarly with θ replaced by $\bar{\theta}$.
Rewriting the SUSY transformation in Eq. 1.39 with Φ_L given in Eq. 1.44,

$$\begin{aligned}\delta_S\Phi_L = \quad & \sqrt{2}\alpha^\alpha\psi_\alpha + 2\alpha^\alpha\theta^\beta\epsilon_{\alpha\beta}F + 2i\theta^\alpha\sigma^\mu_{\alpha\dot{\beta}}\bar{\alpha}^{\dot{\beta}}\partial_\mu\phi + 2\sqrt{2}i\theta^\alpha\sigma^\mu_{\alpha\dot{\beta}}\bar{\alpha}^{\dot{\beta}}\theta^\beta\partial_\mu\psi_\beta \\ \equiv \quad & \delta_S\phi + \sqrt{2}\theta\delta_S\psi + \theta\theta\delta_S F. \end{aligned} \tag{1.45}$$

Hence after the transformation is applied on the left-chiral superfield, we get back the same superfield. This implies that the SUSY algebra is close. Explicitly, the transformations of the different fields are given by

$$\delta_S\phi = \sqrt{2}\alpha\psi \tag{1.46}$$

$$\delta_S\psi = \sqrt{2}\alpha F + i\sqrt{2}\sigma^\mu\bar{\alpha}\partial_\mu\phi \tag{1.47}$$

$$\delta_S F = -i\sqrt{2}\partial_\mu\psi\sigma^\mu\bar{\alpha}. \tag{1.48}$$

Note that the component field F, which is the $(\theta\theta)$-component of the left-handed chiral superfield, transforms as a space-time total derivative. Hence any action written using this component will be invariant under SUSY transformations. The dimension of the superfield is the same as that of its scalar component and ψ has a dimension as any other standard fermions.

$$[\Phi] = [\phi] = 1, \quad [\psi] = \tfrac{3}{2}.$$

From Eq. 1.44, it follows

$$[\theta] = -\tfrac{1}{2}, \quad [F] = 2,$$

i.e, the field $F(x)$ has a dimension of $(mass)^2$ unlike an ordinary scalar field and is called an auxiliary field as it can be eliminated using the equations of motion of the fields obtained through the Lagrangian. The scalar field $\phi(x)$ is called the supersymmetric partner of $\psi(x)$.

The chiral superfields can describe fermions and Higgs boson of the SM along with their superpartners. However, to describe gauge bosons and their superpartners, gauginos, we need to consider vector superfields.

Vector superfields:

The vector superfields (V) are considered to be self-conjugate:

$$V(x, \theta, \bar{\theta}) \equiv V^{\dagger}(x, \theta, \bar{\theta}). \tag{1.49}$$

In component form:

$$\begin{aligned} V(x,\theta,\bar{\theta}) = \quad & \left(1 + \frac{1}{4}\theta\theta\bar{\theta}\bar{\theta}\partial_\mu\partial^\mu\right) C(x) + \left(i\theta + \frac{1}{2}\theta\theta\sigma^\mu\bar{\theta}\partial_\mu\right)\chi(x) + \frac{i}{2}\theta\theta\left[M(x) + iN(x)\right] \\ & + \left(-i\bar{\theta} + \frac{1}{2}\bar{\theta}\bar{\theta}\sigma^\mu\theta\partial_\mu\right)\bar{\chi}(x) - \frac{i}{2}\bar{\theta}\bar{\theta}\left[M(x) - iN(x)\right] \\ & -\theta\sigma_\mu\bar{\theta}A^\mu(x) + i\theta\theta\bar{\theta}\bar{\lambda}(x) - i\bar{\theta}\bar{\theta}\theta\lambda(x) + \frac{1}{2}\theta\theta\bar{\theta}\bar{\theta}D(x), \end{aligned} \tag{1.50}$$

where, C, M and N are real scalar fields, χ and λ are Weyl spinors and A_μ is a vector field. V is called a vector superfield because of the presence of this vector field. D is an auxiliary field.

A general non-abelian SUSY gauge transformation acting on V is described as

$$e^{gV} \rightarrow e^{-ig\Lambda^\dagger} e^{gV} e^{ig\Lambda}, \tag{1.51}$$

where $\Lambda(x,\theta,\bar{\theta})$ represents a chiral superfield and g is the gauge coupling. For an abelian gauge symmetry this transformation can be simplified as

$$V \to V + i(\Lambda - \Lambda^\dagger). \tag{1.52}$$

One can choose the "Wess-Zumino" gauge

$$\chi(x) = C(x) = M(x) = N(x) \equiv 0, \tag{1.53}$$

to remove some unphysical degrees of freedom. In this gauge,

$$V = -\theta\sigma_\mu\bar{\theta}A^\mu(x) + i\theta\theta\bar{\theta}\bar{\lambda}(x) - i\bar{\theta}\bar{\theta}\theta\lambda(x) + \frac{1}{2}\theta\theta\bar{\theta}\bar{\theta}D(x). \tag{1.54}$$

One can define a field strength tensor(W_α) and its conjugate ($\bar{W}_{\dot{\alpha}}$) as

$$\begin{aligned} W_\alpha &= -\frac{1}{4}\bar{D}^2 e^V D_\alpha e^{-V}, \\ \bar{W}_{\dot{\alpha}} &= -\frac{1}{4}D^2 e^V \bar{D}_{\dot{\alpha}} e^{-V}. \end{aligned} \tag{1.55}$$

This field strength tensor is a chiral superfield:

$$\bar{D}_{\dot{\beta}} W_\alpha = 0, \quad D_\beta \bar{W}_{\dot{\alpha}} = 0, \tag{1.56}$$

which in Wess-Zumino gauge, is written as a polynomial over the component fields:

$$W_\alpha = T^a \left(-i\lambda^a_\alpha + \theta_\alpha D^a - \frac{i}{2}(\sigma^\mu\bar{\sigma}^\nu\theta)_\alpha F^a_{\mu\nu} + \theta^2\sigma^\mu D_\mu\bar{\lambda}^a \right), \tag{1.57}$$

where,

$$F^a_{\mu\nu} = \partial_\mu A^a_\nu - \partial_\nu A^a_\mu + f^{abc}A^b_\mu A^c_\nu, \quad D_\mu\bar{\lambda}^a = \partial\bar{\lambda}^a + f^{abc}A^b_\mu\bar{\lambda}^c. \tag{1.58}$$

However, in Abelian gauge, this field strength tensor can be simplified as

$$W_\alpha = -\frac{1}{4}\bar{D}^2 D_\alpha V, \quad \bar{W}_{\dot{\alpha}} = \frac{1}{4}D^2\bar{D}_{\dot{\alpha}}V. \tag{1.59}$$

1.2.2 Supersymmetric Lagrangian

Supersymmetric Lagrangian is constructed using superfield method. Let us first start with the Lagrangian which has no local gauge invariance. In the superfield notation, the SUSY invariant Lagrangian is a polynomial of superfields. The most general SUSY invariant Lagrangian for a chiral superfield (Φ) has the form

$$\mathcal{L} = \Phi_i^\dagger\Phi_i\Big|_{\theta\theta\bar{\theta}\bar{\theta}} + \left[\left(\lambda_i\Phi_i + \frac{1}{2}m_{ij}\Phi_i\Phi_j + \frac{1}{3}g_{ijk}\Phi_i\Phi_j\Phi_k \right)\Big|_{\theta\theta} + h.c. \right]. \tag{1.60}$$

The first term in Eq. 1.60 represents a kinetic term. It consists of both the chiral and anti-chiral superfields and is a function of the Grassmanian parameters θ and $\bar{\theta}$. Expanding this term in θ and $\bar{\theta}$ produces the usual kinetic terms for the corresponding component fields. The subsequent terms together form what is called the superpotential. It is composed of the chiral superfields and the hermitian conjugated counterpart consisting of the anti-chiral superfields.

Eq. 1.60 can be written more efficiently in superspace. The action in that case is an integral over the superspace. The space-time Lagrangian density is [27, 37]

$$\mathcal{L} = \int d^2\theta d^2\bar{\theta}\Phi_i^\dagger\Phi_i + \int d^2\theta \left[\left(\lambda_i\Phi_i + \frac{1}{2}m_{ij}\Phi_i\Phi_j + \frac{1}{3}g_{ijk}\Phi_i\Phi_j\Phi_k\right) + h.c.\right] \quad (1.61)$$

Using the rules of Grassmanian integration [38]

$$\int d\theta_\alpha = 0, \qquad \int \theta_\alpha d\theta_\beta = \delta_{\alpha\beta}, \quad (1.62)$$

one performs the integration and obtain from Eq. 1.61,

$$\begin{aligned}\mathcal{L} \quad &= \partial^\mu\phi_i^*\partial_\mu\phi_i + i\bar{\psi}_i\bar{\sigma}^\mu\partial_\mu\psi_i + F_i^*F_i + \\ &\left[\lambda_iF_i + m_{ij}\left(\phi_iF_j - \frac{1}{2}\psi_i\psi_j\right) + y_{ijk}\left(\phi_i\phi_jF_k - \psi_i\psi_j\phi_k\right) + h.c\right]. \quad (1.63)\end{aligned}$$

Now let us consider the gauge invariant SUSY Lagrangian. It contains gauge invariant interaction terms for the matter and the gauge fields and kinetic terms and self interaction terms of the gauge fields. In the Wess-Zumino gauge the gauge field kinetic terms look like

$$W^\alpha W_\alpha|_{\theta\theta} = -2i\lambda\sigma^\mu D_\mu\bar{\lambda} - \frac{1}{2}F_{\mu\nu}F^{\mu\nu} + \frac{1}{2}D^2 + i\frac{1}{4}\epsilon_{\mu\nu\rho\sigma}F_{\mu\nu}F^{\rho\sigma}. \quad (1.64)$$

The gauge invariant Lagrangian now looks like

$$\begin{aligned}\mathcal{L} \quad &= \frac{1}{4}\int d^2\theta W^\alpha W_\alpha + \frac{1}{4}\int d^2\bar{\theta}\bar{W}_{\dot{\alpha}}\bar{W}^{\dot{\alpha}} \\ &= \frac{1}{2}D^2 - \frac{1}{4}F_{\mu\nu}F^{\mu\nu} - i\lambda\sigma^\mu D_\mu\bar{\lambda}. \quad (1.65)\end{aligned}$$

In order to obtain gauge invariant interaction terms with matter chiral superfields, one has to consider their gauge transformations:

$$\Phi \to e^{-ig\Lambda}\Phi, \quad \Phi^\dagger \to \Phi^\dagger e^{ig\Lambda^\dagger}, \quad V \to V + i\left(\Lambda - \Lambda^\dagger\right). \quad (1.66)$$

The gauge invariant kinetic term is modified

$$\Phi_i^\dagger\Phi_i\left|_{\theta\theta\bar{\theta}\bar{\theta}} \to \Phi_i^\dagger e^{gV}\Phi_i\right|_{\theta\theta\bar{\theta}\bar{\theta}}. \quad (1.67)$$

Then the complete SUSY as well as gauge invariant Lagrangian is as follows

$$\begin{aligned}\mathcal{L}_{inv} \quad &= \frac{1}{4}\int d^2\theta W^\alpha W_\alpha + \frac{1}{4}\int d^2\bar{\theta}\bar{W}_{\dot{\alpha}}\bar{W}^{\dot{\alpha}} + \int d^2\theta d^2\bar{\theta}\Phi_i^\dagger e^{gV}\Phi_i + \\ &\int d^2\theta\left(\frac{1}{2}m_{ij}\Phi_i\Phi_j + \frac{1}{3}y_{ijk}\Phi_i\Phi_j\Phi_k\right) + h.c. \end{aligned} \tag{1.68}$$

Expanding Eq. 1.68 in terms of the component fields and integrating out the auxiliary fields D^a and F_i, one gets the usual Lagrangian.

1.2.3 The Scalar Potential

In SUSY theories the scalar potential consists of two kinds of terms, namely, D-terms and F-terms. The kinetic energy term of the gauge fields give rise to a D-term: $\frac{1}{2}D^aD^a$, where the index a denotes corresponding the gauge groups index. Another D-term is yielded by the matter-gauge interaction term, $gD^a\phi_i^*T_{ij}^a\phi_j$, where T_{ij}^a denote the generators of the corresponding gauge group. Hence

$$\mathcal{L}_D = \frac{1}{2}D^aD^a + gD^a\phi_i^*T_{ij}^a\phi_j. \tag{1.69}$$

The Euler-Lagrange equation gives:

$$D^a = -g\phi_i^*T_{ij}^a\phi_j. \tag{1.70}$$

Substituting Eq. 1.70 into Eq. 1.69, the Lagrangian looks like

$$\mathcal{L}_D = -\frac{1}{2}D^aD^a$$

Here a can run from 1,..,3 for $SU(2)_L$. There is an additional contribution to $\mathcal{L}_D$ coming from $U(1)_Y$ D-term as well. This contribution can be written as $-\frac{1}{2}D'^2$, where, $D' = -g'y_Q\phi^*\phi$, y_Q being the corresponding hypercharge. Hence

$$V_D = \frac{1}{2}\left(\sum D^aD^a + D'^2\right). \tag{1.71}$$

The F-term can be obtained from matter field self-interaction Eq. 1.63. For a general superpotential (W), one can write

$$\mathcal{L}_F = F_i^*F_i + \left(\frac{\partial W}{\partial\phi_i}F_i + h.c.\right). \tag{1.72}$$

The Euler-Lagrange equation gives:

$$F_i^* = -\frac{\partial W}{\partial\phi_i}. \tag{1.73}$$

Substituting Eq. 1.73 into Eq. 1.72,

$$\mathcal{L}_F = -F_i^* F_i$$

Hence,

$$V_F = F_i^* F_i. \tag{1.74}$$

The full potential is given by

$$V = V_D + V_F. \tag{1.75}$$

1.2.4 Supersymmetry Breaking

If SUSY was an exact symmetry, the superparticles would have the same mass as their SM counterparts. But no superpartners of the SM particles have yet been found so far which means they are heavier. Hence SUSY must be a broken symmetry. There are two ways to break the symmetry: spontaneous breaking and explicit breaking.

Breaking SUSY spontaneously means that the vacuum state ($|0\rangle$) is not invariant under the SUSY transformation, i.e, $Q_\alpha|0\rangle \neq 0$ and $Q_{\dot{\alpha}}^\dagger|0\rangle \neq 0$. Hence,

$$\begin{aligned} &\langle 0|Q_{\dot{\alpha}}^\dagger Q_\alpha|0\rangle \neq 0 \\ &\Rightarrow \langle 0|H|0\rangle \neq 0 \end{aligned} \tag{1.76}$$

As a consequence, the vacuum must have a positive energy. On the other hand, for the vacuum state,

$$\langle 0|H|0\rangle = \langle 0|V|0\rangle, \tag{1.77}$$

which means $\langle 0|V|0\rangle \neq 0$, where V is the scalar potential given by Eq. 1.75. Different SUSY and gauge symmetry breaking scenarios are shown in Fig. 1.4 and Fig. 1.5. SUSY is broken whenever the minimum of the potential ($V(\phi_{min})$) is nonzero and the gauge symmetry is broken when the minimum of the potential is attained at a nonzero gauge field configuration, i.e, $\phi_{min} \neq 0$.

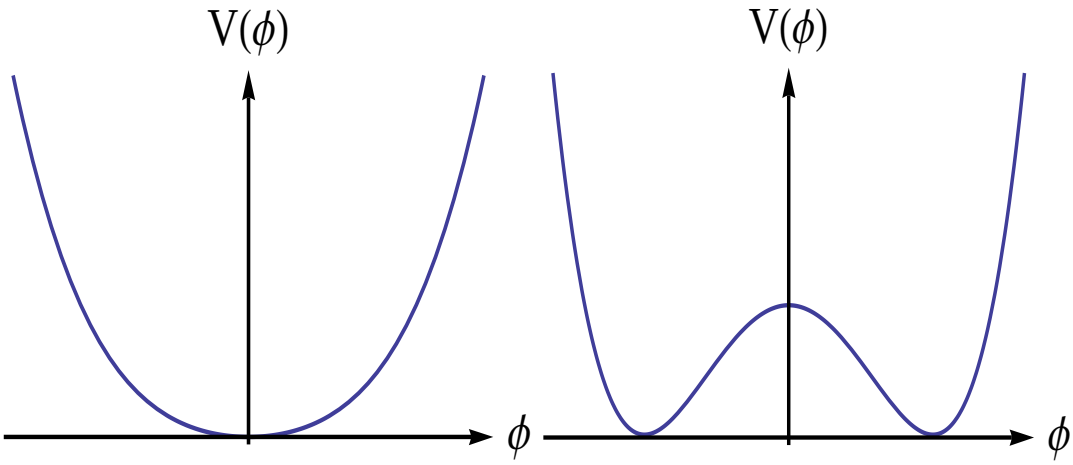

Figure 1.4: The figure on the left panel represents the scenario where both SUSY and gauge symmetry are preserved and the right panel represents gauge symmetry breaking.

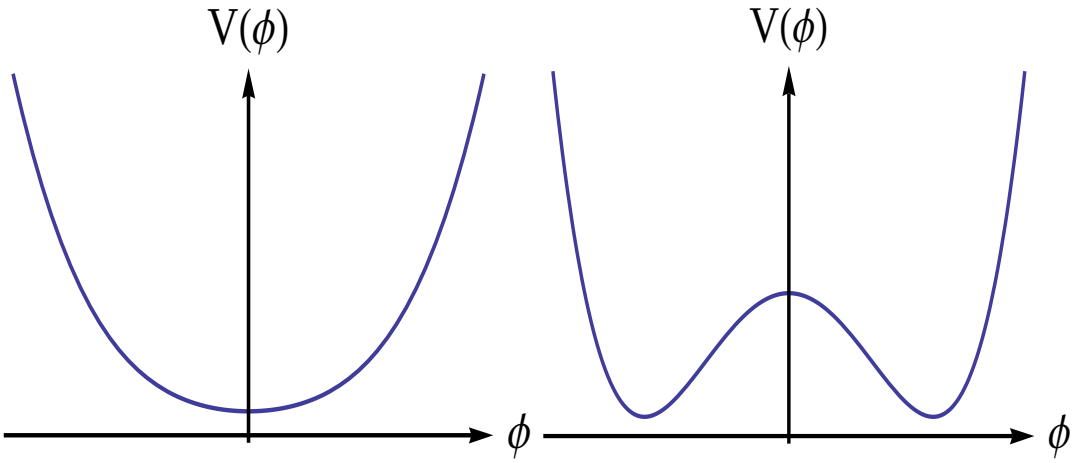

Figure 1.5: The figure on the left panel represents SUSY breaking keeping gauge symmetry preserved while the one on the right panel represents the scenario where both SUSY and the gauge symmetry are broken.

Hence if SUSY is spontaneously broken, it means that F^i and/or D^a cannot vanish in the ground state. Therefore, to achieve spontaneous SUSY breaking, one has to ensure that the equations $F^i = 0$ and $D^a = 0$ are not satisfied simultaneously in the theory for any values of the fields. In a similar way as the electroweak symmetry breaking, a field needs to be introduced which breaks the symmetry by introducing a non-zero vacuum expectation value. Due to the structure of SUSY, this field should be a superfield whose auxiliary F and D terms acquire nonzero vevs. Breaking of the theory through F-term is known as O'Raifeartaigh mechanism [39] and the same

through D-term is known as Fayet-Iliopoulos mechanism [40, 41].

O'Raifeartaigh mechanism:

In this case, one needs several chiral superfields and the superpotential should be chosen in a way that trivial zero vevs for the auxiliary F-fields are absent. Let the superpotential be

$$\mathcal{W} = \lambda\Phi_3 + m\Phi_1\Phi_2 + g\Phi_3\Phi_1^2. \tag{1.78}$$

Then the equations of motion for the auxiliary fields are:

$$\begin{aligned} F_1^* &= m\phi_2 + 2g\phi_1\phi_3, \\ F_2^* &= m\phi_1, \\ F_3^* &= \lambda + g\phi_1^2. \end{aligned} \tag{1.79}$$

The above equations have no solutions with $\langle F_i \rangle = 0$ and SUSY is broken spontaneously. The drawback of this mechanism is a lot of arbitrariness in the choice of the superpotential.

Fayet-Iliopoulos mechanism:

It is also possible to generate an expectation value for a D-term. We have, from the definition of V,

$$\mu^2 \int d^4\theta V = \mu^2 D. \tag{1.80}$$

This is known as "Fayet-Iliopoulos D term". This is a gauge and SUSY invariant term by itself, but can lead to spontaneous SUSY breaking. The simplemost model exhibiting this mechanism is a SUSY $U(1)$ gauge theory with a single chiral superfield of charge q in which the auxiliary component $D(x)$ of the vector superfield V develops a non-zero vev, i.e, $\langle D(x) \rangle \neq 0$. The drawback of this mechanism is the necessity of $U(1)$ gauge invariance.

For both these breaking mechanisms described above, the SUSY particle spectrum follows certain sum rules, known as the supertrace sum rules which states that the supertrace of the tree-level squared-mass eigenvalues, defined with a weighted sum over all particles with spin j, $STr(m^2) \equiv \sum(-1)^j(2j+1)Tr(m_j^2) = 0$ [42]. This theorem is valid only for sets of states with same quantum numbers. A vanishing supertrace, however, needs some of the SUSY particles to be lighter compared to their SM counterpart, which has not been observed so far experimentally. However, this relation only holds true at the tree level and for renormalizable theories.

A way out to this problem is to break SUSY spontaneously in a sector which only couples to the SM sector via loops or via non-renormalizable operators. The SUSY-breaking sector is referred to as "hidden" sector [43] and the SM sector as the "visible" sector. Although we do not know the exact mechanism for SUSY breaking, this scenario by far remains the most popular one. These two sectors interact with each other by the exchange of some "messenger" fields. These fields mediate the information of SUSY breaking from the hidden sector to the visible sector. In the visible sector, the explicit SUSY breaking terms are known as soft SUSY breaking terms. These terms consist of mass terms for scalars and gauginos and trilinear scalar couplings. We discuss more about this later. As a consequence of SUSY being broken in the "hidden" sector, the form of the soft SUSY-breaking terms do not depend on the mechanism of spontaneous SUSY-breaking itself, but rather on the mechanism for mediating the SUSY-breaking information to the "visible" sector. Depending upon the various messenger fields, there exist different scenarios:

- **Gravity mediation:** In this framework [44], gravitational interactions play the role of messenger sector. Supersymmetry is broken spontaneously in the hidden sector. This information is then communicated to the MSSM sector through gravitational sector leading to the soft terms. Since gravitational interactions play an important role only at very high energies, $M_{Planck} \sim 10^{19}$ GeV, the breaking information is passed on to the visible sector only at those scales. A particular class of supergravity mediated supersymmetry breaking models are those which go under the name of "minimal" supergravity (mSUGRA). One further considers a grand unified theory (GUT) group G to break into the SM gauge group $SU(3)_C \otimes SU(2)_L \otimes U(1)_Y$ at the gauge coupling unification scale $M_G \sim 10^{16}$ GeV. The soft terms are assigned with unified values at M_G:

  - a universal gaugino mass parameter, $m_{1/2}$,
  - a universal scalar mass parameter, m_0,
  - a universal trilinear coupling parameter, A_0.

  Apart from these, there are two more independent parameters in mSUGRA scenario, $\tan\beta$ and $sign(\mu)$ (these parameters will be introduced later). One of the special features of this model is that with only these five parameters, it can determine the entire soft spectrum.

- **Gauge mediation:** The key idea behind this mechanism [45] is to use gauge interactions instead of gravity to mediate the supersymmetry breaking from the

hidden to the visible MSSM sector. In this case supersymmetry breaking can be communicated at much lower energies ~ 100 TeV.

Apart from these two there also exist other messenger field scenarios, namely, anomaly mediation [46], gaugino mediation [47] and several others [48] which we shall not discuss here.

Now that we are familiar with the general framework of SUSY, in the next section we discuss about the simplest supersymmetric model, obtained by minimal extension of the SM, known as the minimal supersymmetric SM (MSSM).

1.2.5 Minimal Supersymmetric Standard Model: Particle content

The MSSM is based on the same gauge group as SM:

$$SU(3)_c \otimes SU(2)_L \otimes U(1)_Y \tag{1.81}$$

The MSSM contains minimum number of new particles and new interactions required to construct a consistent SUSY theory. Below we discuss the particle content of the model in brief.

The SM fermions are associated with complex scalar bosons (sfermions) with the same quantum numbers and they both belong to a chiral superfield. The gauge bosons appear with the corresponding spin 1/2 fermions known as gauginos to form a vector supermultiplet. Unlike the Standard Model, in MSSM one requires to have two Higgs doublets with opposite hypercharges to cancel the triangle anomalies [49] and also to give masses to the isospin +1/2 and -1/2 fermions in a SUSY invariant [50,51] way. As a result of introducing two Higgs doublet in the model, now there are five Higgs bosons in total: two CP-even, one CP-odd and two charged [52]. The Higgs doublets have their corresponding fermionic superpartners, known as the Higgsinos. The higgsinos will mix with the gauginos to produce two charginos and four neutralinos in the physical basis. The field content of the MSSM is summerised in Table 1.2.

1.2.6 The superpotential and SUSY breaking Lagrangian

The superpotential must be gauge invariant and renormalizable. The most general MSSM superpotential consists of the following terms:

$$W_{MSSM} = \epsilon_{ab}\left[\mu \widehat{H}_u^a \widehat{H}_d^b - y_{u_{ij}} \widehat{Q}_i^a \widehat{H}_u^b \widehat{U}_j^c + y_{d_{ij}} \widehat{Q}_i^a \widehat{H}_d^b \widehat{D}_j^c + y_{e_{ij}} \widehat{L}_i^a \widehat{H}_d^b \widehat{E}_j^c\right], \tag{1.82}$$

Superfields	Boson fields	Fermion fields	$SU(3)_c$	$SU(2)_L$	$U(1)_Y$
$\widehat{G}_A$	G_A^μ	$\widetilde{G}_A$	8	1	0
$\widehat{W}_a$	W_a^μ	$\widetilde{W}_a$	1	3	0
$\widehat{B}$	B^μ	$\widetilde{B}$	1	1	0
$\widehat{L}_i = \begin{pmatrix} \widehat{\nu}_L \\ \widehat{e_L^-} \end{pmatrix}_i$	$\left(\widetilde{\nu}_L, \widetilde{e_L^-} \right)_i$	$\left(\nu_L, e_L^- \right)_i$	1	2	-1
$\widehat{E}_i^c$	$\widetilde{e}_{R_i}^-$	$e_{R_i}^-$	1	1	-2
$\widehat{Q}_i = \begin{pmatrix} \widehat{u}_L \\ \widehat{d}_L \end{pmatrix}_i$	$\left(\widetilde{u}_L, \widetilde{d}_L \right)_i$	$\left(u_L, d_L \right)_i$	3	2	$\frac{1}{3}$
$\widehat{U}_i^c$	$\widetilde{u}_{R_i}$	u_{R_i}	3	1	$\frac{4}{3}$
$\widehat{D}_i^c$	$\widetilde{u}_{R_i}$	d_{R_i}	3	1	$-\frac{2}{3}$
$\widehat{H}_d = \begin{pmatrix} \widehat{h}_d^0 \\ \widehat{h}_d^- \end{pmatrix}_i$	$\left(h_d^0, h_d^- \right)_i$	$\left(\widetilde{h}_d^0, \widetilde{h}_d^- \right)_i$	1	2	-1
$\widehat{H}_u = \begin{pmatrix} \widehat{h}_u^+ \\ \widehat{h}_u^0 \end{pmatrix}_i$	$\left(h_u^+, h_u^0 \right)_i$	$\left(\widetilde{h}_u^+, \widetilde{h}_u^0 \right)_i$	1	2	1

Table 1.2: MSSM particle content with the corresponding gauge quantum numbers. Here i(=1,2,3) indicates the three generations of SM fermions, a(=1,2,3) indicates the three W-bosons and A(=1,2,3,...,8) indicates the eight gluons. There exists one anti-particle multiplet for each supermultiplet corresponding to the charge-conjugated SM particles and their superpartners.

where a,b(=1,2) are the $SU(2)_L$ indices, $y_{u,d,e}$ are the 3×3 Yukawa coupling matrices and

$$\epsilon_{ab} = \begin{pmatrix} 0 & 1 \\ -1 & 0 \end{pmatrix}.$$

The lepton and quark masses are generated after electroweak symmetry breaking by the vevs of the neutral Higgs components.

$$\langle H_u \rangle = \frac{1}{\sqrt{2}} \begin{pmatrix} 0 \\ v_u \end{pmatrix}, \quad \langle H_d \rangle = \frac{1}{\sqrt{2}} \begin{pmatrix} v_d \\ 0 \end{pmatrix}, \tag{1.83}$$

where $\frac{v_u}{v_d} \equiv \tan\beta$. As discussed earlier, the effect of spontaneous SUSY breaking in the hidden sector is reflected by addition of the soft terms to the SUSY Lagrangian in

visible sector. The most general soft SUSY breaking [53–57] Lagrangian is given by

$$
\begin{aligned}
-\mathcal{L}_{soft\ breaking} &= m^2_{Q_{ij}}\widetilde{Q}^\dagger_i\widetilde{Q}_j + m^2_{U_{ij}}\widetilde{u}^\dagger_{R_i}\widetilde{u}_{R_j} + m^2_{D_{ij}}\widetilde{d}^\dagger_{R_i}\widetilde{d}_{R_j} + m^2_{L_{ij}}\widetilde{L}^\dagger_i\widetilde{L}_j + m^2_{E_{ij}}\widetilde{e}^\dagger_{R_i}\widetilde{e}_{R_j} \\
&+\epsilon^{ab}\left(A_{u_{ij}}y_{u_{ij}}\widetilde{Q}_{ia}H_{u_b}\widetilde{u}^\dagger_{R_j} + A_{d_{ij}}y_{d_{ij}}\widetilde{Q}_{ia}H_{d_b}\widetilde{d}^\dagger_{R_j} + A_{e_{ij}}y_{e_{ij}}\widetilde{L}_{ia}H_{d_b}\widetilde{e}^\dagger_{R_j} + h.c\right) \\
&+m^2_{H_u}H^\dagger_u H_u + m^2_{H_d}H^\dagger_d H_d + B_\mu\left(\epsilon^{ab}H_{u_a}H_{d_b} + h.c\right) \\
&+\frac{1}{2}[M_1\bar{\widetilde{B}}\widetilde{B} + M_2\bar{\widetilde{W}}^a\widetilde{W}_a + M_3\bar{\widetilde{G}}^A\widetilde{G}_A + h.c]
\end{aligned}
\tag{1.84}
$$

where $i,j(=1,2,3)$ are the generation indices, and $a(=1,2,3)$, $A(=1,2,....,8)$ are the $SU(2)_L$ and $SU(3)_C$ indices respectively. M_1, M_2 and M_3 are the respective gaugino masses associated with $U(1)_Y$, $SU(2)_L$ and $SU(3)_C$ gauge groups. m^2_Q, m^2_U, m^2_D, m^2_L, m^2_E are the 3×3 complex hermitian matrices in family space. $m^2_{H_u}$ and $m^2_{H_d}$ are squared mass parameters and B_μ is the bilinear Higgs mixing coefficient. A_u, A_d and A_e are the trilinear couplings and appear as 3×3 complex matrices.

1.2.7 Particle masses in MSSM

- **Slepton mass matrix:**
  The relevant Lagrangian contains off-diagonal mass terms for the sleptons in the basis $(\widetilde{\ell}_L,\widetilde{\ell}_R)$,where ℓ stands for e, μ, or τ. Hence one has to diagonalize the mass matrix to obtain physical mass eigenstates. The mass squared matrices look like

$$
\mathcal{M}^2_{\widetilde{\ell}} = \begin{pmatrix} m^2_L + m^2_\ell - M^2_Z(\frac{1}{2} - \sin^2\theta_W)\cos2\beta & m_\ell(A_\ell - \mu\tan\beta) \\ m_\ell(A_\ell - \mu\tan\beta) & m^2_E + m^2_\ell - M^2_Z\sin^2\theta_W\cos2\beta \end{pmatrix} \tag{1.85}
$$

  Since the off-diagonal term in the above mass matrix is proportional to the corresponding lepton mass, for the first two generations, mixing between the left and right-handed(L-R) states is negligible. Hence the physical mass eigenstates are essentially the same as the corresponding diagonal entries. However, for the third generation, the mixing can be quite significant.

  Sneutrinos, on the other hand, have no right-handed states. The mass squared term is given by

$$
\mathcal{M}^2_{\widetilde{\nu}} = m^2_L + \frac{1}{2}M^2_Z\cos2\beta. \tag{1.86}
$$

- **Squark mass matrix:**
  The up-type and down type mass squared matrices in the basis $(\widetilde{q}_L,\widetilde{q}_R)$, where q stands for either up-type (u,c,t) or down-type (d,s,b) quarks, look like:

$$
\mathcal{M}^2_{\widetilde{u}} = \begin{pmatrix} m^2_Q + m^2_u - M^2_Z(\frac{1}{2} - \frac{2}{3}\sin^2_W)\cos2\beta & m_u(A_u - \mu\cot\beta) \\ m_u(A_u - \mu\cot\beta) & m^2_U + m^2_u + \frac{2}{3}M^2_Z\sin^2_W\cos2\beta \end{pmatrix} \tag{1.87}
$$

$$\mathcal{M}^2_{\tilde{d}} = \begin{pmatrix} m_Q^2 + m_d^2 - M_Z^2(\frac{1}{2} - \frac{1}{3}\sin^2_W)\cos2\beta & m_d(A_d - \mu\tan\beta) \\ m_d(A_d - \mu\tan\beta) & m_D^2 + m_d^2 - \frac{1}{3}M_Z^2\sin^2_W\cos2\beta \end{pmatrix} \quad (1.88)$$

The L-R mixing of the third generation is significant due to large top mass. Mixing in the bottom sector is large for a large value of tanβ. As in the sleptonic case, due to very small quark masses the L-R mixing for first and second generation of squarks are negligible.

- **Chargino mass matrix:**
  Charginos ($\widetilde{\chi}^{\pm}_{1,2}$) arise due to mixing between Winos ($\widetilde{W}^{\pm}$) and charged Higgsinos ($H^{\pm}$). They are four component Dirac spinors. Since there are two independent mixings between ($\widetilde{W}^{-}$, $\widetilde{H}^{-}$) and ($\widetilde{W}^{+}$, $\widetilde{H}^{+}$) states, we need two unitary matrices in order to diagonalize the mass matrix. By introducing the notation,

$$\psi^- = \begin{pmatrix} \widetilde{W}^- \\ \widetilde{H}^- \end{pmatrix}, \quad \psi^+ = \begin{pmatrix} \widetilde{W}^+ \\ \widetilde{H}^+ \end{pmatrix}$$

and

$$\Psi^{\pm} = \begin{pmatrix} \psi^+ \\ \psi^- \end{pmatrix}$$

The relevant part of the Lagrangian in the above mentioned basis is of the form

$$\mathcal{L}^{mass}_{\widetilde{\chi}^{\pm}} = \frac{1}{2}(\Psi^{\pm})^T Y^{\pm}\Psi^{\pm} + h.c. \quad (1.89)$$

Here

$$Y^{\pm} = \begin{pmatrix} 0 & X^T \\ X & 0 \end{pmatrix}, \quad (1.90)$$

and

$$X = \begin{pmatrix} M_2 & -\sqrt{2}m_W\sin\beta \\ -\sqrt{2}m_W\cos\beta & \mu \end{pmatrix} \quad (1.91)$$

Now, two-component mass eigenstates can be written as

$$\chi_i^+ = V_{ij}\psi_j^+, \quad (1.92)$$

$$\chi_i^- = U_{ij}\psi_j^-, \quad (1.93)$$

where i, j =1,2 and U and V are unitary matrices, constructed in such a way that

$$U^* X V^{\dagger} = M_D^{\pm}. \quad (1.94)$$

The chargino masses appear as the diagonal entries of $M_D^{\pm}$. The two-component spinors $\chi_i^{\pm}$ can be arranged in a four-component Dirac-spinor as

$$\widetilde{\chi}_i = \begin{pmatrix} \chi_i^+ \\ \bar{\chi}_i^- \end{pmatrix}, \qquad i = 1, 2. \tag{1.95}$$

Thus the two chargino mass eigenvalues are

$$\begin{aligned} M^2_{\widetilde{\chi}^+_{1,2}} = \tfrac{1}{2}\{M_2^2 + \mu^2 + 2m_W^2 \mp [(M_2^2 - \mu^2)^2 + 4m_W^4 \cos^2 2\beta \\ + 4m_W^2(M_2^2 + \mu^2 + 2M_2\mu \sin 2\beta)]^{1/2}\}. \end{aligned} \tag{1.96}$$

- **Neutralino mass matrix:**
  The neutral gauginos ($\widetilde{B}$, $\widetilde{W}^3$) and neutral higgsinos ($\widetilde{H}_u^0$, $\widetilde{H}_d^0$) mix among themselves to produce neutralino ($\widetilde{\chi}^0$) mass eigenstates. The relevant Lagrangian looks like

$$\mathcal{L}^{mass}_{\widetilde{\chi}^0} = \frac{1}{2}(\psi^0)^T Y^0 \psi^0 + h.c, \tag{1.97}$$

  where in the basis $\psi^0 \equiv (\widetilde{B}, \widetilde{W}^3, \widetilde{H}_d^0, \widetilde{H}_u^0)$ the matrix Y^0 is of the form

$$Y^0 = \begin{pmatrix} M_1 & 0 & -M_Z \cos\beta \sin\theta_W & M_Z \sin\beta \sin\theta_W \\ 0 & M_2 & M_Z \cos\beta \cos\theta_W & -M_Z \sin\beta \cos\theta_W \\ -M_Z \cos\beta \sin\theta_W & M_Z \cos\beta \cos\theta_W & 0 & -\mu \\ M_Z \sin\beta \sin\theta_W & -M_Z \sin\beta \cos\theta_W & -\mu & 0 \end{pmatrix} \tag{1.98}$$

  Note that Y^0 is symmetric and can be diagonalized by a unitary matrix, N to obtain the neutralino mass eigenvalues:

$$N^* Y^0 N^\dagger = M_D^0. \tag{1.99}$$

  M_D^0 is the diagonal neutralino mass matrix.

- **Higgs boson masses:**
  The Higgs scalar fields in the MSSM consist of two complex $SU(2)_L$ doublets i.e, eight real, scalar degrees of freedom. After the electroweak symmetry breaking, three of these degrees of freedom become the longitudinal modes of the massive vector bosons, Z^0 and $W^{\pm}$. The remaining five are the Higgs boson mass eigenstates consisting of one CP-odd neutral scalar (A_0), a positively charged scalar (H^+) and its conjugate, a negatively charged scalar (H^-) along with two CP-even

neutral scalars (h_0 and H_0). The tree level masses of these particles are given by

$$m^2_{A_0} = m^2_1 + m^2_2, \tag{1.100}$$

$$m^2_{H^\pm} = m^2_{A_0} + m^2_W, \tag{1.101}$$

$$m^2_{h_0,H_0} = \frac{1}{2}\left(m^2_{A_0} + m^2_Z \mp \sqrt{(m^2_{A_0} + m^2_Z)^2 - 4m^2_Z m^2_{A_0}\cos^2 2\beta}\right), \tag{1.102}$$

where $m^2_1 = m^2_{H_d} + \mu^2$ and $m^2_2 = m^2_{H_u} + \mu^2$. Whereas the masses of A_0, H_0 and $H^\pm$ can be arbitrarily large, the mass of h_0 is bounded from above [58, 59]. From the above relations it can be derived that at tree level [60, 61],

$$m_{h_0} < |\cos 2\beta| M_Z. \tag{1.103}$$

It suggests that the lightest Higgs boson mass can even be lighter than the Z-boson mass. However, this scenario is already ruled out from LEP searches [62, 63]. The large radiative corrections coming mainly from top quark and top squark loops contribute largely to enhance the Higgs boson mass. In the limit where the top squark masses ($m_{\tilde{t}_1}$, $m_{\tilde{t}_2}$) are larger than the top quark mass (m_t), the one loop radiative correction contribution [64–67] is given by

$$\Delta(m^2_{h_0}) = \frac{3}{4\pi^2} v^2 y_t^4 \sin^4\beta \ln\left(\frac{m_{\tilde{t}_1} m_{\tilde{t}_2}}{m^2_t}\right). \tag{1.104}$$

This correction added with the other relevant correction terms provides a limit on the lightest Higgs boson mass,

$$m_{h^0} \lesssim 130 \text{ GeV}. \tag{1.105}$$

There exist quite a few detailed analyses on the MSSM Higgs boson and their phenomenological implications in the literature [68].

1.2.8 R-parity in Supersymmetry

In addition to the terms in the superpotential of the MSSM there may be other gauge invariant and renormalizable terms which can also be included:

$$W_{\not R_P} = \epsilon_{ab}\left[\mu_i \widehat{L}^a_i \widehat{H}^b_2 + \lambda_{ijk}\widehat{L}^a_i \widehat{L}^b_j \widehat{E}^c_k + \lambda'_{ijk}\widehat{L}^a_i \widehat{Q}^b_j \widehat{D}^c_k\right] + \lambda''_{ijk}\widehat{U}^c_i \widehat{D}^c_j \widehat{D}^c_k \tag{1.106}$$

The first three terms violate lepton number (L) and the fourth term violates baryon number (B) both by one unit. Although no baryon or lepton number violating processes have ever been found, these conservations are accidental in SM. This is a consequence of the fact that it is not possible to write any renormalizable term within the framework

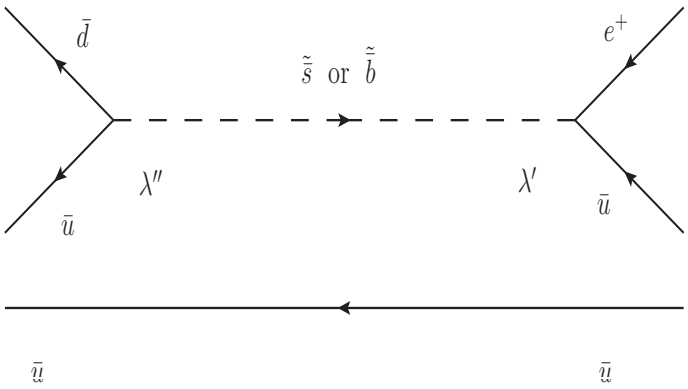

Figure 1.6: A sample diagram showing a typical proton decay ($p \to e^+\pi^0$) via squark exchange in R-parity violating SUSY scenario.

of the SM that violates B or L. However, if both B and L violating couplings were present simultaneously in the superpotential, the proton would no longer be stable and would decay, for example, via a squark exchange as shown in Fig. 1.6. Experimental evidence tells us that the proton lifetime is very large $\geq 10^{33}$ years [69]. Thus products of these couplings (e.g, λ'' and λ') which can lead to proton decay have to be extremely small, typically $\sim 10^{-20}$ [70].

A more natural way to deal with this problem is to add a new discrete symmetry to ensure that there are no B or L violating terms in the renormalizable MSSM superpotential. This new symmetry is called R-parity [71–73] and for a particle it is defined as

$$R_P = (-1)^{3(B-L)+2s}, \tag{1.107}$$

where, "s" is the spin of the corresponding particle. One could, in principle, just impose B and L conservations and thus discard all the terms in Eq. 1.106, but both these conservation laws are known to be violated by non-perturbative electroweak effects. Neither B or L can therefore be regarded as a fundamental symmetry. Instead, imposing R-parity conservation forbids terms like the ones in Eq. 1.106 while allowing all the interactions of the MSSM.

All the sleptons, squarks, gauginos and higgsinos carry $R_P = -1$ whereas all the SM particles and gauge bosons have $R_P = +1$. In R-parity conserving theory, there can be no mixing between $R_P = -1$ and $R_P = +1$ terms. Also, every interaction vertex in the theory must contain an even number of $R_P = -1$ particles. These properties have some very interesting phenomenological consequences:

- The SUSY partners can only be pair produced from the SM particles.

- All other superparticles eventually decay into a final state with the lightest supersymmetric particle (LSP) and the decay products must contain an odd number of LSP's.
- The LSP cannot further decay into any SM particles, making it absolutely stable. Additionally, if this LSP is electrically neutral and interacts weakly with ordinary matter, it can be a very good candidate for non-baryonic DM.

Since the LSP's are stable and can escape detection at the colliders, they give rise to missing energy signals for R-parity conserving SUSY scenarios. The missing energy is particularly high in R-parity conserving SUSY scenarios as the sparticles are always pair produced and their decay products consists of at least one LSP. This novel missing energy signature is being extensively searched for at the LHC as a probe for R-parity conserving SUSY models.

1.3 Neutrino Physics

If neutrinos are massive, their flavor changes while they propagate. As a consequence, a neutrino which is originally produced as electron neutrino can be detected as muon or tau neutrino. This oscillating effect explains the deficits found in solar and atmospheric neutrino experiments. Neutrinos are produced by charged current weak interactions as flavor eigenstates, $\nu_\alpha \equiv (\nu_e, \nu_\mu, \nu_\tau)$. The mass eigenbasis, $\nu_i \equiv (\nu_1, \nu_2, \nu_3)$ is related to the flavor eigenbasis by a unitary matrix:

$$|\nu_\alpha\rangle = U^*_{\alpha i}|\nu_i\rangle, \tag{1.108}$$

where U is known as Pontecorvo-Maki-Nakagawa-Sakata (PMNS) matrix and is given by:

$$U_{PMNS} = \begin{pmatrix} c_{12}c_{13} & s_{12}c_{13} & s_{13}e^{-i\delta} \\ -s_{12}c_{23} - c_{12}s_{23}s_{13}e^{i\delta} & c_{12}c_{23} - s_{12}s_{23}s_{13}e^{i\delta} & s_{23}c_{13} \\ s_{12}s_{23} - c_{12}c_{23}s_{13}e^{i\delta} & -c_{12}s_{23} - s_{12}c_{23}s_{13}e^{i\delta} & c_{23}c_{13} \end{pmatrix}. \tag{1.109}$$

Here $s_{ij} = \sin\theta_{ij}$, $c_{ij} = \cos\theta_{ij}$ and δ is the Dirac CP-violating phase. In case of Majorana neutrinos, two additional phases appear in the mixing matrix. Although the production mechanism of the neutrino is flavor diagonal, the quantum mechanical evolution is mass diagonal. One can compute the final state $|\nu_i(t)\rangle$ at time t starting from the initial state $|\nu_i(t_0)\rangle$ at time t_0,

$$|\nu_i(t)\rangle = e^{iE_i(t-t_0)}|\nu_i(t_0)\rangle, \tag{1.110}$$

where $E_i^2 = p^2 + m_i^2$. The probability of flavor eigenstate ν_α oscillating into ν_β is given by,

$$P(\nu_\alpha \to \nu_\beta) = \sum_{j,k=1}^{6} U^*_{\alpha k} U_{\beta k} U_{\alpha j} U^*_{\beta j} exp\left(-i\frac{\Delta m^2_{kj} L}{2E}\right), \tag{1.111}$$

where L is the oscillation length and $\Delta m^2_{kj} \equiv m^2_k - m^2_j$. Eq. 1.111 indicates that neutrino oscillation is not sensitive to the absolute masses of the neutrinos, but the mass square differences. Neutrino oscillation experiments over the years have found two mass square differences, Δm^2_{21}, responsible for solar neutrino oscillations, and $|\Delta m^2_{31}|$, responsible for atmospheric neutrino oscillations, the solar and atmospheric mixing angles θ_{12} and θ_{23} and the reactor angle θ_{13}. There is an ambiguity over the sign of Δm^2_{31}. Hence two types of neutrino mass spectrum are possible, namely normal hierarchy ($m_1 < m_2 < m_3$, $\Delta m^2_{31} > 0$) and inverted hierarchy ($m_3 < m_1 < m_2$, $\Delta m^2_{31} < 0$). For normal hierarchy, the best fit values along with their 3σ ranges [74] are provided in Table 1.3. Since the neutrino oscillation data are not sensitive to the

Parameter	Best Fit ($\pm 1\sigma$)	3σ Range
$\Delta m^2_{21}[10^{-5}$ eV$^2]$	$7.58^{+0.22}_{-0.26}$	6.99 - 8.18
$\lvert\Delta m^2_{31}\rvert[10^{-3}$ eV$^2]$	$2.35^{+0.12}_{-0.09}$	2.06 - 2.67
$\sin^2\theta_{12}$	$0.312^{+0.018}_{-0.015}$	0.265 - 0.364
$\sin^2\theta_{23}$	$0.42^{+0.08}_{-0.03}$	0.34 - 0.64
$\sin^2\theta_{13}$	$0.025^{+0.007}_{-0.008}$	0.005 - 0.050

Table 1.3: The best-fit values and 3σ allowed ranges of the 3-neutrino oscillation parameters, derived from a global fit of the current neutrino oscillation data including T2K [75] and MINOS [76].

absolute value of the neutrino masses, we cannot measure m_ν from these oscillation experiments. There are three main experimental sources to obtain information on the absolute scale of neutrino mass.

- *Tritium beta decay experiments*:
  As pointed out by Fermi theory, the shape of electron spectrum near the endpoint is highly sensitive to the scale of neutrino masses. Experimental setups at Mainz [77] and Troitsk [78] have applied this idea to study neutrino mass using tritium (^3H) as the decaying nucleus and hence source of the electron and a massive neutrino (m_i):

$$^3H \to ^3 He + e^- + \bar{\nu}. \tag{1.112}$$

These experiments measure an effective neutrino mass $m_\beta = \sqrt{\sum_{i=1}^{3} |U_{ei}|^2 m_i^2}$, where U is the PMNS matrix. The existing bound obtained from these experiments so far is:

$$m_\beta < 2.2 \text{ eV } (95\% \ c.l). \tag{1.113}$$

- *Neutrinoless double beta decay experiments*:
  Another way to determine the absolute scale of neutrino masses and the Majorana nature of the neutrinos is the search for neutrinoless double beta decay ($0\nu\beta\beta$). These are lepton number violating processes, like

$$N(A, Z) \to N(A, Z + 2) + e^{\pm} + e^{\mp}. \tag{1.114}$$

  These type of processes are possible only for Majorana nature of the neutrinos. The decay rate is proportional to m_ν^2 and is suppressed by several orders of magnitude from the $2\nu\beta\beta$ decay mode. These two decay modes can be differentiated from the energy spectrum of the electrons. In $0\nu\beta\beta$ mode, the electrons are expected to be more energetic as there are no energy loss due to the final state neutrinos. These experiments can measure

$$m_{\beta\beta} = \sum_{i=1}^{3} U_{ei}^2 m_i. \tag{1.115}$$

  Heidelberg-Moscow experiment [79] provided the most stringent bound on the half-life of ^{76}Ge so far:

$$T_{1/2}^{0\nu}(^{76}Ge) > 1.9 \times 10^{25} y \ (90\% \ c.l). \tag{1.116}$$

  IGEX experiment [80] on the other hand obtained a similar lower bound:

$$T_{1/2}^{0\nu}(^{76}Ge) > 1.57 \times 10^{25} y \ (90\% \ c.l). \tag{1.117}$$

  The future experiments GERDA [81], CUORE [82] and EXO [83] with increased sensitivities are expected to probe further. The bound on $m_{\beta\beta}$ does have large error due to the uncertainties involved in calculating the nuclear matrix elements [85]. However, the detection of $0\nu\beta\beta$ will confirm the existence of a new type of particle, a Majorana particle even if the effective neutrino mass cannot be measured with high accuracy.

  Applying Heidelberg-Moscow collaboration results and taking into account the uncertainties, one obtains

$$m_{\beta\beta} \lesssim 0.2 - 0.6 \text{ eV}. \tag{1.118}$$

- *Cosmological observations*:
  The most stringent constraint on the neutrino masses come from cosmological observations. If the neutrinos are really massive and the masses are of eV order, they would constitute a hot DM component. This type of DM reduces structure formation at small scales ($\sim$ 1 - 10 Mpc). Hence by studying density fluctuations in the CMB and the large scale structure distributions of galaxies, the experimentalists put a strong bound [84] on the sum of neutrino masses

$$\sum_{i=1}^{3} m_i \lesssim 0.3 - 1.0 \text{ eV}. \tag{1.119}$$

1.3.1 Neutrino mass

As already discussed, the neutrinos in the SM remain massless due to the absence of right-handed neutrinos. The neutrino masses can be either Dirac or Majorana type.

- *Dirac mass*:
  One can just add right-handed neutrinos, singlet under SM gauge groups, to write the corresponding Yukawa term $Y_\nu H L \nu_R$ leading to a neutrino mass, $m_D = Y_\nu \langle H \rangle$ after EWSB as in the cases of other SM fermions. Then it is evident that, for a 174 GeV Higgs vev, to achieve a sub-eV neutrino mass, Y_ν must be of the order of 10^{-11}. Since the right-handed neutrinos are gauge singlets, they do not have any gauge interactions and couple to the rest of the particles through the Yukawa coupling. Hence their interactions are highly suppressed making this scenario phenomenologically uninteresting.

- *Majorana mass*:
  Charge conjugation of a field is defined as

$$\widehat{C} : \psi \to \psi^c = C\bar{\psi}^T \tag{1.120}$$

  where $\widehat{C}$ is the charge-conjugation operator. The particles for whom $\psi = \psi^c$ are known as the Majorana particles. Then the corresponding mass term can be written as:

$$-\mathcal{L}_m = \frac{1}{2}\left[\psi_L^T C M \psi_L + h.c\right]. \tag{1.121}$$

  Here $\psi = (\psi_1, ..., \psi_n)^T$ is a vector in flavor space and M is a $n \times n$ matrix. A Majorana mass term breaks not only the family lepton number but the total lepton number as well. Note that, due to the anti-commutation properties of the fermionic fields, the matrix M is symmetric.

Kinematically, the Dirac and Majorana mass terms are indistinguishable. However, a Majorana mass term is the reason $0\nu\beta\beta$ has a non-vanishing amplitude, but the source of this mass term also remains to be explained. An important difference between the Dirac and Majorana neutrino mass terms is that the Dirac mass terms remain invariant under $U(1)$ transformations, but the Majorana mass terms do not. It breaks all the charges that the field (ψ) has by two units. Thus if electric charge is exactly conserved, there cannot be any charged particles with Majorana mass. Therefore, among all the fermions only neutrinos can be Majorana particles.

Higher dimensional operators:

One can incorporate a relevant mass term by adding a dimension five operator, known as the Weinberg operator [86] to the Lagrangian

$$W = \frac{1}{\Lambda} L_i L_j H H, \tag{1.122}$$

where $L_{i,j}$ are the SM doublets and H is the standard Higgs doublet. Λ is a mass scale where the operator is generated. This term breaks the lepton number by two units just as in the case of a Majorana mass term. After EWSB, the Higgs fields gets vev and W reduces to a Majorana mass term. A pictorial representation of generation of this mass term is shown in Fig. 1.7 The Weinberg operator points to the fact that lepton number

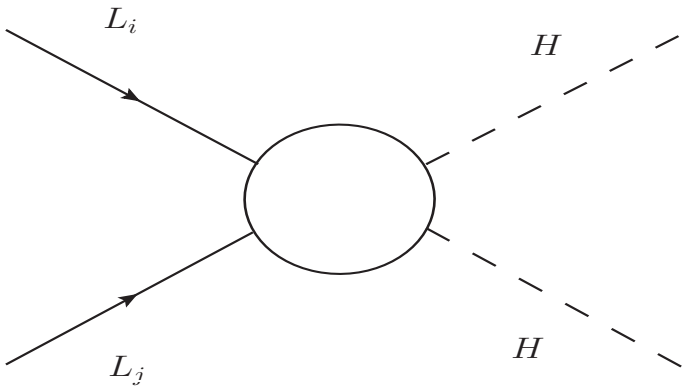

Figure 1.7: Weinberg dimension five operator responsible for generating neutrino masses.

conservation is rather accidental since non-renormalizable operators like this violate it. Different realizations of this dimension five operator are possible as we discuss below.

Seesaw mechanism:

The most popular way of realization of this effective theory is the seesaw mechanism. In the simplemost seesaw theory one additional SM fermionic singlet (N_R) is added

to the SM particle content for each generation. Then the two terms relevant to the neutrino masses that are added to the Lagrangian looks like

$$\mathcal{L}_\nu = \frac{1}{2}\sum_{i=1}^{3} M_{N_i}\bar{N}^c_{R_i}N_{R_i} + \sum_{i,j=1}^{3} Y_{\nu_{ij}}H\bar{L}_i N_{R_j} + h.c. \tag{1.123}$$

Here M_N is the Majorana mass term of the right-handed heavy neutrino field and Y_ν is the Yukawa parameter that controls the left-right mixing between the neutrino states. After EWSB, the Higgs field acquires a vev(v) and subsequently the Yukawa term gives rise to a Dirac mass term ($m_D \equiv Y_\nu \times v$) for the neutrinos. In the basis (ν_L, N^c_R) the neutrino mass matrix looks like

$$m_\nu = \begin{pmatrix} 0 & m_D \\ m_D^T & M_N \end{pmatrix}. \tag{1.124}$$

Using

$$Tr(m_\nu) = M_N \quad \text{and} \quad |Det(m_\nu)| = m_D^T m_D, \tag{1.125}$$

and under the approximation, $M_N >> m_D$, we get the eigenvalues of m_ν:

$$m_{\nu_1} \simeq \frac{m_D^T m_D}{M_N}, \quad m_{\nu_2} \simeq M_N. \tag{1.126}$$

Now, as a result of its mixing with the heavy singlet state, the massless neutrino has a non-zero mass. Smallness of this mass depends either on the smallness of the Yukawa parameter or the largeness of the seesaw scale, M_N. which is equivalent to Λ appearing in Eq. 1.122. This mechanism is known as type I seesaw mechanism [87–91]. There are other types of seesaw mechanisms as well.

Another way to write the Weinberg operator (Eq. 1.122) is

$$\frac{1}{M}(L^T\vec{\tau}L)(H^T\vec{\tau}H), \tag{1.127}$$

where τ^i's are the usual Pauli matrices. This can be incorporated in the theory by adding an $SU(2)_L$ bosonic triplet $\vec{\Delta} \equiv (\Delta^{++}, \Delta^{+}, \Delta^{0})$ which couple to SM leptons. This is known as type II seesaw mechanism [92–95]. In this case the scale (Λ) appearing in Weinberg operator is

$$\frac{1}{\Lambda} = \frac{f\mu}{M^2}, \tag{1.128}$$

where, the $LL\Delta$ and $HH\Delta$ couplings are denoted by f and μ respectively and M is the mass of the triplet, Δ. Similar to the previous case, when the Higgs field gets vev, neutrinos get masses

$$m_\nu = \frac{f\mu v^2}{M^2}. \tag{1.129}$$

Type III seesaw mechanism [96] introduces a fermionic $SU(2)_L$ triplet Σ with hypercharge, $Y = 0$. If three families of Σ is added to the SM particle content, the additional terms in the Lagrangian reads:

$$-\mathcal{L}_\Sigma = Y_\Sigma H L \Sigma + \frac{1}{2}\Sigma M_\Sigma \Sigma + h.c. \tag{1.130}$$

Here Y_Σ and M_Σ are 3×3 matrices. The neutrino mass now reads

$$m_\nu = \frac{Y_\Sigma^2 v^2}{2M_\sigma}. \tag{1.131}$$

The neutrino mass expression is similar to the one obtained for type I seesaw case.

R-parity violating SUSY scenario:

Just like the SM, R-parity conserving SUSY, on its own is not sufficient to provide non-zero masses to neutrinos. R-parity violating SUSY models are, however, capable of explaining neutrino oscillation data. If R-parity is violated, there is no conserved quantum number that can distinguish between a down-type Higgs doublet and a lepton doublet. These fields in general mix to generate neutrino mass terms. One neutrino obtains its mass at tree level depending upon the mixing between the Higgs and the sneutrinos [97–108]. The other two neutrinos become massive at one loop level and those masses are smaller compared to the tree level neutrino mass due to a suppression by the loop factor.

Bilinear R-parity violation is the minimal extension of the MSSM that incorporates lepton number violation. It is represented by the term $\mu_i L_i H_2$ in Eq. 1.106. As a result, we get a 7×7 neutralino-neutrino mass matrix, which after diagonalization gives mass to one of the massless neutrinos. This tree level contribution generates the atmospheric neutrino mass scale, whereas, in order to generate the solar neutrino mass scale one needs to consider the additional corrections coming from bottom-sbottom, tau-stau and neutralino-sneutrino one loop contributions [97–111].

Apart from the bilinear term, a general RPV superpotential also consists of lepton number violating λ and λ' terms. These terms give rise to nonzero neutrino masses at one loop level via lepton-slepton or quark-squark loops [107]. These contributions are suppressed by square of the λ and λ' couplings and square of charged lepton or down type quark masses apart from the loop suppression factor. Thus these contributions are usually very small.

One very important feature of R-parity violating neutrino mass models is their accessibility at the present colliders. The phenomenological aspects of this neutrino mass generation mechanism have been studied extensively in the literature [112–119].

1.4 Dark Matter

Fritz Zwicky postulated the existence of a non-luminous matter from his observation that the velocities of galaxies in the Coma cluster far exceeded the velocities expected based on the gravitational potential of only the luminous matter [120]. Over the years several other studies have pointed towards the existence of the Dark Matter (DM), e.g, rotation curves of galaxies [121], gravitational lensing [122] and temperature fluctuations of the cosmic microwave background (CMB) [18]. The current relic abundance of the DM is measured as the ratio of its density and the critical matter density required for the closure of the universe

$$\Omega_{DM} = \frac{\rho_{DM}}{\rho_c}. \tag{1.132}$$

ρ_c can be written in terms of Hubble expansion rate (H) and Newton's gravitational constant (G_N)

$$\rho_c = \frac{3H^2}{8\pi G_N}. \tag{1.133}$$

A scaling parameter h is used to write: $H = 100h$ km/s/Mpc, where 1 pc=3.2615 light year= 3.0856×10^{18} cm and accordingly, h takes the value 0.705 ± 0.013. The DM can be "hot", "warm" or "cold". Hot dark matter is composed of particles that have zero or very small non-zero mass (e.g, neutrinos). The Special Theory of Relativity requires that nearly massless particles move at nearly the speed of light. Such high velocities of "hot" dark matter cause it to wipe out structure on small scales and thus this particular kind of DM is disfavored from the structure formation arguments. "Cold" dark matter (CDM) particles on the other hand, are massive and move slowly compared to the speed of light and interact very weakly with the visible matter. "Warm" DM has properties intermediate between that of "hot" and "cold" DM candidates and its mass can be of the keV range. Cold DM can provide the most dominant contribution to the DM relic density and is composed of non-baryonic and non relativistic particle. Ordinary baryonic matter density is smaller than Ω_{CDM} by one order of magnitude. For this thesis, we shall only concentrate on the cold DM. The most recent measurement of the cold DM relic abundance (Ω_{CDM}) is provided by PLANCK experiment [15]:

$$\Omega_{CDM}h^2 = 0.1199 \pm 0.0027. \tag{1.134}$$

Among several candidates for a cold DM, the most popular are the axions [123] and weakly interacting massive particles (WIMPs). The properties of a WIMP can be probed through its scattering against different target nuclei [124] as well as through its

annihilation into different possible final states [125]. In the subsequent subsections we shall discuss about the WIMP relic density calculation , different detection techniques opted by the DM detection experiments and how their results affect the choice of DM candidates in SUSY theories.

1.4.1 Relic Density

A weakly interacting stable particle provides the correct order of magnitude of the relic density if we assume the universe to be in thermal equilibrium at the time the DM decouples from the thermal bath. This is called the "WIMP miracle". The evolution of WIMP (χ) number density (n_χ) in the thermal bath of the early universe obeys the Boltzman equation:

$$\frac{dn_\chi}{dt} + 3Hn_\chi = - < \sigma_A|v| > (n_\chi^2 - n_{eq}^2), \tag{1.135}$$

where the factor $< \sigma_A|v| >$ is called the thermal averaged annihilation cross-section of the DM and n_{eq} is the equilibrium number density. v is the relative velocity between the annihilating DM particles measured in center of mass frame. In case of an exact thermal equilibrium, the forward and backward processes of WIMP annihilation and creation are same, but as the universe cools down with the decrease of temperature, the annihilation rate surpasses creation rate. Now if the thermal equilibrium was to be maintained, n_χ would fall exponentially. However, the WMAP and subsequent measurement of relic density predicts a much larger value. These results can only be explained if the equilibrium is broken at some point of time during the evolution. The annihilation rate (Γ_{ann}) is given by

$$\Gamma_{ann} =< \sigma_A|v| > n_\chi. \tag{1.136}$$

The deviation from equilibrium occurs when $\Gamma_{ann}(T_f) \approx H(T_f)$. This scenario is known as the "freeze-out". Using this freeze-out condition one can solve for the freeze-out temperature (T_f). For weak scale inputs,

$$T_f \approx m_\chi/20. \tag{1.137}$$

Using T_f one can also find the comoving number density at freeze-out. The Hubble constant can be written as

$$H = 1.66 g_*^{1/2} T^2/m_{Planck}, \tag{1.138}$$

where T denotes temperature and g_* counts the number of relativistic degrees of freedom. The ratio of the comoving number density to entropy can be assumed to be

constant as the universe cools. Then using entropy as a function of temperature, $s \approx 0.4 g_* T^3$, we can write

$$\left(\frac{n_\chi}{s}\right)_{present} = \left(\frac{n_\chi}{s}\right)_{freeze-out} \approx \frac{10^2}{m_\chi m_{Planck} g_*^{1/2} < \sigma_A v >}. \tag{1.139}$$

The present DM number density can be converted to units of the critical density, $\rho_c = 10^{-5} h^2$ GeVcm^{-3} using the entropy at present, $s \approx 4000$ cm^{-3}

$$\Omega_{DM} h^2 = \frac{m_\chi n_\chi}{\rho_c} \approx 0.1 \left(\frac{3 \times 10^{-26} \text{ cm}^3/\text{s}}{< \sigma_A |v_f| >}\right), \tag{1.140}$$

where, $v_f = 1/\sqrt{20}$. Hence the WIMP relic density is independent of its mass and is inversely proportional to its annihilation cross-section. Thus requiring a relic density also constrains the value of its annihilation cross-section.

1.4.2 Detection of the DM

The DM detection techniques can be broadly divided into two categories, namely, direct and indirect detection.

Direct Detection:

The idea behind direct detection technique is a very simple one. If the galaxy has certain abundance of WIMPs, they must be passing through the Earth. Hence studying the interaction of such particles with matter, e.g, studying the recoil energy of the target nuclei, can reveal a lot about the WIMP properties [126]. The detectors are buried deep underground to eliminate backgrounds coming from cosmic rays. The most important factors for the calculation of the signal in direct detection experiments are the density and the velocity distribution of WIMPs in the solar neighborhood and the WIMP-nucleon scattering cross-section. Using these information one can calculate the rate of WIMP-nucleon scattering events expected in an experiment per unit time, per unit detector material mass.
The scattering rate is approximately given by [127]

$$R \approx \sum_i N_i n_\chi < \sigma_{i\chi} >, \tag{1.141}$$

where i runs over the nuclei species present in the detector and N_i is the number of target nuclei in the detector, n_χ is the local WIMP density and $< \sigma_{i\chi} >$ is the WIMP nuclei scattering cross-section averaged over the relative WIMP velocity with respect to the detector. Scintillators like NaI, semi-conductors like Ge and noble liquids like Xe are typically used as detector materials.

The scattering processes can be divided into two classes; elastic and inelastic scattering. The elastic scattering involves the interaction of the WIMP with a target nuclei as a whole making the nucleus to recoil. This recoil energy is then measured to obtain an energy spectrum that reveals various WIMP properties. Current experiments can detect recoils of considerable lower energy, as low as 1-10 keV. Inelastic scattering on the other hand involves WIMP interaction with the orbital electrons in the target. As a result, the electrons are either excited or target is ionized. Also the WIMP can interact with the nuclei putting it in an excited state. This process involves both recoil of the nuclei and emission of a photon immediately afterwards [128]. However, such signatures have large background coming from natural radioactivity.

The elastic scattering can be divided into two categories, namely spin-dependent and spin-independent scattering depending on their classes of couplings. The spin-dependent axial-vector interactions result in a scattering cross-section proportional to $J(J+1)$, where J is the total angular momentum of the particle, rather than the number of nucleons. For spin independent scalar scattering, the cross-section increases with the square of the nuclear atomic number. Hence heavier target nuclei are favored while searching for spin-independent scattering. For sufficiently heavy target nuclei, this cross-section dominates over the spin-dependent one. As a result, bounds on DM obtained coming from spin-independent scattering are more severe than that coming from spin-dependent scattering.

LUX [129] experiment provides the strongest bound so far from direct detection searches. Other direct detection experiments include CDMS [130], XENON [131, 132], ZEPLIN [133], EDELWEISS [134], CRESST [135], CoGeNT [136], DAMA [137], etc. Future run of LUX [138] and XENON1T [139] are expected to improve the results by several orders of magnitude in the next few years.

Indirect Detection:

Indirect search of DM involves study of the final state particles produced in DM annihilations. Since the annihilation rate of WIMP is proportional to the square of the DM density, the searches are carried out close to the places that are expected to have large WIMP density, e.g, sun, earth and the galactic center. The annihilation products searched for include gamma-rays, neutrinos and anti-matter.

The most likely source of gamma-rays coming from WIMP annihilation is the galactic center. The WIMP pair annihilation can produce charged fermions in the final state which then can radiate gamma-rays. Also the quarks in the final state go through hadronization and in the process neutral pions are created. These pions can then decay into pairs of gamma-rays. A large number of photons with varying energies are

created in this process giving rise to a continuous spectrum. Alternatively, a pair of WIMPs can directly produce a pair of photons via some loop induced processes and thus producing a monochromatic photon energy spectrum. This production rate is usually small because of loop suppression, but since the energy of these photons depend on the WIMP mass, for its large value the generated photons will be highly energetic. If detected, these photons can provide an obvious proof for the existence of DM. The continuum γ-ray flux is typically 2-3 orders of magnitude higher than that of monochromatic γ-rays. Recently, an excess in photon energy spectrum was observed at low energy close to the galactic center [140] by the Fermi Large Area Telescope (Fermi-LAT). Photons originated from DM annihilation can explain the situation perfectly well [141]. With improved sensitivity in the ongoing experiments, a discovery may just be around the corner.

Neutrinos can also be an important probe for the WIMPs. The WIMPs slowly gather at the centers of large gravitating bodies until the capture rate and the annihilation rate come into an equilibrium. Sun is a close enough object where these rates are at equilibrium which produces a steady flow of neutrinos generated from the WIMP annihilation. Neutrinos being very weakly interacting, escape the sun unlike most of the other particles. Neutrino telescopes focus on this neutrino flux coming out of the sun. Depending upon the WIMP mass and its composition it decays into different final states involving charged fermions and gauge bosons which then decay into neutrinos among other products. The differential neutrino flux from WIMP annihilation is given by

$$\frac{dN_\nu}{dE_\nu} = \frac{\Gamma_A}{4\pi D^2} \sum_f B_X^f \frac{dN_\nu^f}{dE_\nu}, \tag{1.142}$$

where, Γ_A is the annihilation rate of WIMP, D is the distance of the detector from the source, f is the WIMP pair annihilation final states and B_X^f are the branching ratios of the final state. dN_ν^f/dE_ν are the energy distributions of neutrinos generated by the final state, f. This detection, then heavily depends on the WIMP mass, the annihilation rate and WIMP density within the sun. Among several DM experiments AMANDA [142], Super-Kamiokande [143] and IceCube [144] are looking for this sort of DM signal.

Pair annihilation of DM is expected to produce equal number of particles and anti-particles. The products of these DM annihilations in the galaxies would therefore give rise to an anti-particle signal in cosmic rays which is relatively rare, making it an excellent signal for DM detection. The quarks produced through WIMP annihilation undergo harmonizations to produce anti-protons. Positrons can be created as secondary products coming from final state gauge bosons. Unlike γ-rays and neutri-

nos, these particles are charged and therefore are affected by electromagnetic fields and lose energy due to radiation. Experimentalists therefore study the flux of anti-particles from the galactic halo as a whole. An excess in positron flux was first observed by the HEAT [145] and AMS [146] experiments and was confirmed afterwards by PAMELA [147, 148]. The Fermi-LAT also observed excess in cosmic ray electron and positron flux over the expected background. If interpreted as a DM signal, this observation puts severe constraints on annihilation channels. A sharp rise in the positron fraction indicates a hard lepton spectrum [149,150], while the lack of anti-proton excess strongly constrains hadronic annihilation modes of the DM [151]. However, one requires further data to determine the fact that these kind of excesses are really originated from DM annihilation or they are coming from some astrophysical sources unknown to us so far.

1.4.3 DM candidates

Many extensions of the SM indeed require the introduction of new particles, some of which could be DM candidates. Perhaps the most popular candidate for particle DM is the lightest supersymmetric particle (LSP) in R-parity conserving supersymmetric (SUSY) models [127, 152]. In the Minimal Supersymmetric extension of the SM (MSSM), the lightest neutralino is the usual DM candidate, as the other viable candidate, namely the scalar superpartner of the left-handed (LH) neutrino, is strongly disfavored by a combination of relic density, direct detection and invisible decay width of the SM Z-boson constraints [153]. More specifically, the unsuppressed coupling of the LH sneutrino to the SM Z-boson leads to a large cross-section for elastic scattering with the target nuclei in direct detection devices [154]; such cross-sections are already ruled out experimentally over almost the entire viable mass range [132]. By the same argument, their large Z-coupling leads to far too rapid annihilation for the LH sneutrinos and too small a relic density compared to the WMAP-measured value [18]. One could make them very light (of order GeV) [155] in order to suppress the annihilation rate as well as to evade the direct detection bounds due to the limited sensitivity of the experiments at low masses. However, a very light sneutrino is excluded by the measurement of the Z invisible decay width at LEP [156].

Recent data from three DM direct detection experiments, namely DAMA [137], CoGeNT [136] and CRESST [135] have suggested the hints of a light DM with mass in the 10-100 GeV range and cross section in the range $10^{-3} - 10^{-6}$ pb for elastic scattering off nucleons. Though there is no unanimity among these results and several other experiments [130,132–134,157,158] do not see any such positive hints of a DM, it has certainly generated considerable curiosity in a light DM scenario which can explain

some/all of these hints of positive detection while being consistent with the null results from other direct detection experiments [159]. Therefore, it may not be premature to examine some beyond SM scenarios accommodating a light DM candidate in case any of these positive hints are confirmed in near future. However, neither of the most recent searches by XENON [131] and LUX [138] direct detection experiments has found any evidence of a light DM and as a result, put stringent constraint on the direct detection cross-section.

If we assume gaugino mass unification in pure MSSM, the LEP searches on SUSY put a lower bound on the lightest neutralino mass around 50 GeV [63], and the recent LHC data push this bound to more than about 200 GeV [160]. Even if we do not assume gaugino mass unification, one could derive a lower limit on the neutralino LSP mass of ~ 20 GeV [161] just requiring the observed DM relic density, together with the LEP constraints on chargino and slepton masses. Therefore, if the DM indeed turns out to be very light as suggested by some of the recent experiments [135–137], we need to go beyond the universal MSSM scenario. Since MSSM anyway cannot be a complete theory and needs to be extended to accommodate the observed small neutrino masses, it would be interesting to see if these extensions can also provide a viable light DM candidate while satisfying both collider and relic density constraints as well as other low-energy constraints in the leptonic sector.

In the next chapter, we discuss one such extension of the MSSM to accommodate neutrino oscillation data. We consider a special kind of seesaw scenario in the MSSM framework and call it supersymmetric inverse seesaw model. We take into account both the minimal and general extension of MSSM to accommodate inverse seesaw. Our aim is to see if we can find a light DM candidate in this R-parity conserving model consistent with all the DM and collider experimental bounds. In the subsequent chapters we explore the feasibility of collider search of this model in different lepton and/or jet associated missing energy channels.

Bibliography

[1] E. S. Abers and B. W. Lee, Phys. Rept. **9**, 1 (1973) .

[2] M. A. B. Beg and A. Sirlin, Phys. Rept. **88**, 1 (1982).

[3] D. J. Gross and F. Wilczek, Phys. Rev. Lett. **30**, 1343 (1973).

[4] H. D. Politzer, Phys. Rev. Lett. **30**, 1346 (1973).

[5] S. L. Glashow, Nucl. Phys. **22**, 579 (1961).

[6] S. Weinberg, Phys. Rev. Lett. **19**, 1264 (1967).

[7] G. Aad *et al.* [ATLAS Collaboration], Phys. Lett. B **716**, 1 (2012) [arXiv:1207.7214 [hep-ex]].

[8] S. Chatrchyan *et al.* [CMS Collaboration], Phys. Lett. B **716**, 30 (2012) [arXiv:1207.7235 [hep-ex]].

[9] V. Khachatryan *et al.* [CMS Collaboration], arXiv:1407.0558 [hep-ex].

[10] G. Aad *et al.* [ATLAS Collaboration], arXiv:1408.7084 [hep-ex].

[11] S. Weinberg, Phys. Rev. D **19**, 1277 (1979).

[12] L. Susskind, Phys. Rev. D **20**, 2619 (1979).

[13] T. Schwetz, M. A. Tortola and J. W. F. Valle, New J. Phys. **10**, 113011 (2008) [arXiv:0808.2016 [hep-ph]].

[14] M. C. Gonzalez-Garcia, M. Maltoni and J. Salvado, JHEP **1004**, 056 (2010) [arXiv:1001.4524 [hep-ph]].

[15] P. A. R. Ade *et al.* [Planck Collaboration], arXiv:1303.5076 [astro-ph.CO].

[16] D. H. Weinberg, M. J. Mortonson, D. J. Eisenstein, C. Hirata, A. G. Riess and E. Rozo, [arXiv:1201.2434 [astro-ph.CO]].

[17] P. A. R. Ade *et al.* [Planck Collaboration], arXiv:1303.5062 [astro-ph.CO].

[18] E. Komatsu *et al.* [WMAP Collaboration], Astrophys. J. Suppl. **192**, 18 (2011) [arXiv:1001.4538 [astro-ph.CO]].

[19] S. Weinberg, Rev. Mod. Phys. 61, 1 (1989).

[20] A. G. Cohen, D. B. Kaplan and A. E. Nelson, Ann. Rev. Nucl. Part. Sci. **43**, 27 (1993) [hep-ph/9302210]; A. Riotto and M. Trodden, Ann. Rev. Nucl. Part. Sci. **49**, 35 (1999) [hep-ph/9901362]; M. Dine and A. Kusenko, Rev. Mod. Phys. **76**, 1 (2003) [hep-ph/0303065]; J. M. Cline, hep-ph/0609145.

[21] K. Hagiwara, A. D. Martin, D. Nomura and T. Teubner, Phys. Rev. D **69**, 093003 (2004) [hep-ph/0312250].

[22] T. Aaltonen *et al.* [CDF Collaboration], Phys. Rev. D **83**, 112003 (2011) [arXiv:1101.0034 [hep-ex]].

[23] P. Ramond, Phys. Rev. D **3**, 2415 (1971).

[24] J. Wess and B. Zumino, Nucl. Phys. B **70**, 39 (1974).

[25] J. Wess and B. Zumino, Phys. Lett. B **49**, 52 (1974).

[26] S. Ferrara, J. Wess and B. Zumino, Phys. Lett. B **51**, 239 (1974).

[27] J. Wess and J. Bagger Supersymmetry and Supergravity, Princeton University Press, 1983 (World Scientific).

[28] H. E. Haber and G. L. Kane, Phys. Rept. **117**, 75 (1985).

[29] M. Drees, hep-ph/9611409.

[30] M. Dine, hep-ph/9612389.

[31] D. I. Kazakov, hep-ph/0012288.

[32] A. Bilal, hep-th/0101055.

[33] M. Drees, R. Godbole and P. Roy, Hackensack, USA: World Scientific (2004) 555 p; H. Baer and X. Tata, Cambridge, UK: Univ. Pr. (2006) 537 p

[34] I. Simonsen, hep-ph/9506369.

[35] S. P. Martin, "A Supersymmetry primer," [hep-ph/9709356].

[36] I. J. R. Aitchison, hep-ph/0505105.

[37] S. J. Gates, M. T. Grisaru, M. Rocek and W. Siegel, hep-th/0108200.

[38] F. A. Berezin, Pure Appl. Phys. **24**, 1 (1966).

[39] L. O'Raifeartaigh, Nucl. Phys. B **96**, 331 (1975).

[40] P. Fayet and J. Iliopoulos, Phys. Lett. B **51**, 461 (1974).

[41] P. Fayet, Nuovo Cim. A **31**, 626 (1976).

[42] S. Ferrara, L. Girardello and F. Palumbo, Phys. Rev. D **20**, 403 (1979).

[43] L. J. Hall, J. D. Lykken and S. Weinberg, Phys. Rev. D **27**, 2359 (1983); S. K. Soni and H. A. Weldon, Phys. Lett. B **126**, 215 (1983); I. Affleck, M. Dine and N. Seiberg, Nucl. Phys. B **256**, 557 (1985).

[44] H. P. Nilles, Phys. Lett. B **115**, 193 (1982); A. H. Chamseddine, R. L. Arnowitt and P. Nath, Phys. Rev. Lett. **49**, 970 (1982); P. Nath, R. L. Arnowitt and A. H. Chamseddine, Nucl. Phys. B **227**, 121 (1983); R. Barbieri, S. Ferrara and C. A. Savoy, Phys. Lett. B **119**, 343 (1982); E. Cremmer, P. Fayet and L. Girardello, Phys. Lett. B **122**, 41 (1983); L. E. Ibanez, Phys. Lett. B **118**, 73 (1982); H. P. Nilles, M. Srednicki and D. Wyler, Phys. Lett. B **120**, 346 (1983).

[45] M. Dine and A. E. Nelson, Phys. Rev. D **48**, 1277 (1993) [hep-ph/9303230]; M. Dine, A. E. Nelson and Y. Shirman, Phys. Rev. D **51**, 1362 (1995) [hep-ph/9408384]; M. Dine, A. E. Nelson, Y. Nir and Y. Shirman, Phys. Rev. D **53**, 2658 (1996) [hep-ph/9507378].

[46] L. Randall and R. Sundrum, Nucl. Phys. B **557**, 79 (1999) [hep-th/9810155]; G. F. Giudice, M. A. Luty, H. Murayama and R. Rattazzi, JHEP **9812**, 027 (1998) [hep-ph/9810442].

[47] D. E. Kaplan, G. D. Kribs and M. Schmaltz, Phys. Rev. D **62**, 035010 (2000) [hep-ph/9911293]; Z. Chacko, M. A. Luty, A. E. Nelson and E. Ponton, JHEP **0001**, 003 (2000) [hep-ph/9911323].

[48] K. A. Intriligator and N. Seiberg, Class. Quant. Grav. **24**, S741 (2007) [hep-ph/0702069].

[49] S. L. Adler and W. A. Bardeen, Phys. Rev. **182**, 1517 (1969).

[50] P. Fayet, Nucl. Phys. B **90**, 104 (1975); Phys. Lett. B **64**, 159 (1976); Phys. Lett. B **69**, 489 (1977); Phys. Lett. B **84**, 416 (1979).

[51] L. Alvarez-Gaume and E. Witten, Nucl. Phys. B **234**, 269 (1984).

[52] A. Djouadi, Phys. Rept. **459**, 1 (2008) [hep-ph/0503173].

[53] S. Dimopoulos and H. Georgi, Nucl. Phys. B **193**, 150 (1981).

[54] N. Sakai, Z. Phys. C **11**, 153 (1981).

[55] L. Girardello and M. T. Grisaru, Nucl. Phys. B **194**, 65 (1982).

[56] L. J. Hall and L. Randall, Phys. Rev. Lett. **65**, 2939 (1990).

[57] D. J. H. Chung, L. L. Everett, G. L. Kane, S. F. King, J. D. Lykken and L. -T. Wang, Phys. Rept. **407**, 1 (2005) [hep-ph/0312378].

[58] J. A. Casas, J. R. Espinosa, M. Quiros and A. Riotto, Nucl. Phys. B **436**, 3 (1995) [Erratum-ibid. B **439**, 466 (1995)] [hep-ph/9407389].

[59] J. A. Casas, J. R. Espinosa and M. Quiros, Phys. Lett. B **342**, 171 (1995) [hep-ph/9409458].

[60] J. F. Gunion, H. E. Haber, G. L. Kane and S. Dawson, Front. Phys. **80**, 1 (2000); hep-ph/9302272.

[61] J. F. Gunion and H. E. Haber, Nucl. Phys. B **272**, 1 (1986) [Erratum-ibid. B **402**, 567 (1993)].

[62] R. Barate *et al.* [LEP Working Group for Higgs boson searches and ALEPH and DELPHI and L3 and OPAL Collaborations], Phys. Lett. B **565**, 61 (2003) [hep-ex/0306033].

[63] Nakamura K et al. (Particle Data Group) 2010 J. Phys. G37 075021.

[64] H. E. Haber and R. Hempfling, Phys. Rev. Lett. **66**, 1815 (1991).

[65] Y. Okada, M. Yamaguchi and T. Yanagida, Prog. Theor. Phys. **85**, 1 (1991); Phys. Lett. B **262**, 54 (1991).

[66] J. R. Ellis, G. Ridolfi and F. Zwirner, Phys. Lett. B **257**, 83 (1991); Phys. Lett. B **262**, 477 (1991).

[67] J. R. Espinosa and M. Quiros, Phys. Lett. B **266**, 389 (1991).

[68] J. F. Gunion and H. E. Haber, Nucl. Phys. B **278**, 449 (1986); Nucl. Phys. B **307**, 445 (1988); hep-ph/9301205.

[69] Super-K: Y. Hayato et al. [Super-Kamiokande Collaboration], Phys. Rev. Lett. **83**, 1529 (1999); [arXiv:hep-ex/9904020].

[70] G. Bhattacharyya, arXiv:hep-ph/9709395.

[71] G. R. Farrar and P. Fayet, Phys. Lett. B **76**, 575 (1978).

[72] N. Sakai and T. Yanagida, Nucl. Phys. B **197**, 533 (1982).

[73] S. Dimopoulos, S. Raby and F. Wilczek, Phys. Lett. B **112**, 133 (1982).

[74] D. V. Forero, M. Tortola and J. W. F. Valle, Phys. Rev. D **86**, 073012 (2012) [arXiv:1205.4018 [hep-ph]].

[75] K. Abe *et al.* [T2K Collaboration], Phys. Rev. Lett. **107**, 041801 (2011) [arXiv:1106.2822 [hep-ex]].

[76] P. Adamson *et al.* [MINOS Collaboration], Phys. Rev. Lett. **101**, 131802 (2008) [arXiv:0806.2237 [hep-ex]]; P. Adamson *et al.* [MINOS Collaboration], Phys. Rev. Lett. **106**, 181801 (2011) [arXiv:1103.0340 [hep-ex]].

[77] H. Barth, L. Bornschein, B. Degen, L. Fleischmann, M. Przyrembel, H. Backe, A. Bleile and J. Bonn *et al.*, Prog. Part. Nucl. Phys. **40**, 353 (1998).

[78] V. M. Lobashev, V. N. Aseev, A. I. Belesev, A. I. Berlev, E. V. Geraskin, A. A. Golubev, O. V. Kazachenko and Y. .E. Kuznetsov *et al.*, Phys. Lett. B **460**, 227 (1999).

[79] H. V. Klapdor-Kleingrothaus, A. Dietz, L. Baudis, G. Heusser, I. V. Krivosheina, S. Kolb, B. Majorovits and H. Pas *et al.*, Eur. Phys. J. A **12**, 147 (2001) [hep-ph/0103062].

[80] C. E. Aalseth *et al.* [IGEX Collaboration], Phys. Rev. D **65**, 092007 (2002) [hep-ex/0202026].

[81] G. Zuzel [GERDA Collaboration], Acta Phys. Polon. B **41**, 1469 (2010).

[82] E. Guardincerri [CUORE Collaboration], PoS EPS **-HEP2009**, 274 (2009).

[83] D. Akimov, G. Bower, M. Breidenbach, R. Conley, E. Conti, M. Danilov, R. DeVoe and Z. Djurcic *et al.*, Nucl. Phys. Proc. Suppl. **138**, 224 (2005).

[84] J. Lesgourgues and S. Pastor, Phys. Rept. **429**, 307 (2006) [astro-ph/0603494].

[85] O. Civitarese and J. Suhonen, Nucl. Phys. A **729**, 867 (2003) [nucl-th/0208005]; S. R. Elliott and J. Engel, J. Phys. G **30**, R183 (2004) [hep-ph/0405078].

[86] S. Weinberg, Phys. Rev. Lett. **43**, 1566 (1979).

[87] P. Minkowski, Phys. Lett. **B67**, 421 (1977).

[88] M. Gell-Mann, P. Ramond, and R. Slansky, (1979), print-80-0576 (CERN).

[89] T. Yanagida, in KEK lectures, proceedings of the Workshop on Unified Theory and Baryon Number in the Universe, KEK, edited by O. Sawada and A. Sugamoto (1979).

[90] R. N. Mohapatra and G. Senjanovic, Phys. Rev. Lett. 44, 912 (1980).

[91] J. Schechter and J. W. F. Valle, Phys. Rev. D **22**, 2227 (1980).

[92] W. Konetschny and W. Kummer, Phys. Lett. B **70**, 433 (1977).

[93] T. P. Cheng and L. F. Li, Phys. Rev. D **22**, 2860 (1980).

[94] R. N. Mohapatra and G. Senjanovic, Phys. Rev. D **23**, 165 (1981).

[95] G. Lazarides, Q. Shafi and C. Wetterich, Nucl. Phys. B **181**, 287 (1981).

[96] R. Foot, H. Lew, X. G. He and G. C. Joshi, Z. Phys. C **44**, 441 (1989).

[97] L. J. Hall and M. Suzuki, Nucl. Phys. B **231**, 419 (1984).

[98] I. H. Lee, Phys. Lett. B **138**, 121 (1984).

[99] I. H. Lee, Nucl. Phys. B **246**, 120 (1984).

[100] S. Dawson, Nucl. Phys. B **261**, 297 (1985).

[101] H. P. Nilles and N. Polonsky, Nucl. Phys. B **484**, 33 (1997) [hep-ph/9606388].

[102] R. Hempfling, Nucl. Phys. B **478**, 3 (1996) [hep-ph/9511288].

[103] F. de Campos, M. A. Garcia-Jareno, A. S. Joshipura, J. Rosiek and J. W. F. Valle, Nucl. Phys. B **451**, 3 (1995) [hep-ph/9502237].

[104] S. Roy and B. Mukhopadhyaya, Phys. Rev. D **55**, 7020 (1997) [hep-ph/9612447].

[105] M. A. Diaz, J. C. Romao and J. W. F. Valle, Nucl. Phys. B **524**, 23 (1998) [hep-ph/9706315].

[106] A. S. Joshipura and S. K. Vempati, Phys. Rev. D **60**, 111303 (1999) [hep-ph/9903435].

[107] Y. Grossman and H. E. Haber, Phys. Rev. D **59**, 093008 (1999) [hep-ph/9810536].

[108] M. Bisset, O. C. W. Kong, C. Macesanu and L. H. Orr, Phys. Rev. D **62**, 035001 (2000) [hep-ph/9811498].

[109] M. Hirsch, M. A. Diaz, W. Porod, J. C. Romao and J. W. F. Valle, Phys. Rev. D **62**, 113008 (2000) [Erratum-ibid. D **65**, 119901 (2002)] [hep-ph/0004115].

[110] M. A. Diaz, M. Hirsch, W. Porod, J. C. Romao and J. W. F. Valle, Phys. Rev. D **68**, 013009 (2003) [Erratum-ibid. D **71**, 059904 (2005)] [hep-ph/0302021].

[111] Y. Grossman and S. Rakshit, Phys. Rev. D **69**, 093002 (2004) [hep-ph/0311310].

[112] B. Mukhopadhyaya, S. Roy and F. Vissani, Phys. Lett. B **443**, 191 (1998) [hep-ph/9808265].

[113] S. Y. Choi, E. J. Chun, S. K. Kang and J. S. Lee, Phys. Rev. D **60**, 075002 (1999) [hep-ph/9903465].

[114] W. Porod, M. Hirsch, J. Romao and J. W. F. Valle, Phys. Rev. D **63**, 115004 (2001) [hep-ph/0011248].

[115] J. C. Romao, M. A. Diaz, M. Hirsch, W. Porod and J. W. F. Valle, Phys. Rev. D **61**, 071703 (2000) [hep-ph/9907499].

[116] D. Restrepo, W. Porod and J. W. F. Valle, Phys. Rev. D **64**, 055011 (2001) [hep-ph/0104040].

[117] A. Bartl, M. Hirsch, T. Kernreiter, W. Porod and J. W. F. Valle, JHEP **0311**, 005 (2003) [hep-ph/0306071].

[118] F. de Campos, O. J. P. Eboli, M. B. Magro, W. Porod, D. Restrepo, M. Hirsch and J. W. F. Valle, JHEP **0805**, 048 (2008) [arXiv:0712.2156 [hep-ph]].

[119] F. De Campos, O. J. P. Eboli, M. Hirsch, M. B. Magro, W. Porod, D. Restrepo and J. W. F. Valle, Phys. Rev. D **82**, 075002 (2010) [arXiv:1006.5075 [hep-ph]].

[120] F. Zwicky, "Spectral displacement of extra galactic nebulae," Helv. Phys. Acta **6**, 110 (1933).

[121] V. C. Rubin and W. K. Ford, Jr., Astrophys. J. **159**, 379 (1970).

[122] D. Walsh, R. F. Carswell and R. J. Weymann, Nature **279**, 381 (1979).

[123] W. M. Yao *et al.* [Particle Data Group Collaboration], J. Phys. G **33**, 1 (2006).

[124] R. J. Gaitskell, Ann. Rev. Nucl. Part. Sci. **54**, 315 (2004).

[125] J. Carr, G. Lamanna and J. Lavalle, Rept. Prog. Phys. **69**, 2475 (2006).

[126] A. Drukier and L. Stodolsky, Phys. Rev. D **30**, 2295 (1984); M. W. Goodman and E. Witten, Phys. Rev. D **31**, 3059 (1985).

[127] G. Jungman, M. Kamionkowski and K. Griest, Phys. Rept. **267**, 195 (1996) [hep-ph/9506380].

[128] J. R. Ellis, R. A. Flores and J. D. Lewin, Phys. Lett. B **212**, 375 (1988).

[129] D. S. Akerib *et al.* [LUX Collaboration], Phys. Rev. Lett. **112**, 091303 (2014) [arXiv:1310.8214 [astro-ph.CO]].

[130] Z. Ahmed *et al.* [CDMS Collaboration], Phys. Rev. Lett. **102**, 011301 (2009) [arXiv:0802.3530 [astro-ph]].

[131] J. Angle *et al.* [XENON Collaboration], Phys. Rev. Lett. **100**, 021303 (2008) [arXiv:0706.0039 [astro-ph]].

[132] E. Aprile *et al.* [XENON100 Collaboration], Phys. Rev. Lett. **109**, 181301 (2012) [arXiv:1207.5988 [astro-ph.CO]].

[133] G. J. Alner, H. M. Araujo, A. Bewick, C. Bungau, B. Camanzi, M. J. Carson, R. J. Cashmore and H. Chagani *et al.*, Astropart. Phys. **28**, 287 (2007) [astro-ph/0701858 [ASTRO-PH]]; G. J. Alner *et al.* [UK Dark Matter Collaboration], Astropart. Phys. **23**, 444 (2005).

[134] V. Sanglard *et al.* [EDELWEISS Collaboration], Phys. Rev. D **71**, 122002 (2005) [astro-ph/0503265].

[135] G. Angloher, C. Bucci, P. Christ, C. Cozzini, F. von Feilitzsch, D. Hauff, S. Henry and T. .Jagemann *et al.*, Astropart. Phys. **23**, 325 (2005) [astro-ph/0408006].

[136] C. E. Aalseth *et al.* [CoGeNT Collaboration], Phys. Rev. Lett. **101**, 251301 (2008) [Erratum-ibid. **102**, 109903 (2009)] [arXiv:0807.0879 [astro-ph]].

[137] R. Bernabei *et al.* [DAMA Collaboration], Eur. Phys. J. C **56**, 333 (2008) [arXiv:0804.2741 [astro-ph]].

[138] D. S. Akerib *et al.* [LUX Collaboration], Nucl. Instrum. Meth. A **704**, 111 (2013) [arXiv:1211.3788 [physics.ins-det]].

[139] E. Aprile [XENON1T Collaboration], Springer Proc. Phys. **148**, 93 (2013) [arXiv:1206.6288 [astro-ph.IM]].

[140] M. Su, T. R. Slatyer and D. P. Finkbeiner, Astrophys. J. **724**, 1044 (2010) [arXiv:1005.5480 [astro-ph.HE]].

[141] D. Hooper and T. R. Slatyer, Phys. Dark Univ. **2**, 118 (2013) [arXiv:1302.6589 [astro-ph.HE]].

[142] J. Ahrens *et al.* [AMANDA Collaboration], Phys. Rev. D **66**, 032006 (2002) [astro-ph/0202370].

[143] S. Desai *et al.* [Super-Kamiokande Collaboration], Phys. Rev. D **70**, 083523 (2004) [Erratum-ibid. D **70**, 109901 (2004)] [hep-ex/0404025].

[144] R. Abbasi *et al.* [ICECUBE Collaboration], Phys. Rev. Lett. **102**, 201302 (2009) [arXiv:0902.2460 [astro-ph.CO]].

[145] S. W. Barwick *et al.* [HEAT Collaboration], Astrophys. J. **482**, L191 (1997) [astro-ph/9703192].

[146] M. Aguilar *et al.* [AMS-01 Collaboration], Phys. Lett. B **646**, 145 (2007) [astro-ph/0703154 [ASTRO-PH]].

[147] O. Adriani, G. C. Barbarino, G. A. Bazilevskaya, R. Bellotti, M. Boezio, E. A. Bogomolov, L. Bonechi and M. Bongi *et al.*, Phys. Rev. Lett. **102**, 051101 (2009) [arXiv:0810.4994 [astro-ph]].

[148] O. Adriani *et al.* [PAMELA Collaboration], Nature **458**, 607 (2009) [arXiv:0810.4995 [astro-ph]].

[149] I. Cholis, L. Goodenough, D. Hooper, M. Simet and N. Weiner, Phys. Rev. D **80**, 123511 (2009) [arXiv:0809.1683 [hep-ph]].

[150] M. Cirelli, M. Kadastik, M. Raidal and A. Strumia, Nucl. Phys. B **813**, 1 (2009) [Addendum-ibid. B **873**, 530 (2013)] [arXiv:0809.2409 [hep-ph]].

[151] F. Donato, D. Maurin, P. Brun, T. Delahaye and P. Salati, Phys. Rev. Lett. **102**, 071301 (2009) [arXiv:0810.5292 [astro-ph]].

[152] K. Griest and M. Kamionkowski, Phys. Rept. **333**, 167 (2000).

[153] T. Hebbeker, Phys. Lett. **B470**, 259 (1999) [arXiv:hep-ph/9910326].

[154] T. Falk, K. A. Olive and M. Srednicki, Phys. Lett. B **339**, 248 (1994) [hep-ph/9409270].

[155] J. S. Hagelin, G. L. Kane and S. Raby, Nucl. Phys. **B241**, 638 (1984); L. E. Ibanez, Phys. Lett. **B137**, 160 (1984).

[156] The LEP Electroweak Working Group, `http://lepewwg.web.cern.ch/LEPEWWG`.

[157] M. Felizardo *et al.* [SIMPLE Collaboration], Phys. Rev. Lett. **108**, 201302 (2012) [arXiv:1106.3014 [astro-ph.CO]].

[158] A. Geringer-Sameth and S. M. Koushiappas, Phys. Rev. Lett. **107**, 241303 (2011) [arXiv:1108.2914 [astro-ph.CO]].

[159] P. J. Fox, J. Liu and N. Weiner, Phys. Rev. D **83**, 103514 (2011) [arXiv:1011.1915 [hep-ph]]; J. Kopp, T. Schwetz and J. Zupan, JCAP **1203**, 001 (2012) [arXiv:1110.2721 [hep-ph]]; C. Kelso, D. Hooper and M. R. Buckley, Phys. Rev. D **85**, 043515 (2012) [arXiv:1110.5338 [astro-ph.CO]]; M. T. Frandsen, F. Kahlhoefer, C. McCabe, S. Sarkar and K. Schmidt-Hoberg, JCAP **1201**, 024 (2012) [arXiv:1111.0292 [hep-ph]]; P. Gondolo and G. B. Gelmini, JCAP **1212**, 015 (2012), arXiv:1202.6359 [hep-ph]; R. Foot, Phys. Rev. D **86**, 023524 (2012) [arXiv:1203.2387 [hep-ph]].

[160] For global fits of the cMSSM, see e.g., O. Buchmueller *et al.*, Eur. Phys. J. C **72**, 2020 (2012) arXiv:1112.3564 [hep-ph]; L. Roszkowski, E. M. Sessolo and Y. -L. S. Tsai, Phys. Rev. D **86**, 095005 (2012) arXiv:1202.1503 [hep-ph]; C. Strege, G. Bertone, D. G. Cerdeno, M. Fornasa, R. R. de Austri and R. Trotta, JCAP **1203**, 030 (2012) [arXiv:1112.4192 [hep-ph]]; J. Ellis and K. A. Olive, Eur. Phys. J. C **72**, 2005 (2012) [arXiv:1202.3262 [hep-ph]]; A. Fowlie *et al.*, Phys. Rev. D **86**, 075010 (2012) arXiv:1206.0264 [hep-ph]; S. Akula, P. Nath and G. Peim, Phys. Lett. B **717**, 188 (2012) arXiv:1207.1839 [hep-ph]; C. Beskidt, W. de Boer, D.I. Kazakov, F. Ratnikov, Eur. Phys. J. C **72**, 2166 (2012) arXiv:1207.3185 [hep-ph].

[161] D. Hooper, T. Plehn, Phys. Lett. **B562**, 18 (2003) [hep-ph/0212226].

[162] H. K. Dreiner, S. Heinemeyer, O. Kittel, U. Langenfeld, A. M. Weber, G. Weiglein, Eur. Phys. J. **C62**, i 547 (2009) [arXiv:0901.3485 [hep-ph]]; E. Kuflik, A. Pierce, K. M. Zurek, Phys. Rev. **D81**, 111701 (2010) [arXiv:1003.0682 [hep-ph]]; N. Fornengo, S. Scopel, A. Bottino, Phys. Rev. **D83**, 015001 (2011) [arXiv:1011.4743 [hep-ph]]; L. Calibbi, T. Ota, Y. Takanishi, JHEP **1107**, 013 (2011) [arXiv:1104.1134 [hep-ph]]; *ibid.* arXiv:1112.0219 [hep-ph].

Chapter 2

Supersymmetric Inverse Seesaw

Seesaw has so far been the simplemost mechanism for neutrino mass generation. As mentioned earlier, it introduces three $SU(2)_L \times U(1)_Y$ singlet right handed neutrinos with Majorana masses, M_{N_i}, in the theory. To maintain smallness of the neutrino masses, these Majorana mass terms need to be much larger than the weak scale while keeping a sizable left-right mixing yukawa coupling. The Yukawa coupling needs to be kept large (~ 0.1) in order to make the model "visible" at the collider. However, in order to keep the Yukawa coupling large and simultaneously fit the neutrino oscillation data, one has to push the scale of the model far above the present collider limit. An order of magnitude estimation from Eq. 1.126 for the lightest mass eigenvalue reveals that for a neutrino mass to be ~ 0.01 eV and Yukawa coupling ~ 0.1, the seesaw scale must be $\sim 10^{13}$ GeV. Here we shall be considering a scenario that is phenomenologically more interesting, namely, inverse seesaw mechanism.

Inverse seesaw model extends the particle content of the SM by the addition of a pair of singlet leptons, N_i^c and S_i, per generation, with i denoting the generation index running over 1,2,3. Within this scenario, the smallness of the neutrino mass is taken care of by a small lepton number violating parameter, μ_S. Hence one can keep an $\mathcal{O}(0.1)$ Dirac neutrino Yukawa coupling and still the lepton number conserving mass scale of singlet neutrinos can be brought down below TeV order satisfying all the existing neutrino oscillation data. This makes the model testable at the present collider experiments like the LHC.

In the supersymmetric version of the inverse seesaw mechanism [1, 2], all the light neutrino masses can be generated at tree-level by adding three pairs of SM singlet superfields: $\widehat{N}_i^c$ and $\widehat{S}_i$ (with i = 1, 2, 3) having lepton number -1 and $+1$ respectively. Several embeddings of this set up have been discussed in the literature within the MSSM gauge group [3] as well as with extended gauge symmetries such as $SU(2)_L \times SU(2)_R \times U(1)_{B-L}$ [4–6], $SU(2)_L \times U(1)_Y \times U(1)_{B-L}$ [7,8] and $SU(2)_L \times U(1)_Y \times U(1)_R$ [9]. In

this thesis, we choose to work within the MSSM gauge group. The superpotential for the Supersymmetric Inverse seesaw Model (SISM) is given by

$$\mathcal{W}_{\rm SISM} = \mathcal{W}_{\rm MSSM} + \epsilon_{ab} y_\nu^{ij} \widehat{L}_i^a \widehat{H}_u^b \widehat{N}_j^c + M_{R_{ij}} \widehat{N}_i^c \widehat{S}_j + \mu_{S_{ij}} \widehat{S}_i \widehat{S}_j \,, \tag{2.1}$$

μ_S being the only (tiny) source of lepton number violation in the superpotential. The soft SUSY-breaking Lagrangian is given by

$$\begin{aligned} \mathcal{L}_{\rm SISM}^{\rm soft} &= \mathcal{L}_{\rm MSSM}^{\rm soft} - \left[m_N^2 \widetilde{N}^{c\dagger} \widetilde{N}^c + m_S^2 \widetilde{S}^\dagger \widetilde{S} \right] \\ &\quad - \left[\epsilon_{ab} A_\nu^{ij} \widetilde{L}_i^a \widetilde{N}_j^c H_u^b + B_{M_R}^{ij} \widetilde{N}_i^c \widetilde{S}_j + B_{\mu_S}^{ij} \widetilde{S}_i \widetilde{S}_j + \text{h.c.} \right] . \end{aligned} \tag{2.2}$$

Light neutrino mass

As a result of the LH neutrinos mixing with the singlet ones, the tree level neutrino mass matrix is 9×9 in the basis $\{\nu_L, N^c, S\}$:

$$\mathcal{M}_\nu = \begin{pmatrix} \mathbf{0} & M_D & \mathbf{0} \\ M_D^T & \mathbf{0} & M_R \\ \mathbf{0} & M_R^T & \mu_S \end{pmatrix} , \tag{2.3}$$

where,

$$M_D = v_u y_\nu \tag{2.4}$$

is the Dirac neutrino mass matrix, $v_u = v \sin\beta$ being the vev of the $\widehat{H}_u$ superfield in MSSM, with $v \simeq 174$ GeV. Eq. 2.3 can be simply written as in a type-1 seesaw case:

$$\mathcal{M}_\nu = \begin{pmatrix} \mathbf{0} & M_D' \\ {M_D'}^T & X \end{pmatrix} , \tag{2.5}$$

where,

$$M_D' = (M_D \;\; 0) \text{ and } X = \begin{pmatrix} \mathbf{0} & M_R \\ M_R^T & \mu_S \end{pmatrix} . \tag{2.6}$$

In the limit $\|\mu_S\| \ll \|M_D\| \ll \|M_R\|$ (where $\|M\| \equiv \sqrt{\text{Tr}(M^\dagger M)}$), the lighter mass eigenvalue of the matrix defined in Eq. 2.5 comes out to be

$$M_\nu = {M_D'}^T X^{-1} M_D' . \tag{2.7}$$

Substituting X^{-1} and M_D' in Eq. 2.7, we can rewrite this eigenvalue in terms of M_D, M_R and μ_S. This eigenvalue is the effective 3×3 light neutrino mass matrix:

$$M_\nu = \left[M_D M_R^{T^{-1}} \right] \mu_S \left[(M_R^{-1}) M_D^T \right] + \mathcal{O}(\mu_S^2) \equiv F \mu_S F^T + \mathcal{O}(\mu_S^2) \,, \tag{2.8}$$

where, $F = M_D M_R^{T^{-1}}$. As can be seen from Eq. (2.8), the smallness of neutrino mass now additionally depends on the small lepton-number violating parameter μ_S instead of just the smallness of the Dirac mass M_D and/or heaviness of M_R as in the canonical type-I seesaw case. For $\mu_S \sim \mathcal{O}(\text{keV})$, we can easily bring down M_R to $\mathcal{O}(\text{TeV})$ range even with comparatively large Dirac Yukawa couplings of $\mathcal{O}(0.1)$, thus leading to a rich collider phenomenology [10–15] as well as observable lepton flavor violation (LFV) effects [4, 16–26].

In the limit $\mu_S \to 0$, the lepton number remains conserved in the theory and the three light neutrinos remain massless as in the SM. Hence the smallness of μ_S is technically natural in the 't Hooft sense [27], since $\mu_S \to 0$ restores a larger symmetry. The smallness of μ_S can be explained by some other mechanisms, e.g, radiative corrections [28] or extra dimensions [29].

Note that, the gauge symmetry $SU(2)_L \times U(1)_Y$ allows for additional entries in the singlet sector, i.e, non-zero $\nu_L S$ and $N^c N$ terms in the superpotential. The presence of only the $N^c N$ term does not spoil anything in the light neutrino sector as this term does not appear in the light effective 3×3 neutrino mass matrix given in Eq. 2.8. However, it can affect the heavy neutrino and sneutrino masses in the model, as the coefficient of this term may not be as small as the μ_S term which has to be $\mathcal{O}(keV)$ to accommodate neutrino oscillation data. We do not consider this scenario for the present purpose. On the other hand, the $\nu_L S$ term will in general affect the light neutrino study by appearing in Eq. 2.8 but the lepton number violating coupling y_s in $y_s \widehat{L} \widehat{H}_u \widehat{S}$ term in the corresponding superpotential can be made very small (sub eV order) to denounce its effect. There are models where y_s serves as the parameter responsible for small neutrino masses instead of μ_S, known as the linear seesaw mechanism [9]. For the present purpose we ignore both these terms. These terms can be naturally eliminated by extending the SM gauge group so that these additional terms in the superpotential are forbidden by some symmetry (see, for instance, refs. [4, 5]).

Fitting Neutrino Oscillation data

The effective light neutrino mass matrix is usually diagonalized by the unitary PMNS matrix. However, due to its mixing with heavy neutrinos in the matrix structure of $\mathcal{M}_\nu$ in Eq. 2.3, the light neutrino mixing matrix will receive additional non-unitary contributions. Thus, the full (non-unitary) light neutrino mixing matrix $\mathcal{U}$ diagonalizing the light neutrino mass matrix in Eq. 2.8 has to be derived from the 9×9 unitary matrix $\mathcal{V}$ diagonalizing the full mass matrix given in Eq. 2.3, i.e,

$$\mathcal{V} \mathcal{M}_\nu \mathcal{V}^T = \text{diag}(m_i, m_{R_j}), \quad (i = 1, 2, 3;\ j = 1, 2, ..., 6), \tag{2.9}$$

and by decomposing it into the blocks

$$\mathcal{V}_{9\times9} = \begin{pmatrix} \mathcal{U}_{3\times3} & \mathcal{K}_{3\times6} \\ \mathcal{K}'_{6\times3} & \mathcal{N}_{6\times6} \end{pmatrix}. \tag{2.10}$$

For $\|M_D\| \ll \|M_R\|$, it is sufficient to expand $\mathcal{U}$ up to leading order in $F = M_D M_R^{T^{-1}}$:

$$\mathcal{U} \simeq \left(\mathbf{1} - \frac{1}{2}FF^\dagger\right) U \equiv (\mathbf{1} - \eta)U \tag{2.11}$$

where U denotes the unitary PMNS matrix that diagonalizes the light neutrino mass matrix and $\eta = \frac{1}{2}FF^\dagger$ is a measure of the non-unitarity. We choose to work with diagonal M_R and M_D, and accordingly fit μ_S to be consistent with the neutrino oscillation data. We use the global fit values for the oscillation parameters as given in Table 1.3.

Sneutrino mass matrix

In the scalar sector, the relevant terms for sneutrino mass matrix can be obtained following the prescription in Section 1.2.3. Apart from the D-term and F-term contributions, there are additional terms arising from the soft terms in Eq. 2.2. Due to mixing between doublet and singlet sneutrinos we have a 9×9 complex (or 18×18 real) sneutrino mass squared matrix. Assuming CP conservation in the soft SUSY-breaking Lagrangian in Eq. 2.2, we can decompose this mass matrix into two 9×9 real block-diagonal matrices corresponding to CP-even and CP-odd sneutrino states. The corresponding mass term in the Lagrangian looks like

$$\mathcal{L}_{\widetilde{\nu}} = \frac{1}{2}(\phi^R, \phi^I) \begin{pmatrix} \mathcal{M}_+^2 & \mathbf{0} \\ \mathbf{0} & \mathcal{M}_-^2 \end{pmatrix} \begin{pmatrix} \phi^R \\ \phi^I \end{pmatrix}, \tag{2.12}$$

where $\phi^{R,I} = (\widetilde{\nu}_{L_i}^{R,I}, \widetilde{N}_j^{c^{R,I}}, \widetilde{S}_k^{R,I})$ $(i, j, k = 1, 2, 3)$ and

$$\mathcal{M}_\pm^2 = \begin{pmatrix} m_{\widetilde{L}}^2 + M_D M_D^T + \frac{1}{2}m_Z^2 \cos 2\beta & \pm(v_u A_\nu - \mu M_D \cot\beta) & M_D M_R \\ \pm(v_u A_\nu - \mu M_D \cot\beta)^T & m_N^2 + M_R M_R^T + M_D^T M_D & B_{M_R} \pm M_R \mu_S \\ M_R^T M_D^T & B_{M_R}^T \pm \mu_S M_R^T & m_S^2 + \mu_S^2 + M_R^T M_R \pm B_{\mu_S} \end{pmatrix},$$

where $m_{\widetilde{L}}^2$ denote the soft SUSY-breaking mass squared term for $SU(2)_L$-doublet sleptons. The real symmetric CP-even and CP-odd mass squared matrices $\mathcal{M}_\pm^2$ can be diagonalized by 9×9 orthogonal matrices $\mathcal{G}_\pm$ as follows:

$$\mathcal{G}_\pm \mathcal{M}_\pm^2 \mathcal{G}_\pm^T = \text{diag}\left(m_{\widetilde{\nu}_i^{R,I}}^2\right) \quad (i = 1, 2, \cdots, 9). \tag{2.13}$$

The corresponding eigenvalues of $\mathcal{M}_\pm^2$ are almost degenerate in nature, with the degeneracy between $\widetilde{\nu}_i^R$ and $\widetilde{\nu}_i^I$ lifted only due to the small lepton number breaking parameter μ_S and B_{μ_S}. In the subsequent chapters, $\widetilde{\nu}_1^R$ is referred to as $\widetilde{\nu}_1$ and $\widetilde{\nu}_1^I$ as $\widetilde{\nu}_2$. Similarly, $\widetilde{\nu}_2^R$ is referred to as $\widetilde{\nu}_3$ and $\widetilde{\nu}_2^I$ as $\widetilde{\nu}_4$, etc. Here we consider a scenario where the lightest sneutrino mass eigenstate is the LSP, and as a result, also serve as a DM candidate.

2.1 Minimal Supersymmetric Inverse Seesaw Model

In the Minimal Supersymmetric Inverse Seesaw Model (MSISM) the particle content of the MSSM is extended by only one pair of SM singlet fields $\widehat{N}^c$ and $\widehat{S}$ having lepton number -1 and $+1$ respectively instead of three. The tree level neutrino mass matrix now is a 5×5 matrix in the basis (ν_L, N^c, S), where, $L = e, \mu, \tau$. The mass matrix looks similar to the one in Eq. 2.3:

$$\mathcal{M}_\nu = \begin{pmatrix} 0 & 0 & 0 & M_{D_1} & 0 \\ 0 & 0 & 0 & M_{D_2} & 0 \\ 0 & 0 & 0 & M_{D_3} & 0 \\ M_{D_1} & M_{D_2} & M_{D_3} & 0 & M_R \\ 0 & 0 & 0 & M_R & \mu_S \end{pmatrix}, \tag{2.14}$$

where, M_{D_i} is defined as before and the effective 3×3 light neutrino mass matrix looks similar to Eq. 2.8. After diagonalization, this effective mass matrix gives rise to just one non-zero neutrino mass. In order to satisfy neutrino oscillation data one requires a second non-zero neutrino mass eigenvalue which is originated from the sneutrino-antisneutrino loop [30, 31] as shown in Fig 2.1. The correction term is proportional to the mass splitting of sneutrino states. This feature is analogous to the R-parity

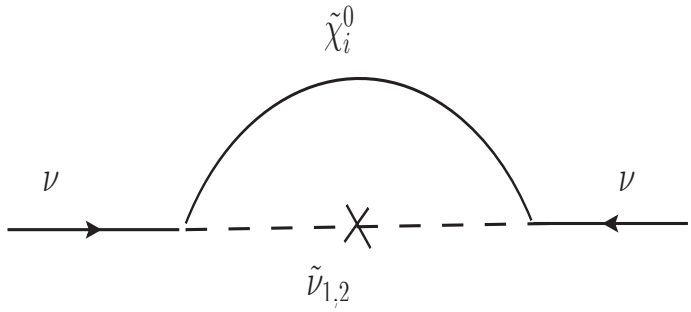

Figure 2.1: One-loop contribution to the neutrino mass due to sneutrino mass splitting.

violating [32] models of light neutrino mass generation with bilinear terms [33–43]. Issues of neutrino mass generation in MSISM have been addressed in ref. [9, 18]. A model of neutrino mass generation where the origin of neutrino mass is radiative and suppressed by inverse seesaw scale has been advocated in [44].

The sneutrino mass squared matrix is now a 10×10 matrix. Assuming CP-conservation, this matrix can be decomposed into two 5×5 block matrices in the basis $(\widetilde{\nu}_{L_i}^R, \widetilde{N}^{c^R}, \widetilde{S}^R)$ and $(\widetilde{\nu}_{L_i}^L, \widetilde{N}^{c^I}, \widetilde{S}^I)$ corresponding to CP-even and CP-odd sneutrino fields respectively as in Eq. 2.12.

2.1.1 Phenomenological aspects

In SUSY inverse seesaw, in addition to assigning neutrino mass, the singlet scalars, having mixed with the doublet sneutrinos, can be good thermal cold dark matter candidate. Apart from the neutrino masses and mixing, the SUSY inverse seesaw model has also been analysed earlier in various context:

- *LFV Signatures:* The non-negligible mixing between the light and heavy neutrinos leads to enhanced rate of the LFV processes like $\ell_\alpha^- \to \ell^-\beta$, $\mu \to eee$, etc, which have been studied in this context [4, 16–18, 45]. Note that the LFV decay rates are usually suppressed by the light neutrino masses in canonical type-I seesaw [46], but in inverse seesaw model these processes can occur irrespective of the lightness of these masses [47].

- *Dark Matter:* As discussed in the Section 1.4, cMSSM is in tension with a light neutralino or sneutrino LSP. Supersymmetric inverse seesaw model, on the other hand, provides us with a very natural DM candidate in R-parity conserving scenario in the form of a singlet sneutrino. Being mostly a singlet, this DM is not very strictly restricted from the direct detection cross-section limit. This DM scenario has been studied in some detail in refs. [3, 9, 10, 15, 48].

- *Collider signatures:* Having a large neutrino Yukawa coupling and the seesaw scale at sub-TeV range simultaneously makes the inverse seesaw mechanism very interesting regarding collider search at the LHC. The SUSY version of the model has been explored in various lepton and jet associated final states at different center of mass energies at the LHC [10, 12, 15].

- *Non-unitarity effects:* This scenario can also be tested from the observation of any kind of non-unitarity in the PMNS matrix that can be searched in the neutrino oscillation experiments [49, 50]. As described earlier in this chapter, the non-unitarity parameters can be large depending on how much mixing is allowed between the light and heavy neutrino states.

Inverse seesaw model have also been studied in detail in the context of leptogenesis [51–53] which dynamically generate the matter-antimatter asymmetry of our universe via the out-of-equilibrium decays of heavy right-handed neutrinos. For the present thesis, we mainly concentrate on the DM and collider aspects of this model. We study various signals in order to probe the model at the LHC. We also study the minimal version of the model from the aspect of a novel correlation between a collider and a neutrino physics observable that is a unique feature of this kind of models.

Bibliography

[1] R. N. Mohapatra, Phys. Rev. Lett. **56**, 561 (1986).

[2] R. N. Mohapatra and J. W. F. Valle, Phys. Rev. D **34**, 1642 (1986).

[3] C. Arina, F. Bazzocchi, N. Fornengo, J. C. Romao and J. W. F. Valle, Phys. Rev. Lett. **101**, 161802 (2008) [arXiv:0806.3225 [hep-ph]].

[4] P. S. B. Dev and R. N. Mohapatra, Phys. Rev. D **81**, 013001 (2010) [arXiv:0910.3924 [hep-ph]].

[5] P. S. B. Dev and R. N. Mohapatra, Phys. Rev. D **82**, 035014 (2010) [arXiv:1003.6102 [hep-ph]].

[6] H. An, P. S. B. Dev, Y. Cai and R. N. Mohapatra, Phys. Rev. Lett. **108**, 081806 (2012) [arXiv:1110.1366 [hep-ph]].

[7] S. Khalil, H. Okada and T. Toma, JHEP **1107**, 026 (2011) [arXiv:1102.4249 [hep-ph]].

[8] L. Basso, O. Fischer and J. J. van der Bij, Phys. Rev. D **87**, 035015 (2013) [arXiv:1207.3250 [hep-ph]].

[9] V. De Romeri and M. Hirsch, JHEP **1212**, 106 (2012) [arXiv:1209.3891 [hep-ph]].

[10] P. S. B. Dev, S. Mondal, B. Mukhopadhyaya and S. Roy, JHEP **1209**, 110 (2012) [Erratum-ibid. **1311**, 169 (2013)] [arXiv:1207.6542 [hep-ph]].

[11] C. -Y. Chen and P. S. B. Dev, Phys. Rev. D **85**, 093018 (2012) [arXiv:1112.6419 [hep-ph]].

[12] S. Mondal, S. Biswas, P. Ghosh and S. Roy, JHEP **1205**, 134 (2012) [arXiv:1201.1556 [hep-ph]].

[13] A. Das and N. Okada, Phys. Rev. D **88**, no. 11, 113001 (2013) arXiv:1207.3734 [hep-ph].

[14] P. Bandyopadhyay, E. J. Chun, H. Okada and J. -C. Park, JHEP **1301**, 079 (2013) [arXiv:1209.4803 [hep-ph]].

[15] S. Banerjee, P. S. B. Dev, S. Mondal, B. Mukhopadhyaya and S. Roy, JHEP **1310**, 221 (2013) [arXiv:1306.2143 [hep-ph]].

[16] F. Deppisch and J. W. F. Valle, Phys. Rev. D **72**, 036001 (2005) [hep-ph/0406040].

[17] F. Deppisch, T. S. Kosmas and J. W. F. Valle, Nucl. Phys. B **752** (2006) 80 [hep-ph/0512360].

[18] M. Hirsch, T. Kernreiter, J. C. Romao and A. Villanova del Moral, JHEP **1001**, 103 (2010) [arXiv:0910.2435 [hep-ph]].

[19] W. Abdallah, A. Awad, S. Khalil and H. Okada, Eur. Phys. J. C **72**, 2108 (2012) [arXiv:1105.1047 [hep-ph]].

[20] A. Abada, D. Das and C. Weiland, JHEP **1203**, 100 (2012) [arXiv:1111.5836 [hep-ph]].

[21] M. Hirsch, F. Staub and A. Vicente, Phys. Rev. D **85**, 113013 (2012) [arXiv:1202.1825 [hep-ph]].

[22] A. Abada, D. Das, A. Vicente and C. Weiland, JHEP **1209**, 015 (2012) [arXiv:1206.6497 [hep-ph]].

[23] M. Malinsky, T. Ohlsson and H. Zhang, Phys. Rev. D **79**, 073009 (2009) [arXiv:0903.1961 [hep-ph]].

[24] M. Malinsky, T. Ohlsson, Z. -z. Xing and H. Zhang, Phys. Lett. B **679**, 242 (2009) [arXiv:0905.2889 [hep-ph]].

[25] R. L. Awasthi and M. K. Parida, Phys. Rev. D **86**, 093004 (2012) [arXiv:1112.1826 [hep-ph]].

[26] R. L. Awasthi, M. K. Parida and S. Patra, JHEP **1308**, 122 (2013) arXiv:1302.0672 [hep-ph].

[27] G.t.Hooft, in G.t Hooft et al. (eds.), Proceedings of the 1979 Cargese Summer Institute on Recent Developments in Gauge Theories, Plenum Press (1979).

[28] E. Ma, Phys. Rev. D **80**, 013013 (2009) [arXiv:0904.4450 [hep-ph]]; F. Bazzocchi, D. G. Cerdeno, C. Munoz and J. W. F. Valle, Phys. Rev. D **81**, 051701 (2010) [arXiv:0907.1262 [hep-ph]].

[29] N. Arkani-Hamed, L. J. Hall, D. Tucker-Smith and N. Weiner, Phys. Rev. D **63**, 056003 (2001) [hep-ph/9911421]; S. C. Park, K. Wang and T. T. Yanagida, Phys. Lett. B **685**, 309 (2010) [arXiv:0909.2937 [hep-ph]]; C. S. Fong, R. N. Mohapatra and I. Sung, Phys. Lett. B **704**, 171 (2011) [arXiv:1107.4086 [hep-ph]].

[30] M. Hirsch, H. V. Klapdor-Kleingrothaus, and S. G. Kovalenko, *B-L violating masses in softly broken supersymmetry*, *Phys. Lett.* **B398** (1997) 311–314, [hep-ph/9701253].

[31] Y. Grossman and H. E. Haber, *Sneutrino mixing phenomena*, *Phys. Rev. Lett.* **78** (1997) 3438–3441, [hep-ph/9702421].

[32] R. Barbier *et. al.*, *R-parity violating supersymmetry*, *Phys. Rept.* **420** (2005) 1–202, [hep-ph/0406039].

[33] L. J. Hall and M. Suzuki, *Explicit R-Parity Breaking in Supersymmetric Models*, *Nucl. Phys.* **B231** (1984) 419.

[34] I.-H. Lee, *Lepton number violation in softly broken supersymmetry*, *Phys. Lett.* **B138** (1984) 121.

[35] I.-H. Lee, *Lepton Number Violation in Softly Broken Supersymmetry. 2*, *Nucl. Phys.* **B246** (1984) 120.

[36] R. Hempfling, *Neutrino Masses and Mixing Angles in SUSY-GUT Theories with explicit R-Parity Breaking*, *Nucl. Phys.* **B478** (1996) 3–30, [hep-ph/9511288].

[37] S. Roy and B. Mukhopadhyaya, Phys. Rev. D **55**, 7020 (1997) [hep-ph/9612447].

[38] B. Mukhopadhyaya, S. Roy and F. Vissani, Phys. Lett. B **443**, 191 (1998) [hep-ph/9808265].

[39] Y. Grossman and H. E. Haber, *Neutrino masses and sneutrino mixing in R-parity violating supersymmetry*, hep-ph/9906310.

[40] M. Hirsch, M. A. Diaz, W. Porod, J. C. Romao, and J. W. F. Valle, *Neutrino masses and mixings from supersymmetry with bilinear R-parity violation: A theory for solar and atmospheric neutrino oscillations*, *Phys. Rev.* **D62** (2000) 113008, [hep-ph/0004115].

[41] S. Davidson and M. Losada, *Neutrino masses in the R_p violating MSSM*, *JHEP* **05** (2000) 021, [hep-ph/0005080].

[42] A. Abada, S. Davidson, and M. Losada, *Neutrino masses and mixings in the MSSM with soft bilinear R(p) violation*, *Phys. Rev.* **D65** (2002) 075010, [hep-ph/0111332].

[43] Y. Grossman and S. Rakshit, *Neutrino masses in R-parity violating supersymmetric models*, *Phys. Rev.* **D69** (2004) 093002, [hep-ph/0311310].

[44] E. Ma, *Radiative inverse seesaw mechanism for nonzero neutrino mass*, *Phys. Rev.* **D80** (2009) 013013, [0904.4450].

[45] D. Ibanez, S. Morisi and J. W. F. Valle, Phys. Rev. D **80**, 053015 (2009) [arXiv:0907.3109 [hep-ph]].

[46] A. Ilakovac and A. Pilaftsis, Nucl. Phys. B437, 491 (1995) [hep-ph/9403398]; A. Abada, C. Biggio, F. Bonnet, M. B. Gavela and T. Hambye, JHEP 0712, 061 (2007) [arXiv:0707.4058 [hep-ph]].

[47] J. Bernabeu, A. Santamaria, J. Vidal, A. Mendez, and J. W. F. Valle, Phys. Lett. B **187**, 303 (1987); M. C. Gonzalez-Garcia and J. W. F. Valle, Mod. Phys. Lett. A **7**, 477 (1992).

[48] Z. Kang, J. Li, T. Li, T. Liu and J. Yang, arXiv:1102.5644 [hep-ph].

[49] S. Antusch, C. Biggio, E. Fernandez-Martinez, M. B. Gavela and J. Lopez-Pavon, JHEP **0610**, 084 (2006) [hep-ph/0607020].

[50] S. Goswami and T. Ota, Phys. Rev. D **78**, 033012 (2008) [arXiv:0802.1434 [hep-ph]]; S. Antusch, M. Blennow, E. Fernandez-Martinez and J. Lopez-Pavon, Phys. Rev. D **80**, 033002 (2009) [arXiv:0903.3986 [hep-ph]].

[51] J. Garayoa, M. C. Gonzalez-Garcia and N. Rius, JHEP **0702**, 021 (2007) [hep-ph/0611311].

[52] P. -H. Gu and U. Sarkar, Phys. Lett. B **694**, 226 (2010) [arXiv:1007.2323 [hep-ph]].

[53] S. Blanchet, P. S. B. Dev and R. N. Mohapatra, Phys. Rev. D **82**, 115025 (2010) [arXiv:1010.1471 [hep-ph]].

Chapter 3

Exploring novel correlations in trilepton channels in MSISM

In this chapter, we discuss the signatures of the minimal supersymmetric version of the inverse seesaw model (MSISM) with just one generation of singlet pairs at the LHC. In the case when one of the singlet sneutrinos is the LSP, the phenomenology at the LHC can be very interesting. This is because in this model the neutrino Yukawa coupling can be large and can lead to lepton flavor violating (LFV) coupling of the sneutrinos with a charged lepton and the chargino. These couplings are related to the observed neutrino mixing angles and hence by studying the collider signatures of this model it is possible to study the relation between neutrino physics and the physics at the high energy colliders.

Supersymmetric particle searches from 19 fb^{-1} data, collected by ATLAS and CMS for pp collision at center-of-mass energy, $\sqrt{s} = 7$ and 8 TeV, has found no excess over the expected SM background. In the context of the constrained minimal supersymmetric standard model (CMSSM), searches by ATLAS exclude squarks and gluinos with masses below 950 GeV [1] at 95% C.L. for some particular choice of other parameters. The results from CMS extend the mass limit to 1.2 TeV [2]. However, the third generation squarks can still be somewhat lighter, particularly in the context of a more general MSSM scenario. This is the reason, in this work, we choose to work with a spectrum where the squarks of the first two generations and the gluinos are very heavy (~ 1 TeV) and the electroweak sector is relatively light so that the lighter chargino and neutralinos can be produced at the LHC. If in the production or in the decay chain the lighter chargino ($\tilde{\chi}_1^\pm$) appears then it can have a decay into a charged lepton (ℓ) via $\tilde{\chi}_1^\pm \to \ell^\pm + \tilde{\nu}$, where $\tilde{\nu}$ represents the singlet sneutrino LSP. The ratios of the decay branching ratios into different charged lepton flavors can be shown to correlate with the neutrino mixing angles [3]. Our aim in this chapter is to look at these correlations

by studying the trilepton + $\not{E}_T$ signature from the associated production of the lighter chargino ($\tilde{\chi}_1^\pm$) and the second lightest neutralino ($\tilde{\chi}_2^0$) at the LHC [4].

Similar correlations also appear in the decay of the LSP in the model of bilinear R-parity violation [5–12], spontaneous R-parity violation [13] and in $\mu\nu$SSM [14–16]. In these models correlations with neutrino mixing angles have been studied in various context in the case of a neutralino LSP decays as well as for other LSPs including the chargino [11]. The final states discussed in these cases generally include $multi-leptons\ +\ jets\ +\ \not{E}_T$ along with the presence of displaced vertices originating from the long-lived LSP. Here we have studied this correlation in the decay of the chargino in minimal supersymmetric inverse seesaw model (MSISM) through the cleaner $trilepton\ +\ \not{E}_T$ final state in the absence of any displaced vertex [4].

In MSISM, the atmospheric neutrino mixing angle (θ_{23}) correlates not only with the ratio of the branching ratios of the lighter chargino ($\tilde{\chi}_1^\pm$) decay modes but also with ratio of the branching ratios of lepton flavor violating decays, $\tau/\mu \to \ell+\gamma$, where $\ell = e, \mu$ [3]. On the other hand, trilepton signals ($3l$, with or without tau lepton(s)) have been extensively studied for a long time as an important probe for supersymmetric models [17–28] (see also references [3,4,6,7] of ref. [19]). Besides, a hadronically quiet event like this always has the favor of reducible backgrounds. Moreover, multi-lepton signals have already been considered as an important probe for seesaw models [29, 30]. Being motivated by these features together with the novel correlations mentioned earlier, we aim to perform a detailed analysis of trilepton $(3\ell, 2\ell + 1\tau) + \not{E}_T$ signals for the MSISM taking into account possible SM backgrounds.

As mentioned earlier, we search for the trilepton signatures, arising from the decay of $\tilde{\chi}_2^0\tilde{\chi}_1^\pm$ pair. In our chosen parameter points the associated production of the lightest chargino with the next-to-lightest neutralino, $pp \to \tilde{\chi}_2^0\tilde{\chi}_1^\pm + X$ can occur with a detectable rate at the LHC. In addition, the lighter chargino and the second lightest neutralino decays via two body leptonic modes with large branching ratios. The final state signal will produce three charged lepton and missing energy signature ($3\ell + \not{E}_T$ or $2\ell + 1\tau + \not{E}_T$), because of the presence of the stable singlet sneutrino LSP. It is interesting to note that in our analysis the lightest neutralino $\tilde{\chi}_1^0$ decays into a singlet scalar LSP and a light neutrino. Both of these decay products escape detection and thus $\tilde{\chi}_1^0$ can be thought of as a virtual LSP, which also yields the missing energy signature at an accelerator experiment similar to that by an LSP. We investigate three body final states like 3ℓ ($\ell = e, \mu$) and also $2\ell + \tau$-jet. Final states with more than one tau lepton have been dropped for small τ detection efficiency [31]. In the course of present analysis we choose to work with non-universal gaugino masses but maintain $M_2 > M_1$, where $M_1(M_2)$ are the soft masses for $U(1)(SU(2))$ gaugino(s). It has also

been assumed that $\mu > M_2$, where μ is the coefficient of the only bilinear term in the superpotential of the minimal supersymmetric standard model (MSSM). With such a choice, $\tilde{\chi}_2^0, \tilde{\chi}_1^\pm$ are essentially gaugino like. Moreover, since the first two generation squark masses are heavy, the process $pp \to \tilde{\chi}_2^0 \tilde{\chi}_1^\pm$ receives prime contributions from $W^\pm$-boson mediated processes. Three of our benchmark points (BP1, BP3 and BP4 as defined later) are chosen with this criteria. We have, however, also considered the situation when $M_2 > \mu$ for another benchmark point (BP2). However, in a situation like this, $\tilde{\chi}_2^0, \tilde{\chi}_1^\pm$ are higgsino like and consequently yield a smaller cross section for the process $pp \to \tilde{\chi}_2^0 \tilde{\chi}_1^\pm$. We show later that in a scenario like this the trileptonic final state possesses lower significance compared to the $\mu > M_2$ scenario. We will discuss this issue in more detail later in section 3.3. Having heavy squarks is also useful for suppressing flavor violating processes in the quark sector.

The ratio of the branching ratios for $\tilde{\chi}_1^\pm$ decaying into μ and τ channel in MSISM shows sharp correlation with $\tan^2\theta_{23}$ [3]. It is clear that one of the three charged leptons appearing either in $3\ell + \not{E}_T$ or $2\ell + \tau + \not{E}_T$ final states must have its origin in $\tilde{\chi}_1^\pm$ decay. Using this idea we find that the ratio $\frac{\sigma(\mu^\pm + \sum \ell\ell)}{\sigma(\tau^\pm + \sum \ell\ell)}$, with $\ell = e, \mu$ shows nice correlation with $\tan^2\theta_{23}$ even after the application of different kinematical cuts to reduce SM backgrounds [4]. Definitely, that μ and τ are coming from lightest chargino decay. Existence of this final state correlation with neutrino mixing angle along with a large amount of $\not{E}_T$ provides a distinct signature for the MSISM [4].

3.1 Decays of chargino and neutralino

In this section we discuss the decays of the lighter chargino to charged leptons and singlet sneutrinos as well as the decays of the lighter neutralinos. We shall also show how these decays can lead to the final states, that we have proposed to study in this paper. Our choices of the four benchmark points for a detailed collider study will also be presented here.

3.1.1 Chargino decay

For the discussion of chargino decays we shall concentrate on a part of the parameter space where one of the singlet scalars of MSISM is the LSP. Hence this scalar singlet will appear at the end of the supersymmetric cascade decay chains. For the present discussion let us assume that the dominant decay mode of the lighter chargino is in the two body mode

$$\tilde{\chi}_1^\pm \to \tilde{\nu}_a + l_i^\pm, \qquad a = 1, 2, \quad l_i = e,\ \mu,\ \tau, \tag{3.1}$$

where $\tilde{\nu}_1$ and $\tilde{\nu}_2$ correspond to the lightest CP-even and CP-odd sneutrino mass eigenstates (see Chapter 2) respectively. The relevant piece of the Lagrangian for the calculation of this decay width is

$$L_{\ell\tilde{\chi}^-\tilde{\nu}} = \overline{\tilde{\chi}_j^+}(C_{ija}^L P_L + C_{ija}^R P_R) l_i \tilde{\nu}_a + h.c. \ , \tag{3.2}$$

where

$$\begin{aligned} C_{ija}^L &= -\frac{1}{\sqrt{2}}[g\mathbf{V}_{j1}^*(\mathbf{G}_{ai} - i\mathbf{G}_{a,i+5}) - y_\nu^i \mathbf{V}_{j2}^*(\mathbf{G}_{a4} - i\mathbf{G}_{a9})], \\ C_{ija}^R &= \frac{1}{\sqrt{2}} Y_{\ell_i} \mathbf{U}_{j2}(\mathbf{G}_{ai} - i\mathbf{G}_{a,i+5}). \end{aligned} \tag{3.3}$$

The Y_{ℓ_i}s are the charged lepton Yukawa couplings and $\mathbf{U}$, $\mathbf{V}$ are two unitary 2×2 chargino mixing matrices such that $\mathbf{U}^* m_{2\times 2} \mathbf{V}^{-1} = diag(m_{\tilde{\chi}_1^\pm}, m_{\tilde{\chi}_2^\pm})$, where $m_{\tilde{\chi}_1^\pm}, m_{\tilde{\chi}_2^\pm}$ are the two physical chargino masses. The 2×2 mass matrix $m_{2\times 2}$ in the charged gaugino-higgsino basis $\psi^{+^T} = (-i\tilde{\lambda}_2^+ \ \tilde{H}_u^+)$, $\psi^{-^T} = (-i\tilde{\lambda}_2^- \ \tilde{H}_d^-)$ is given by

$$m_{2\times 2} = \begin{pmatrix} M_2 & g v_u \\ \\ g v_d & \mu \end{pmatrix}. \tag{3.4}$$

Here g is the $SU(2)_L$ gauge coupling. v_u and v_d are the up and down type Higgs VEVs respectively.

The corresponding decay widths are given as

$$\Gamma(\tilde{\chi}_1^\pm \to \tilde{\nu}_a + l_i^\pm) = \frac{(m_{\chi_1^\pm}^2 - m_{\tilde{\nu}_a}^2)^2}{32\pi m_{\chi_1^\pm}^3}(\mid C_{i1a}^L \mid^2 + \mid C_{i1a}^R \mid^2). \tag{3.5}$$

The members of *CP* conjugated pair of sneutrinos being nearly mass degenerate ($m_{\tilde{\nu}_1} \approx m_{\tilde{\nu}_2}$) they are unlikely to be distinguished experimentally. Hence we sum over the *CP*-even and *CP*-odd sneutrino states of the *CP* conjugated pair. Thus

$$\Gamma(\tilde{\chi}_1^\pm \to \tilde{\nu}_{1+2} + l_i^\pm) \equiv \sum_{\alpha=1}^{2} \Gamma(\tilde{\chi}_1^\pm \to \tilde{\nu}_\alpha + l_i^\pm). \tag{3.6}$$

One can adjust the parameters μ_S and B_{μ_S}, defined as in Eq. 2.1 and 2.2, in such a way that the tree-level neutrino mass matrix contribution determines the atmospheric mass scale, while the one-loop corrections control the solar mass scale [3]. In such a situation it can be shown that in order to have small reactor neutrino mixing angle and maximal atmospheric neutrino mixing angle, the parameter M_{D_1} has to be considerably smaller than other two Dirac masses and simultaneously, $M_{D_2} \sim M_{D_3}$. The solar neutrino

mixing angle can be kept large by keeping the parameters $\delta_i \equiv A^i_\nu v_u - \mu M_{D_i} \cot\beta$ to be of the same order for all the three flavors, $i = e,\ \mu,\ \tau$. Here A_ν and M_D are same as defined in Eq. 2.2 and 2.4, apart from the fact that in this case, they are not matrices but just numbers. In this case, one can show that the decay width of the lighter chargino, $\Gamma(\tilde{\chi}^\pm_1 \to \tilde{\nu}_{1+2} + l^\pm_i)$ correlates with the corresponding parameter $M^2_{D_i}$. The atmospheric neutrino mixing angle at the same time also behaves as $\tan^2\theta_{23} \sim \frac{M^2_{D_2}}{M^2_{D_3}}$. Hence, one would expect that the ratio of the branching ratios $\frac{Br(\tilde{\chi}^\pm_1 \to \tilde{\nu}_{1+2}+\mu^\pm)}{Br(\tilde{\chi}^\pm_1 \to \tilde{\nu}_{1+2}+\tau^\pm)}$ must correlate with the ratio $\frac{M^2_{D_2}}{M^2_{D_3}}$. This has been shown in Fig. 3.1.

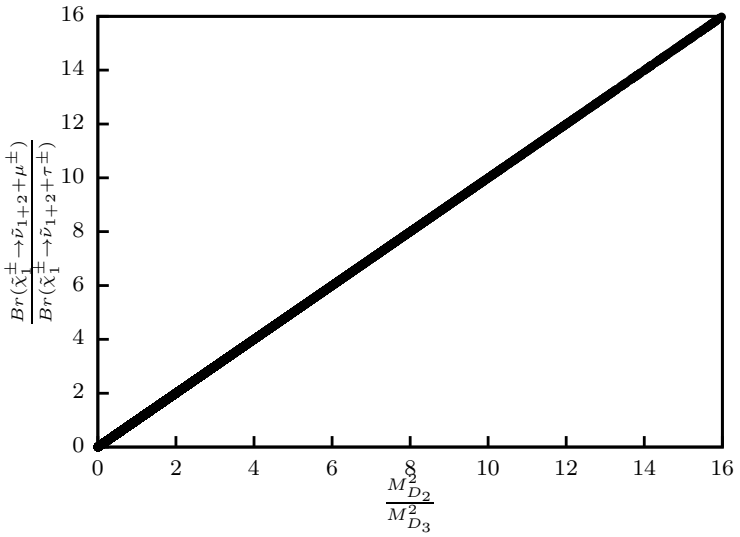

Figure 3.1: Correlation plot for the ratio of the branching ratios $\frac{Br(\tilde{\chi}^\pm_1 \to \tilde{\nu}_{1+2}+\mu^\pm)}{Br(\tilde{\chi}^\pm_1 \to \tilde{\nu}_{1+2}+\tau^\pm)}$ with $\frac{M^2_{D_2}}{M^2_{D_3}}$.

3.1.2 Neutralino decay

In our chosen benchmark points (defined later in this section) the lightest neutralino is the next-to-lightest supersymmetric particle (NLSP) and, decays dominantly through the two body decay channels $\tilde{\chi}^0_1 \to \nu_{l_i} + \tilde{\nu}_{1,2},\ l_i = e, \mu, \tau$. The relevant interaction term of the Lagrangian is:

$$L_{\nu\tilde{\chi}^0\tilde{\nu}} = \bar{\tilde{\chi}}^0_j (A^L_{mjb} P_L + A^R_{mjb} P_R) \nu_m \tilde{\nu}_b + h.c., \tag{3.7}$$

where

$$\begin{aligned} A^L_{mjb} &= \frac{g}{2}(\mathbf{N}^*_{j2} - \tan\theta_W \mathbf{N}^*_{j1})(\mathbf{G}_{bi} - i\mathbf{G}_{b(i+5)}) U^{tr}_{im}, \\ A^R_{mjb} &= -\frac{1}{\sqrt{2}} y^i_\nu U^{tr}_{im} \mathbf{N}_{j4} (\mathbf{G}_{b4} - i\mathbf{G}_{b9}). \end{aligned} \tag{3.8}$$

Here g is the $SU(2)_L$ gauge coupling, θ_W is the weak mixing angle, and $\mathbf{N}$ is the unitary 4x4 neutralino mixing matrix. Although the second lightest neutralino ($\tilde{\chi}_2^0$) decays mostly through the standard MSSM two-body charged lepton-slepton channel ($\tilde{\chi}_2^0 \to \tilde{l}_i^{\pm} + l_i^{\mp}$), some of its branching fraction goes into the decay channels arising from the coupling given in eq. (3.7). Here, we have neglected the charged lepton flavor violating decay of $\tilde{\chi}_2^0$. The decay width of a neutralino ($\tilde{\chi}_j^0$) decaying into neutrino-sneutrino two-body mode is given as

$$\Gamma(\tilde{\chi}_j^0 \to \tilde{\nu}_b + \nu_m) = \frac{(m^2_{\chi_j^0} - m^2_{\tilde{\nu}_b})^2}{32\pi m^3_{\chi_j^0}} (\mid A^L_{mjb} \mid^2 + \mid A^R_{mjb} \mid^2). \tag{3.9}$$

3.1.3 Trilepton signal and the benchmark points

In order to illustrate the trilepton signal we simulate $\tilde{\chi}_2^0\tilde{\chi}_1^{\pm}$ production followed by their two-body decays to produce $3\ell + \not{E}_T$ or $2\ell + \tau - \text{jet} + \not{E}_T$ final states, where $\ell = e, \mu$.

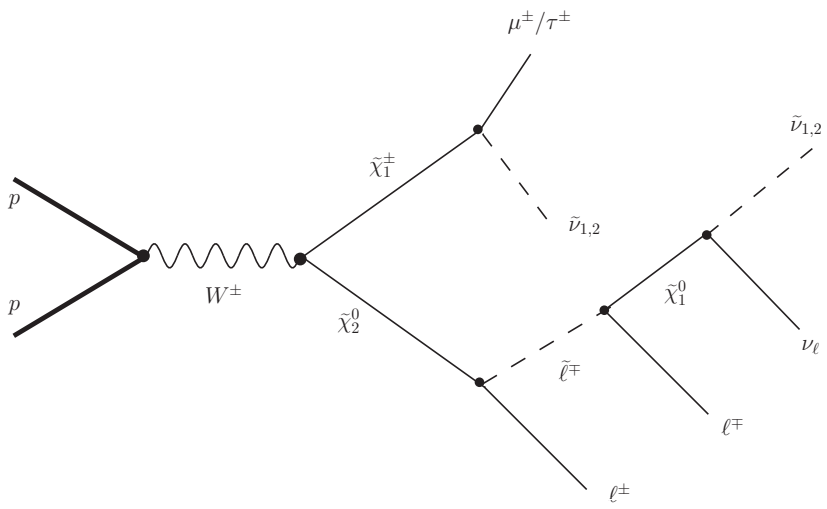

Figure 3.2: Feynman diagram for the process $pp \to 3\ell + \not{E}_T$ or $2\ell + \tau - \text{jet} + \not{E}_T$.

As discussed above the production process and the decay cascades leading to these final states are as follows

$$\begin{aligned}
&pp \to \tilde{\chi}_2^0 + \tilde{\chi}_1^{\pm}, \\
&\tilde{\chi}_1^{\pm} \to \tilde{\nu}_{1,2} + \mu^{\pm}/\tau^{\pm}, \\
&\tilde{\chi}_2^0 \to \tilde{\ell}^{\pm} + \ell^{\mp}, \\
&\tilde{\ell}^{\pm} \to \ell^{\pm} + \tilde{\chi}_1^0, \\
&\tilde{\chi}_1^0 \to \nu_l + \tilde{\nu}_{1,2}.
\end{aligned} \tag{3.10}$$

The Feynman diagram for the above mentioned final states is shown in Fig. 3.2. In the presence of heavy squarks ($\sim 1\ TeV$), this is the leading process for the chosen signal.

Because of the presence of the massive singlet sneutrino LSPs, $\tilde{\nu}_{1,2}$, (quasi-degenerate in masses), we have, for this model, a large amount of missing energy in the final states. In order to have an appreciable signal rate one must have significant production cross section of $\tilde{\chi}_2^0 - \tilde{\chi}_1^\pm$ pair and large branching ratios for the above-mentioned decays. To achieve these we have chosen four benchmark points (BPs) in the parameter space where the detailed collider simulation has been performed. We scanned the whole parameter space to check for charged lepton flavor violating (LFV) decay widths and we found points both above and below the experimental limits in different region of the parameter space. In all of the benchmark points, constraints from LFV decays [32] are satisfied as well as the atmospheric neutrino mixing is near maximal. The input parameters for different benchmark points are given in table 3.1. The choices of the parameters $M_{D_i}^2$ will be shown later. The mass splittings between the second lightest

	BP1	BP2	BP3	BP4
$\tan\beta$	5	10	20	10
μ (GeV)	330	240	280	350
M_1 (GeV)	170	195	160	240
M_2 (GeV)	220	340	240	290
M_3 (GeV)	1100	1100	1100	1100
M_R (GeV)	145	160	140	150
$\mu_s \times 10^9$ (GeV)	7.80	7.81	7.75	7.76
$m_{\nu^c}^2$ (GeV^2)	2500	3025	2500	3025
$m_S^2 \times 10^{-4}$ (GeV^2)	4.0	4.0	4.0	4.8
B_{M_R} (GeV^2)	2500	2500	3500	2500
B_{μ_S} (GeV^2)	10	10	10	10
$M_{\tilde{L}_i}^2 \times 10^{-5}$ (GeV^2)	5.63	5.63	5.63	5.63
$M_{\tilde{e}_{11}^c}^2 \times 10^{-4}$ (GeV^2)	2.99	3.69	2.59	5.86
$M_{\tilde{e}_{22}^c}^2 \times 10^{-4}$ (GeV^2)	2.99	3.69	2.59	5.86
$M_{\tilde{e}_{33}^c}^2 \times 10^{-4}$ (GeV^2)	3.53	7.08	7.90	8.18

Table 3.1: Values of the relevant input parameters for different benchmark points. The quantities $M_{\tilde{e}_{ii}^c}^2$ represent soft squared masses for the right-handed charged sleptons. The choice of $M_{D_i}^2$ parameters are shown in Table 3.3.

neutralino, the charged sleptons and the lightest neutralino are maintained in a way,

that the second lightest neutralino decays only through charged lepton-slepton two body modes and the charged sleptons further decay into the lightest neutralino and charged lepton states. With these considerations we generated the sparticle spectrum using `SuSpect` (version 2.41) [33]. Masses of the neutrino and sneutrino states are computed using a self developed code in `FORTRAN`. Relevant mass spectra for these benchmark points are shown in table 3.2.

The choice of model parameters for different benchmark points are chosen to yield statistically significant final states. As an illustrative example, production cross sections for the $\tilde{\chi}_2^0\tilde{\chi}_1^\pm$ pair with 7 TeV center of mass energy at LHC are in the range of $200 - 300$ fb for the first and third benchmark points. For the fourth benchmark point with relatively heavy $\tilde{\chi}_2^0\tilde{\chi}_1^\pm$ pair (see table 3.2) the production cross section is reduced by a factor of 4(3) compared to the first(third) benchmark point. On the contrary, a higgsino like $\tilde{\chi}_2^0\tilde{\chi}_1^\pm$ pair (BP2) yield a similar production cross-section like BP4, in spite of having a lighter $\tilde{\chi}_2^0\tilde{\chi}_1^\pm$ pair. Thus, the region of parameter space with higgsino like $\tilde{\chi}_2^0\tilde{\chi}_1^\pm$ pair is disfavored for this analysis.

	BP1	BP2	BP3	BP4
$\widetilde{\nu}_1$	153.27	169.18	147.96	159.76
$\widetilde{\nu}_2$	153.27	169.18	147.96	159.76
$\widetilde{\nu}_3$	247.38	256.45	244.81	266.53
$\widetilde{\nu}_4$	247.34	256.42	244.76	266.50
n_4	145.46	160.52	140.42	150.45
n_5	145.46	160.52	140.42	150.45
$\tilde{e}_L, \tilde{\mu}_L$	751.28	751.37	751.39	751.37
$\tilde{e}_R, \tilde{\mu}_R$	178.00	196.97	166.83	245.98
$\tilde{\tau}_1$	193.11	269.48	284.12	289.17
$\tilde{\tau}_2$	751.30	751.40	751.53	751.43
$\tilde{\chi}_1^0$	159.51	172.90	151.80	226.36
$\tilde{\chi}_2^0$	198.11	234.59	207.67	264.16
$\tilde{\chi}_1^\pm$	192.79	215.47	203.72	255.99
$\tilde{\chi}_2^\pm$	363.91	372.89	326.77	391.60

Table 3.2: Relevant mass spectra obtained for four benchmark points with $n_i,\ i = 1, 2, .., 5$ indicating neutrino masses. In the table we show only the heavy neutrino (n_4 and n_5) masses.

Note that hadronically quiet trilepton signal ($3\ell + \not{E}_T$) will get very little contri-

bution from squark-squark, squark-gluino and gluino-gluino pair production. On the other hand, when we have $2\ell + \tau$-jet + $\not{E}_T$ signal, then one should consider all other sources of dilepton + 1-jet + $\not{E}_T$ events where one jet can be faked as a τ-jet. For example, one can have a jet out of a squark decay ($\tilde{q} \to q' + \tilde{\chi}_1^{\pm}$) from one side of the cascade. However, since in this model the squarks are much heavier ($\sim$ 1 TeV) and after incorporating the probability of any jet faking as a τ-jet, the event rate comes out to be negligibly small compared to the one generated from chargino-neutralino production. Hence the main contribution to $2\ell + \tau$-jet + $\not{E}_T$ signal comes from $\tilde{\chi}_2^0\tilde{\chi}_1^{\pm}$ production only.

3.2 Event generation and background analysis

On the basis of the discussion presented in the previous section, let us now provide a detailed description of event generation and subsequently, the background analysis. The decay widths corresponding to the two-body modes shown in eq. (3.10) have been used to modify the branching fractions of the charginos and neutralinos obtained from `SuSpect`. These input files are then fed to `PYTHIA` (version 6.409) [34] for event generation and showering. Initial and final state radiation, decay, hadronization, fragmentation and jet formation are implemented following the standard procedures in `PYTHIA`. Factorization and renormalization scales are set at $\sqrt{\hat{s}}$ (i.e $\mu_R = \mu_F = \sqrt{\hat{s}}$), where $\sqrt{\hat{s}}$ is the parton level centre of mass energy. We have used the leading order CTEQ5L parton distribution functions [35, 36] for the colliding protons. Some of the background events are generated using `ALPGEN` (version 2.14) [37] with default factorization and renormalization scales. The jets are constructed using cone algorithm in PYCELL. Only those jets are constructed which have $p_T > 20$ GeV and $\mid \eta \mid < 2.5$. To simulate detector effects we have taken into account smearing of jet energies by a Gaussian probability density function of width [38] $\sigma(E)/E_j = (0.6/\sqrt{E_j[GeV]}) + 0.03$ where E_j is the unsmeared jet energy.

In order to find three isolated leptons in the final states we impose following cuts and isolation criteria:

I. Leptonic events are selected only if $p_T^{\ell} > 8$ GeV and $\mid \eta^{\ell} \mid < 2.4$.

II. Lepton-lepton separation $\Delta R(\ell, \ell)$ set to be > 0.2, where $\Delta R = \sqrt{(\Delta\eta)^2 + (\Delta\phi)^2}$.

III. Lepton-jet separation $\Delta R(\ell, j)$ chosen to be > 0.5.

IV. The sum of E_T deposits of the hadrons which fall within a cone of $\Delta R \leq 0.2$ around a lepton, must be less than 10 GeV.

A p_T cut of 10 GeV and 17 GeV [31] is applied on final state muons and electrons

respectively, for the analysis at 7 TeV and 14 TeV center of mass energies at the LHC. The τ-jets are counted with $p_T \geq 20$ GeV and $\mid \eta^\tau \mid < 2.4$. The τ's are then counted according to the visible energy bins. A τ-jet is treated as tagged or untagged according to the efficiency (ϵ_τ) of the most efficient algorithm given in [39]. In ref. [39], τ identification efficiency obtained from actual collision data at 7 TeV center of mass energy has also been quoted. The efficiencies obtained from Monte-Carlo simulation and from the data agrees very well. However, for higher luminosity with 14 TeV center of mass energy, a lot of underlying events are expected to be there, which can perhaps bring down the detection efficiency. In this case also we have used the same efficiency as in 7 TeV case hoping the experimentalists can maintain the efficiency as we have now. Unlike τ, detection efficiencies of e and μ are assumed to be 100%.

We have analysed the SM backgrounds in some detail. The dominant background events arise from $t\bar{t}$ and WZ production at the LHC. Apart from these, contributions from ZZ, WW, $Zb\bar{b}$, $Wb\bar{b}$, $Z+jets$, Wt, tb, WWW, $Wt\bar{t}$ events have also been studied at the leading order. We also studied QCD di-jet events. But after putting the cuts to reduce backgrounds as mentioned below we found no trilepton events for 1 fb^{-1} integrated luminosity from these particular QCD events. We use `ALPGEN` for an estimation of $Zb\bar{b}$, $Wb\bar{b}$, Wt, tb, $Z+jets$, WWW, $Wt\bar{t}$ backgrounds. We generate these events at the parton level using `ALPGEN` and fed those partonic events to `PYTHIA` for showering, hadronization, fragmentation, decay, etc. The other events are generated and analysed using `PYTHIA`. It should be mentioned that the importance of these processes have already been emphasized in the literature [25, 40].

The trilepton signal in our model arising out of chargino-neutralino production is accompanied by large missing transverse energy ($\not{E}_T$), because of a pair of singlet sneutrino LSPs and a neutrino. As an example, the $\not{E}_T$ spectrum of background events as well as the signal events ($3\mu + \not{E}_T$) for the first benchmark point (BP1) are shown in fig. 3.3.

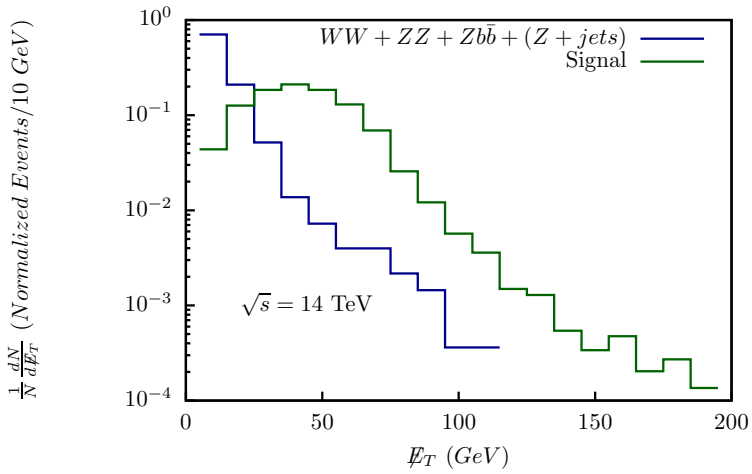

Figure 3.3: $\not{E}_T$ plot for signal events $3\mu + \not{E}_T$ and summed up contribution coming from the $WW, ZZ, Zb\bar{b}, Z + 1\ jet, Z + 2\ jets$ background for LHC at 14 TeV center of mass energy with 1 fb^{-1} of integrated luminosity. The $\not{E}_T$ bin size is chosen to be 10 GeV.

These distributions are obtained without applying any cuts to reduce background events. It is evident from the plot in Fig. 3.3 that a strong $\not{E}_T$ cut will affect the signal cross-section very mildly, but it reduces significantly background events coming from some processes. Therefore, a cut $\not{E}_T > 25$ GeV is applied for background rejection. For some other channels; $t\bar{t}, WZ, Wt\bar{t}, WWW$ the $\not{E}_T$ distributions do not peak before 25 GeV as shown in Fig. 3.4.

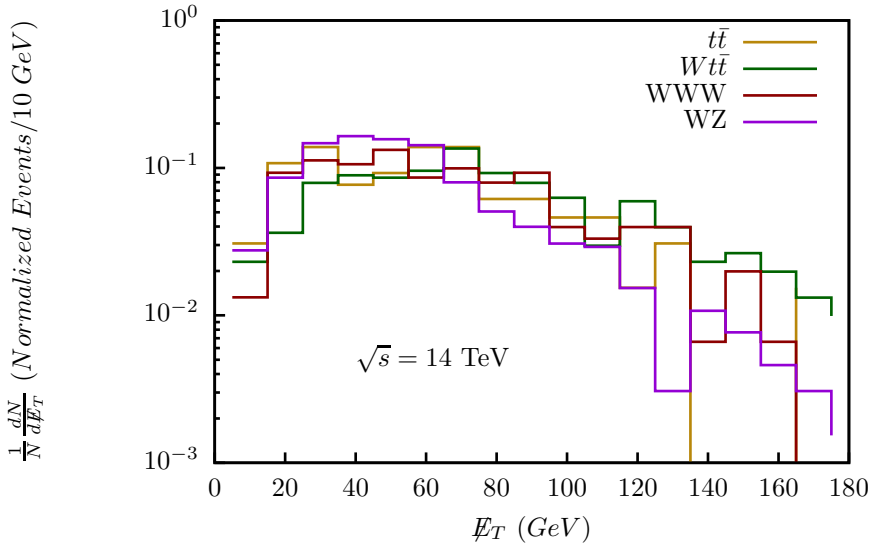

Figure 3.4: $\not{E}_T$ plot for 3μ+$\not{E}_T$ events obtained from $t\bar{t}, WZ, Wt\bar{t}, WWW$ backgrounds for LHC at 14 TeV center of mass energy with 1 fb^{-1} of integrated luminosity. The $\not{E}_T$ bin size is chosen to be 10 GeV.

Hence, the above mentioned $\not{E}_T$ cut does not seriously affect these background events. To reduce these events we have further applied two more cuts. An invariant mass cut on the opposite sign dilepton pair, 80 GeV $> M_{inv}^{\ell\ell} >$ 100 GeV removes backgrounds coming from Z-bosons. To manifest this idea we show invariant mass distribution in Fig. 3.5 constructed from opposite sign muon pairs for signal events and WZ background events.

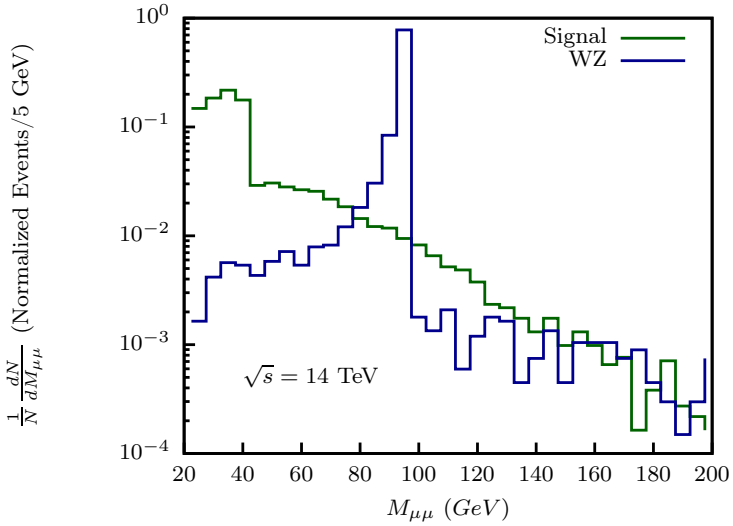

Figure 3.5: $M_{\mu\mu}$ plot for signal events and WZ background for LHC at 14 TeV center of mass energy. The $M_{\mu\mu}$ bin size is chosen to be 5 GeV.

On the other hand, rejection of tagged b-jet events significantly reduces backgrounds coming from $t\bar{t}$ events. A jet (with $\mid \eta \mid < 2.5$) is reconstructed as a b-jet if the ΔR separation between the jet and the b-quark (with $p_T > 5$ GeV) is less than 0.2. The b-jet identification efficiency is taken to be 50%.

In order to perform the collider analysis we have randomly generated $m_{D_i}^2$ and δ_i^2 within certain range: $(\sum_i M_{D_i}^2)^{1/2} \in 10^{[-4,2.6]}$ and $(\sum_i \delta_i^2)^{1/4} \in 10^{[-4,3]}$ [3]. Moreover, we also consider $(\sum M_{D_i}^2)^{1/2} > (\sum_i \delta_i^2)^{1/4}$, such that Dirac neutrino masses give the dominant contribution to the chargino decay [3]. Around each of the four benchmark points we select a set of six to seven points of these randomly generated parameters. These points will be useful for the correlation study discussed later in section 3.3.

Remember that these parameters control the neutrino masses and the mixing angles and our choices of benchmark points are such that the atmospheric neutrino mass scale is determined by the tree level neutrino mass matrix contribution. Before showering in `PYTHIA`, as mentioned earlier, the ratio $\frac{Br(\tilde{\chi}_1^\pm \to \tilde{\nu}_{1+2} + \mu^\pm)}{Br(\tilde{\chi}_1^\pm \to \tilde{\nu}_{1+2} + \tau^\pm)}$ shows a very nice sharp correlation when plotted against $\frac{M_{D_2}^2}{M_{D_3}^2}$ which is a measure of $\tan^2\theta_{23}$. We have done the showering for four benchmark points introduced in table 3.1 and table 3.2 to look for the

ratio $\frac{\sigma(pp\to\mu\sum\ell\ell+\not{E}_T\ )}{\sigma(pp\to\tau\sum\ell\ell+\not{E}_T\ )}$ with $\ell = e, \mu$. Since one μ and one τ in these final states always come from the decay of $\tilde{\chi}_1^\pm$, we would expect that this ratio will also go as $\sim \tan^2\theta_{23}$. Hence, by measuring this ratio from the trilepton signals one can obtain information about the atmospheric neutrino mixing angle at the LHC. On the other hand, a precise measurement of the atmospheric neutrino mixing angle at the oscillation experiments can be used to predict the allowed range of the above ratio at the LHC. In the following section we give a quantitative estimate of this ratio for our choices of benchmark points (along with randomly selected values of $M_{D_i}^2$) and show that for each of these points the various signal events included in the calculation of this ratio can be statistically significant.

3.3 Results

In order to study the correlation between the atmospheric neutrino mixing angle (θ_{23}) and the final states with trilepton + $\not{E}_T$ at the LHC, we look at the ratio of cross sections $\frac{\sigma(pp\to\mu\sum\ell\ell+\not{E}_T\ )}{\sigma(pp\to\tau\sum\ell\ell+\not{E}_T\ )}$, $\ell = e, \mu$. As mentioned in the introduction, in the denominator the τ must always come from the decay of $\tilde{\chi}_1^\pm$ because we are considering final states with only one τ-jet and neglecting lepton flavor violating decays of $\tilde{\chi}_2^0$ and $\tilde{\ell}^\pm$. For the same reason, in the numerator one μ must always also come from the decay of $\tilde{\chi}_1^\pm$. Hence, naively we would expect that this ratio of cross sections will also show nice correlation with the atmospheric neutrino mixing angle θ_{23}.

After applying different cuts to reduce backgrounds and taking into account the τ-tagging efficiency, we find that the ratio of trilepton signal cross section again shows a nice correlation with the atmospheric neutrino mixing angle $\tan^2\theta_{23}$. However, in this case the numbers change from the ratio of branching ratios, discussed earlier and the straight lines obtained are steeper than the one shown in Fig. 3.1. This happens because in our simulation we take the detection efficiency of μ to be 100% as opposed to the τ detection efficiency, which is smaller [31]. Since the branching fractions of τ events are in the denominator of the ratio, the numbers naturally go up.

The cross-sections and the corresponding statistical significance ($\frac{S_x}{\sqrt{B_x+S_x}}$ with $x = e, \mu, \tau$) obtained from our simulation for LHC are shown in this section. Here S_x is defined as the number of $x\sum\ell\ell$ signal events and B_x is defined as the number of corresponding background events. In more simple form significance for the $\mu\sum\ell\ell+\not{E}_T$ channel is defined as $\frac{S_{\mu ee}+S_{\mu\mu\mu}}{\sqrt{S_{\mu ee}+S_{\mu\mu\mu}+B_{\mu ee}+B_{\mu\mu\mu}}}$. In a similar fashion significance for the $\tau\sum\ell\ell+\not{E}_T$ channel can be obtained.

We quote the results below for an integrated luminosity of 25 fb^{-1} for the LHC with 7 TeV and 14 TeV center-of-mass energies. The results are obtained with the

cuts mentioned in section 3.2. Throughout this analysis we have used leading order cross sections for the signals as well as all the backgrounds at the LHC. However, if next-to-leading order (NLO) corrections are included the statistical significance will not change much. For example, if NLO corrections are included the signal cross section at 14 TeV LHC is expected to increase by 1.25 to 1.35 [41]. As discussed above, a large contribution to the background comes from the $t\bar{t}$ events. The NLO cross section for $t\bar{t}$ production at 14 TeV LHC is about 800 pb [42,43] which is about a factor of two larger than the leading order cross section that we have used in our analysis. Thus taking into account the NLO contribution of all the major background events along with the signal event, the significance $S_x/\sqrt{B_x + S_x}$ estimated for our signal, will not change much and remains conservative in comparison to the uncertainties in the production cross sections.

Values of the randomly generated parameters $M^2_{D_i}$, for four chosen benchmark points are presented in table 3.3. For the numerical analysis we choose to vary $M^2_{D_1}$ in the range of $10^{-4} - 10^{-2}$ GeV^2, whereas $M^2_{D_{2,3}}$ are varied within 10^{-2} to 10^2 GeV^2. The δ^2_i are also varied accordingly, but keeping the constraints $(\sum M^2_{D_i})^{1/2} > (\sum \delta^2_i)^{1/4}$. The scale of $M^2_{D_i}$ has a strong influence on the decay processes $\tilde{\chi}^{\pm}_1 \to \tilde{\nu}_{1+2} + \mu^{\pm}/\tau^{\pm}$ and $\tilde{\chi}^0_j \to \tilde{\nu}_b + \nu_m$. In order to achieve a statistically significant trilepton final state originating from $\tilde{\chi}^0_2\tilde{\chi}^{\pm}_1$ pair, we would like to have $Br(\tilde{\chi}^{\pm}_1 \to \tilde{\nu}_{1+2} + \mu^{\pm}/\tau^{\pm})$ to be large and $Br(\tilde{\chi}^0_2 \to \tilde{\nu}_b + \nu_m)$ to be small, simultaneously. However, in the limit $M_{D_i} \sim M_R \sim \mathcal{O}$ (10^2 GeV), the neutrino Yukawa couplings y^i_ν are $\sim \mathcal{O}$ (1). Then as can be seen from eqs. (3.5) and (3.9) both of these decay widths are large and consequently, yields a smaller branching ratio for $\tilde{\chi}^0_2 \to \tilde{\ell}^{\pm} + \ell^{\mp}$. We observe that in this case it is rather difficult to achieve a statistically significant final state particularly for the $\tau \sum \ell\ell + \not{E}_T$ mode.

$M^2_{D_i}$ (GeV^2)	BP1	BP2	BP3	BP4
$M^2_{D_1} \times 10^4$	2.12	3.30	1.58	4.24
$M^2_{D_2}$	71.80	62.96	68.50	80.33
$M^2_{D_3}$	62.45	54.87	66.63	86.00

Table 3.3: Randomly generated values of $M^2_{D_i}$ corresponding to the four benchmark points as indicated in section 3.1.

In the trilepton signals studied in this work, one lepton comes from the lighter chargino ($\tilde{\chi}^{\pm}_1$) decay and the other two same flavor opposite sign leptons come from the second lightest neutralino ($\tilde{\chi}^0_2$) decay. Since the probability of getting electrons from the chargino decay is suppressed compared to muons or taus, events with odd number

of electrons (eee and $e\mu\mu$) should have smaller cross-sections compared to others, which is clearly reflected in the signal cross-sections. This feature is intrinsically related with the small but non-zero reactor neutrino angle [44], which will be discussed again later. In table 3.4 and 3.6 chosen trilepton $+\not{E}_T$ cross sections are shown along with the total standard model background cross section for the LHC at center-of-mass energy, $\sqrt{s} = 7$ and 14 TeV, respectively. The corresponding statistical significance of the signals are shown respectively in table 3.5 and table 3.7.

Tri-lepton events	signal σ (fb)				Background σ (fb)
	BP1	BP2	BP3	BP4	
eee	0.37	0.31	0.50	0.23	8.73
$ee\mu$	9.47	5.37	8.30	3.12	18.91
$e\mu\mu$	1.08	0.49	1.26	0.66	21.15
$\mu\mu\mu$	24.13	8.21	18.85	8.51	23.84
$ee\tau$	2.93	2.14	2.86	1.40	4.60
$\mu\mu\tau$	7.17	3.39	6.99	4.04	13.18

Table 3.4: Cross-section for different trilepton channels are shown here for four different benchmark points along with their total SM background contribution for LHC with $\sqrt{s} = 7$ TeV. Corresponding input parameters and mass spectrum are given in table 3.1, table 3.3 and table 3.2, respectively.

Tri-lepton events	Significance $\frac{S_{x\sum \ell\ell}}{\sqrt{B_{x\sum \ell\ell}+S_{x\sum \ell\ell}}}$			
	BP1	BP2	BP3	BP4
$\mu ee + \mu\mu\mu$	19.23	9.05	16.24	7.89
$\tau ee + \tau\mu\mu$	9.57	5.72	9.37	5.65

Table 3.5: Statistical significance of the studied trilepton signals with integrated luminosity 25 fb^{-1} at the LHC for $\sqrt{s} = 7$ TeV for different benchmark points.

Tri-lepton events	signal σ (fb)				Background σ (fb)
	BP1	BP2	BP3	BP4	
eee	1.29	0.91	1.56	0.75	24.92
$ee\mu$	27.63	15.65	23.50	10.48	91.64
$e\mu\mu$	3.00	1.66	3.59	2.14	117.97
$\mu\mu\mu$	65.42	24.32	53.10	26.47	85.94
$ee\tau$	8.82	6.48	9.11	4.76	29.16
$\mu\mu\tau$	20.11	9.80	18.46	12.48	56.29

Table 3.6: Cross-section for different trilepton channels are shown here for four different benchmark points along with their total SM background contribution for LHC with $\sqrt{s} = 14$ TeV. Corresponding input parameters and mass spectrum are given in table 3.1, table 3.3 and table 3.2, respectively.

Tri-lepton events	Significance $\frac{S_{x\sum \ell\ell}}{\sqrt{B_{x\sum \ell\ell}+S_{x\sum \ell\ell}}}$			
	BP1	BP2	BP3	BP4
$\mu ee + \mu\mu\mu$	28.28	13.55	24.02	12.61
$\tau ee + \tau\mu\mu$	13.53	8.07	12.97	8.50

Table 3.7: Statistical significance of the studied trilepton signals with integrated luminosity 25 fb^{-1} at the LHC for $\sqrt{s} = 14$ TeV for different benchmark points.

We can see from table 3.5 that, at the LHC even with $\sqrt{s} = 7$ TeV, the lowest signal significance for $\tau \sum \ell\ell + \not{E}_T$ final state, that we have obtained, is greater than 3σ for an integrated luminosity of 25 fb^{-1}. Hence, the trilepton $+\not{E}_T$ data for 25 fb^{-1} integrated luminosity at 7 TeV LHC should be able to constrain the theoretical parameter space of this model. These numbers (significance) are much higher for LHC with $\sqrt{s} = 14$ TeV and are shown in table 3.7. It is once again evident from these tables that a higgsino like $\tilde{\chi}_2^0\tilde{\chi}_1^\pm$ pair (BP2) yields statistically less significant specific trilepton final state. In other words for such benchmark points, the significance of the final state trilepton signal is less promising. This situation is comparable to a heavy gaugino like $\tilde{\chi}_2^0\tilde{\chi}_1^\pm$ pair as represented by BP4.

We present the correlation plots, obtained with different randomly generated values of $M_{D_i}^2$ and δ_i^2 around each of the four benchmark points. These are shown in Fig. 3.6

and Fig. 3.7 for the LHC with $\sqrt{s} = 7$ TeV and 14 TeV, respectively. We present these correlations with best fit lines.

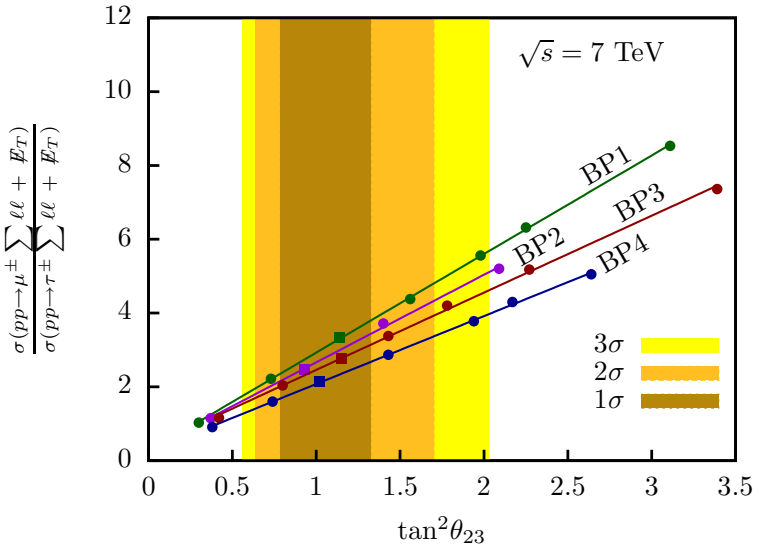

Figure 3.6: Correlation plot ($\frac{\sigma(pp\to\mu^\pm \sum \ell\ell+\not{E}_T)}{\sigma(pp\to\tau^\pm \sum \ell\ell+\not{E}_T)}$ vs $\tan^2\theta_{23}$, with $\ell = e, \mu$) obtained for LHC at $\sqrt{s} = 7$ TeV. Three differently colored vertical strips correspond to 1σ, 2σ and 3σ allowed region for $\tan^2\theta_{23}$, respectively. The benchmark points as given in table 3.1, table 3.2 and table 3.3 are represented by colored ■. Other points, represented by colored •, are obtained with randomly generated $m^2_{D_i}$ and δ^2_i values.

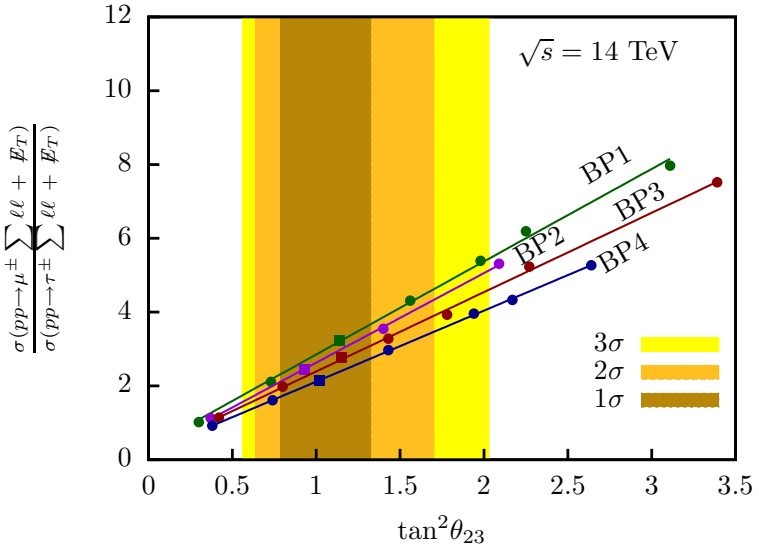

Figure 3.7: Correlation plot ($\frac{\sigma(pp\to\mu^\pm \sum \ell\ell+\not{E}_T)}{\sigma(pp\to\tau^\pm \sum \ell\ell+\not{E}_T)}$ vs $\tan^2\theta_{23}$, with $\ell = e, \mu$) obtained for LHC at $\sqrt{s} = 14$ TeV. Other specifications are the same as in Fig. 3.6.

It can be seen from these figures that the 3σ allowed value of $\tan^2\theta_{23}$ [45] from at-

mospheric neutrino oscillation experiments predict a value of the ratio of cross sections $\frac{\sigma(pp\to\mu\sum\ell\ell+\not{E}_T\ )}{\sigma(pp\to\tau\sum\ell\ell+\not{E}_T\ )}$, $(\ell = e, \mu)$ to be approximately in the range $1.0 - 6$. These predictions can be verified at the LHC or the measured value of this ratio can give an alternative estimate of $\tan^2\theta_{23}$. On the other hand, if this ratio comes out to be very much different from the ones predicted here then one can perhaps conclude that MSISM is not the correct model for explaining neutrino masses and mixing.

Nevertheless, as we can see, from the correlation plots, that there is a different linear relationship for each different kind of benchmark points. In general then, from neutrino oscillation data we cannot give a unique prediction for the ratio of the cross-sections that can be verified at the LHC and help us in constraining the model parameters. In other words, measuring the cross section ratio at the LHC would not allow a prediction of θ_{23} that could be tested against oscillation results. This means that we need other measurements at the LHC to allow such predictions. As an example, to distinguish among the four benchmark points we plot the ratio, $m_{\tilde{\chi}_1^\pm}/m_{\tilde{\nu}_{1,2}}$ with the ratio of cross-sections of μ and τ channels which gives four separate parallel lines for the four benchmark points (Fig. 3.8). One can see from Fig. 3.8 that the ratio $(m_{\tilde{\chi}_1^\pm}/m_{\tilde{\nu}_{1,2}})$

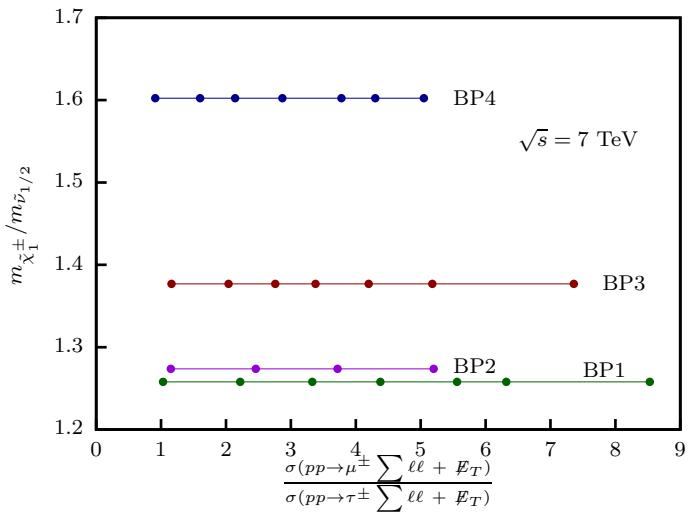

Figure 3.8: $m_{\tilde{\chi}_1^\pm}/m_{\tilde{\nu}_{1,2}}$ plotted against $\frac{\sigma(pp\to\mu^\pm\sum\ell\ell+\not{E}_T\ )}{\sigma(pp\to\tau^\pm\sum\ell\ell+\not{E}_T\ )}$ for $\sqrt{s} = 7$ TeV. The mass ratios increase as the slopes of the straight lines in Fig. 3.6 corresponding to the four benchmark points decrease.

increases as the slope of the straight lines in the correlation plot (Fig. 3.6) corresponding to different benchmark points decreases. This pattern can easily be understood. Increase in the mass ratio indicates greater splitting between the chargino and sneutrino masses. As the splitting increases, the leptons coming from this chargino decay become more energetic (Eq. 3.10). This affects the τ count in the final state more than

the μ count as the detection efficiency for the taus increases with the increase of visible energy of τ decay products [39]. Hence more τ events are expected in the final state for those benchmark points which has greater lighter chargino - LSP mass ratio for a given set of M_{D_i}'s. With the increase of τ events the ratio of the cross-sections plotted in the correlation plots decreases and as a consequence gives smaller slope compared to the previous benchmark point. Now it is clearly understood that if we can determine the lighter chargino-LSP mass ratio, we can distinguish among the four benchmark points.

Mass determination techniques in the context of LHC have been studied extensively. Transverse mass variable (m_{T_2}) [46, 47] is very useful for this purpose. m_{T_2} has also been generalized for the cases where the parent and daughter particles in the two decay chains are not identical [48, 49]. Moreover, final state with more than two invisible particles has also been addressed in ref. [50]. In our case, we observe the following:

- The lightest neutralino $\tilde{\chi}_1^0$ is also invisible, as mentioned earlier in the text.
- One lepton is produced from one side of the cascade and remaining two leptons from the other side of the cascade (Fig. 3.2).
- $\tilde{\chi}_1^\pm$ and $\tilde{\chi}_2^0$ are not mass degenerate but the difference is quite small in the context of mass measurement.

So, we see that daughters of different masses are produced here from nearly identical parents. A mass determination technique similar to refs. [48–50] can be applied here too to determine the masses of the lighter chargino and the sneutrino LSP. However, a detailed analysis in this direction is beyond the scope of the present thesis. Thus we see that measuring the mass ratio ($m_{\tilde{\chi}_1^\pm}/m_{\tilde{\nu}_{1,2}}$), along with the ratio of the trilepton cross-section, can help us pick the correct benchmark point and hence predict the correct value of θ_{23} that could be tested against the oscillation results. On the other hand, a precise determination of $\tan^2\theta_{23}$ from oscillation experiments as well as a measurement of the cross section ratio at the LHC can give a unique prediction of the mass spectrum of the model, that can be verified by mass measurements at the LHC.

In support of our explanation for obtaining different slopes, we present the following analysis. Since this difference among the four benchmark points appears because of taking different τ identification efficiencies for different energy range and for taking separate p_T cuts for μ's and τ's, we can remove this by the following strategy:

- A p_T cut of 20 GeV taken for both μ and τ.
- A uniform τ identification efficiency of 50% applied over the whole energy range.

We have presented the result in Fig. 3.9. This shows the correlation plot for 7 TeV center of mass energy under the above mentioned conditions.

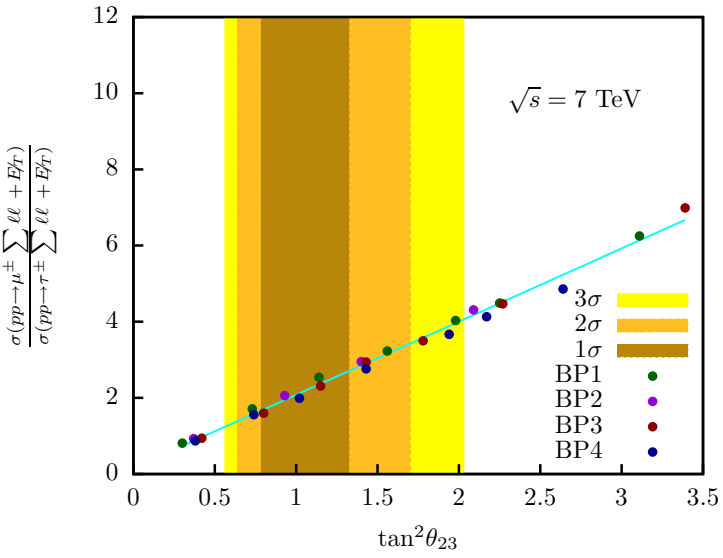

Figure 3.9: Correlation plot ($\frac{\sigma(pp\to\mu^\pm \sum \ell\ell+\not{E}_T\ )}{\sigma(pp\to\tau^\pm \sum \ell\ell+\not{E}_T\ )}$ vs $\tan^2\theta_{23}$) obtained for 7 TeV center of mass energy under the assumption of uniform τ identification efficiency ($\epsilon_\tau \sim 0.5$) and same p_T cut for both μ and τ.

All the benchmark points now lie almost on one straight line. A few points still looks a little bit scattered because of the different isolation criteria used for μ and τ.

Finally, in Table 3.8 we show the ratios $\frac{\sigma(pp\to e\mu\mu+\not{E}_T\ )}{\sigma(pp\to 3\ell+\not{E}_T\ )}$ and $\frac{\sigma(pp\to eee+\not{E}_T\ )}{\sigma(pp\to 3\ell+\not{E}_T\ )}$ for the four benchmark points. Here $\sigma(pp \to 3\ell + \not{E}_T\ )$ indicates the total trilepton cross-section including all possible combinations of e and μ in the final state.

		$\frac{\sigma(pp\to e\mu\mu+\not{E}_T\ )}{\sigma(pp\to 3\ell+\not{E}_T\ )} \times 10^2$	$\frac{\sigma(pp\to eee+\not{E}_T\ )}{\sigma(pp\to 3\ell+\not{E}_T\ )} \times 10^2$
BP1	$\sqrt{s} = 7$ TeV	3.09	1.06
	$\sqrt{s} = 14$ TeV	3.08	1.33
BP2	$\sqrt{s} = 7$ TeV	3.39	2.13
	$\sqrt{s} = 14$ TeV	3.90	2.14
BP3	$\sqrt{s} = 7$ TeV	4.35	1.71
	$\sqrt{s} = 14$ TeV	4.39	1.90
BP4	$\sqrt{s} = 7$ TeV	5.24	1.86
	$\sqrt{s} = 14$ TeV	5.38	1.89

Table 3.8: The ratios $\frac{\sigma(pp\to e\mu\mu+\not{E}_T\ )}{\sigma(pp\to 3\ell+\not{E}_T\ )}$ and $\frac{\sigma(pp\to eee+\not{E}_T\ )}{\sigma(pp\to 3\ell+\not{E}_T\ )}$ for the four benchmark points.

The smallness of these ratios is also a distinct feature of this model and arises due to the smallness of the neutrino reactor angle imposed by neutrino data [44]. In the usual MSSM scenario these ratios are expected to be much higher as there is no suppression of charginos decaying into electrons as we have in this model.

A discussion of these specific trilepton signals remains incomplete without a note on the Tevatron analysis of the considered model. For the four chosen benchmark points we observed no points with significance $\geq 3\sigma$ for the $\tau \sum \ell\ell + \not{E}_T$ final state and simultaneously consistent with the atmospheric neutrino mixing at the 3σ limit. This is a well expected result considering that the Tevatron center-of-mass energy is 1.96 TeV with 12 fb^{-1} of integrated luminosity [51]. For example, the statistical significance for $\tau \sum \ell\ell$ mode for BP1 with $M^2_{D_i}$s given in table 3.3 is computed to be 1.64.

3.4 Summary

We consider the minimal supersymmetric inverse seesaw model and study its characteristic signatures at the LHC. This model, with only one pair of singlet superfields explains existing neutrino oscillation data. The model is rich from phenomenological point of view and can lead to potentially testable signatures at the hadron colliders. In this R-parity conserving model, one of the singlet sneutrino (with a small admixture of the doublet sneutrino) is the lightest supersymmetric particle (LSP) and as a result shows up in the collider as missing energy. Charginos can decay to charged leptons plus singlet sneutrino LSP. The decay patterns of the chargino are controlled by the same parameters which generate the neutrino mixing angles.

In order to study this correlation of the chargino decays and the neutrino mixing angles, we look at specific trilepton + $\not{E}_T$ signatures at the LHC. We show that the ratios of cross sections of this studied trilepton + $\not{E}_T$ final states in certain flavor specific channels ($\mu ee + \not{E}_T$, $\mu\mu\mu + \not{E}_T$, $\tau ee + \not{E}_T$, $\tau\mu\mu + \not{E}_T$) nicely correlate with the atmospheric neutrino mixing angle. We explore different points in the parameter space to study this correlation. A measurement of these cross sections thus provide an interesting test of the minimal supersymmetric inverse seesaw model. The hard missing E_T spectrum makes this trilepton final state statistically significant by reducing certain standard model background events considerably. We adhere to different cuts to reduce the backgrounds coming from some other channels. Motivated by the recent results from the ATLAS and the CMS experiments, we work in a scenario with heavy squarks and gluinos and a relatively light electroweak sector.

The results of our analysis suggest that the theoretical parameter space of this model should already be constrained after the 7 and 8 TeV run of the LHC since there

has been no evidence of any SUSY particles. The cross-section of the trilepton final state that we have considered here is proportional to the fourth power of the relevant Dirac neutrino Yukawa coupling (y_ν). Non observation of any such signal, therefore, may be due to the fact that y_ν values are smaller than what we consider here or the gauginos are simply heavier. However, a 14 TeV run will probe further into the parameter space and unless the gauginos are too heavy or the y_ν parameters are too small, there is a possibility to observe these trilepton signatures in such scenarios. On the other hand, a measured value of the ratio of the trilepton cross-sections in μ and τ channels at the LHC can give us an alternative estimate of $\tan^2\theta_{23}$ and confirm (or rule out) this minimal supersymmetric inverse seesaw model as a possible explanation of neutrino masses and mixing. We also show, as a distinct feature of this model, the cross sections of $pp \to e\mu\mu + \not{E}_T$ and $pp \to eee + \not{E}_T$ are suppressed compared to the total chosen trilepton + $\not{E}_T$ cross section because of the restrictions on the neutrino reactor angle imposed by neutrino data.

Bibliography

[1] ATLAS Collaboration, ATLAS-CONF-2013-062; G. Aad *et al.* [ATLAS Collaboration], JHEP **1310**, 130 (2013) [arXiv:1308.1841 [hep-ex]]; G. Aad *et al.* [ATLAS Collaboration], arXiv:1405.7875 [hep-ex].

[2] CMS Collaboration, SUS-13-013, SUS-13-019, SUS-14-011.

[3] M. Hirsch, T. Kernreiter, J. C. Romao, and A. Villanova del Moral, *Minimal Supersymmetric Inverse Seesaw: Neutrino masses, lepton flavour violation and LHC phenomenology*, *JHEP* **01** (2010) 103, [0910.2435].

[4] S. Mondal, S. Biswas, P. Ghosh and S. Roy, JHEP **1205**, 134 (2012) [arXiv:1201.1556 [hep-ph]].

[5] B. Mukhopadhyaya, S. Roy, and F. Vissani, *Correlation between neutrino oscillations and collider signals of supersymmetry in an R-parity violating model*, *Phys. Lett.* **B443** (1998) 191–195, [hep-ph/9808265].

[6] E. J. Chun and J. S. Lee, *Implication of Super-Kamiokande data on R-parity violation*, *Phys. Rev.* **D60** (1999) 075006, [hep-ph/9811201].

[7] S. Y. Choi, E. J. Chun, S. K. Kang, and J. S. Lee, *Neutrino oscillations and R-parity violating collider signals*, *Phys. Rev.* **D60** (1999) 075002, [hep-ph/9903465].

[8] A. Datta, B. Mukhopadhyaya, and F. Vissani, *Tevatron signatures of an R-parity violating supersymmetric theory*, *Phys.Lett.* **B492** (2000) 324–330, [hep-ph/9910296].

[9] J. Romao, M. Diaz, M. Hirsch, W. Porod, and J. Valle, *A Supersymmetric solution to the solar and atmospheric neutrino problems*, *Phys.Rev.* **D61** (2000) 071703, [hep-ph/9907499].

[10] W. Porod, M. Hirsch, J. Romao, and J. W. F. Valle, *Testing neutrino mixing at future collider experiments*, *Phys. Rev.* **D63** (2001) 115004, [hep-ph/0011248].

[11] M. Hirsch and W. Porod, *Neutrino properties and the decay of the lightest supersymmetric particle*, *Phys.Rev.* **D68** (2003) 115007, [hep-ph/0307364].

[12] F. De Campos, O. Eboli, M. Hirsch, M. Magro, W. Porod, *et. al.*, *Probing Neutrino Oscillations in Supersymmetric Models at the Large Hadron Collider*, *Phys.Rev.* **D82** (2010) 075002, [1006.5075].

[13] M. Hirsch, A. Vicente, and W. Porod, *Spontaneous R-parity violation: Lightest neutralino decays and neutrino mixing angles at future colliders*, *Phys.Rev.* **D77** (2008) 075005, [0802.2896].

[14] P. Ghosh and S. Roy, *Neutrino masses and mixing, lightest neutralino decays and a solution to the mu problem in supersymmetry*, *JHEP* **0904** (2009) 069, [0812.0084].

[15] A. Bartl, M. Hirsch, A. Vicente, S. Liebler, and W. Porod, *LHC phenomenology of the mu nu SSM*, *JHEP* **0905** (2009) 120, [0903.3596].

[16] P. Bandyopadhyay, P. Ghosh, and S. Roy, *Unusual Higgs boson signal in R-parity violating nonminimal supersymmetric models at the LHC*, *Phys.Rev.* **D84** (2011) 115022, [1012.5762].

[17] M. Frank and H. N. Saif, *Trilepton signals from chargino - neutralino production at the CERN p p collider in a supersymmetric left-right model*, *J. Phys.* **G22** (1996) 1653–1660.

[18] **D0** Collaboration, B. Abbott *et. al.*, *Search for the trilepton signature from the associated production of SUSY $\chi_1^\pm \chi_2^0$ gauginos*, *Phys. Rev. Lett.* **80** (1998) 1591–1596, [hep-ex/9705015].

[19] V. D. Barger, C. Kao, and T.-j. Li, *Trilepton signal of minimal supergravity at the Tevatron including tau lepton contributions*, *Phys. Lett.* **B433** (1998) 328–334, [hep-ph/9804451].

[20] V. D. Barger and C. Kao, *Trilepton signature of minimal supergravity at the upgraded Tevatron*, *Phys. Rev.* **D60** (1999) 115015, [hep-ph/9811489].

[21] K. T. Matchev and D. M. Pierce, *Supersymmetry reach of the Tevatron via trilepton, like sign dilepton and dilepton plus tau jet signatures*, *Phys. Rev.* **D60** (1999) 075004, [hep-ph/9904282].

[22] H. Baer, M. Drees, F. Paige, P. Quintana, and X. Tata, *Trilepton signal for supersymmetry at the Fermilab Tevatron revisited*, *Phys. Rev.* **D61** (2000) 095007, [hep-ph/9906233].

[23] K. T. Matchev and D. M. Pierce, *New backgrounds in trilepton, dilepton and dilepton plus tau jet SUSY signals at the Tevatron*, *Phys. Lett.* **B467** (1999) 225–231, [hep-ph/9907505].

[24] M. Bisset, F. Moortgat, and S. Moretti, *Trilepton + top signal from chargino neutralino decays of MSSM charged Higgs bosons at the LHC*, *Eur. Phys. J.* **C30** (2003) 419–434, [hep-ph/0303093].

[25] Z. Sullivan and E. L. Berger, *Trilepton production at the CERN LHC: Standard model sources and beyond*, *Phys. Rev.* **D78** (2008) 034030, [0805.3720].

[26] **CDF** Collaboration, T. Aaltonen *et. al.*, *Search for Supersymmetry in p anti-p Collisions at $\sqrt{s} = 1.96$-TeV Using the Trilepton Signature of Chargino-Neutralino Production*, *Phys. Rev. Lett.* **101** (2008) 251801, [0808.2446].

[27] **D0** Collaboration, V. M. Abazov *et. al.*, *Search for associated production of charginos and neutralinos in the trilepton final state using 2.3 fb-1 of data*, *Phys. Lett.* **B680** (2009) 34–43, [0901.0646].

[28] N. Bhattacharyya and A. Datta, *Tracking down the elusive charginos / neutralinos through τ leptons at the large hadron collider*, *Phys. Rev.* **D80** (2009) 055016, [0906.1460].

[29] F. del Aguila and J. Aguilar-Saavedra, *Distinguishing seesaw models at LHC with multi-lepton signals*, *Nucl.Phys.* **B813** (2009) 22–90, [0808.2468].

[30] F. del Aguila and J. Aguilar-Saavedra, *Electroweak scale seesaw and heavy Dirac neutrino signals at LHC*, *Phys.Lett.* **B672** (2009) 158–165, [0809.2096].

[31] **CMS** Collaboration, G. L. Bayatian *et. al.*, *CMS physics: Technical design report*, . CERN-LHCC-2006-001.

[32] **Particle Data Group** Collaboration, K. Nakamura *et. al.*, *Review of particle physics*, *J. Phys.* **G37** (2010) 075021.

[33] A. Djouadi, J.-L. Kneur, and G. Moultaka, *SuSpect: A Fortran code for the supersymmetric and Higgs particle spectrum in the MSSM*, *Comput. Phys. Commun.* **176** (2007) 426–455, [hep-ph/0211331].

[34] T. Sjostrand, S. Mrenna, and P. Z. Skands, *PYTHIA 6.4 Physics and Manual*, *JHEP* **05** (2006) 026, [hep-ph/0603175].

[35] **CTEQ** Collaboration, H. L. Lai *et. al.*, *Global QCD analysis of parton structure of the nucleon: CTEQ5 parton distributions*, *Eur. Phys. J.* **C12** (2000) 375–392, [hep-ph/9903282].

[36] J. Pumplin *et. al.*, *New generation of parton distributions with uncertainties from global QCD analysis*, *JHEP* **07** (2002) 012, [hep-ph/0201195].

[37] M. L. Mangano, M. Moretti, F. Piccinini, R. Pittau, and A. D. Polosa, *ALPGEN, a generator for hard multiparton processes in hadronic collisions*, *JHEP* **07** (2003) 001, [hep-ph/0206293].

[38] A. J. Barr and C. Gwenlan, *The Race for supersymmetry: Using m(T2) for discovery*, *Phys.Rev.* **D80** (2009) 074007, [0907.2713].

[39] The CMS Collaboration, *Performance of tau reconstruction algorithms in 2010 data collected with CMS*, . CMS PAS TAU-11-001.

[40] N. Bhattacharyya, A. Datta, and S. Poddar, *Lepton Flavours at the Early LHC Experiments as the Footprints of the Dark Matter Producing Mechanisms*, *Phys. Rev.* **D78** (2008) 075030, [0807.0278].

[41] W. Beenakker, M. Klasen, M. Kramer, T. Plehn, M. Spira, and P. Zerwas, *The Production of charginos / neutralinos and sleptons at hadron colliders*, *Phys.Rev.Lett.* **83** (1999) 3780–3783, [hep-ph/9906298].

[42] N. Kidonakis and R. Vogt, *The Theoretical top quark cross section at the Tevatron and the LHC*, *Phys.Rev.* **D78** (2008) 074005, [0805.3844].

[43] M. Cacciari, S. Frixione, M. Mangano, P. Nason, and G. Ridolfi, *The t anti-t cross-section at 1.8-TeV and 1.96-TeV: A Study of the systematics due to parton densities and scale dependence*, *JHEP* **0404** (2004) 068, [hep-ph/0303085].

[44] **T2K** Collaboration, K. Abe *et. al.*, *Indication of Electron Neutrino Appearance from an Accelerator-produced Off-axis Muon Neutrino Beam*, *Phys. Rev. Lett.* **107** (2011) 041801, [1106.2822].

[45] T. Schwetz, M. A. Tortola, and J. W. F. Valle, *Three-flavour neutrino oscillation update*, *New J. Phys.* **10** (2008) 113011, [0808.2016].

[46] C. G. Lester and D. J. Summers, *Measuring masses of semiinvisibly decaying particles pair produced at hadron colliders*, *Phys. Lett.* **B463** (1999) 99–103, [hep-ph/9906349].

[47] A. Barr, C. Lester, and P. Stephens, *m(T2) : The Truth behind the glamour*, *J. Phys.* **G29** (2003) 2343–2363, [hep-ph/0304226].

[48] A. J. Barr, B. Gripaios, and C. G. Lester, *Transverse masses and kinematic constraints: from the boundary to the crease*, *JHEP* **11** (2009) 096, [0908.3779].

[49] P. Konar, K. Kong, K. T. Matchev, and M. Park, *Dark Matter Particle Spectroscopy at the LHC: Generalizing M_{T_2} to Asymmetric Event Topologies*, *JHEP* **04** (2010) 086, [0911.4126].

[50] K. Agashe, D. Kim, D. G. Walker, and L. Zhu, *Using M_{T_2} to Distinguish Dark Matter Stabilization Symmetries*, *Phys.Rev.* **D84** (2011) 055020, [1012.4460].

[51] http://www.fnal.gov/pub/now/tevlum.html.

Chapter 4

Light sneutrino Dark Matter in SISM

In this chapter we discuss the prospect of a light sneutrino DM in the context of SISM. For this purpose, we take a hybrid approach similar to that in Ref. [1], i.e. a low-energy input for the $SU(2)_L$-singlet neutrino sector and for the lepton-number violating soft SUSY-breaking sector while a top-down approach for the MSSM particle spectrum, without necessarily imposing any features of a specific Grand Unified Theory (GUT)-based model. Our goal is to examine if such a minimal Supergravity (mSUGRA) scenario with inverse seesaw can give a light DM candidate satisfying all the existing cosmological, collider as well as low-energy constraints; if so, what are the collider signals for such a scenario and how to distinguish it from a typical cMSSM scenario for similar squark-gluino spectrum at the LHC. In particular, since the sneutrino mass is not directly related to the gaugino masses, and there are additional unknown parameters in the sneutrino mass matrix, we expect the lightest sneutrino to be allowed to have masses in the few GeV range without being in conflict with the collider bounds on gluino and chargino masses.

In fact, we find that in contrast with the pure cMSSM scenario [2], we can have the sneutrino LSP mass in the few GeV range while being consistent with the SUSY search limits; however, the relic density constraint, among others, requires the lightest sneutrino mass to be more than ~ 50 GeV [3]. Though this is not consistent with the CoGeNT-preferred range of ~ 10 GeV [4] for the DM mass, it is within the 2σ-preferred range of CRESST-II [5] and also close to one of the DAMA/LIBRA-preferred mass range [6]. Moreover, the benchmark points we find around 50 GeV DM mass are all consistent with the recent hints of the lightest Higgs boson mass around 125 GeV [7,8], which is difficult to accommodate for a light neutralino DM in pure cMSSM [2,9]). This sneutrino LSP can be searched for at the LHC through a same-sign dilepton+jets+large $\not{E}_T$ signal arising from cascade decays of squarks and gluinos [3].

4.1 Searching for a light DM

In this section we search the parameter space of SISM in order to examine if such a scenario can give a light DM candidate. Then it remains to be checked whether this lightest sneutrino eigenstate has the right admixture of left- and singlet-sneutrino flavors to reproduce the observed relic density while satisfying the constraints from direct and indirect detection experiments as well as from other low-energy sectors.

We observe that the DM relic density for light sneutrino LSPs in the SISM is obtained by resonant enhancement of the annihilation cross section in the Higgs-mediated s-channel process:

$$\widetilde{\nu}_{\rm LSP}\widetilde{\nu}_{\rm LSP} \to f\bar{f}, \tag{4.1}$$

where f denotes the SM fermions, here mainly b and τ. This is illustrated in Fig. 4.1 which was obtained by choosing the input parameters in a sample range

$$\begin{aligned} &m_0 \in [0.1, 2.5]\ \text{TeV},\ m_{1/2} \in [0.65, 2.5]\ \text{TeV},\ A_0 \in [-3, 3]\ \text{TeV}, \\ &\text{diag}(y_\nu) \in [0.01, 0.2],\ (M_R)_{11} \in [100, 800]\ \text{GeV}, \end{aligned} \tag{4.2}$$

and for a fixed $\tan\beta = 10,\ \text{sign}(\mu) = +1,\ (M_R)_{22,33} = 1$ TeV, $B_{\mu_S} = 10^{-4}$ GeV^2, and $B_{M_R} = 10^6$ GeV^2. We have chosen the mSUGRA parameter ranges shown here keeping in mind the LHC exclusion limits on the cMSSM parameter space [10, 11]. We have fixed the sign of the MSSM μ-parameter to be $+1$ throughout our analysis since $\mu < 0$ is strongly disfavored by the muon anomalous magnetic moment as well as by the $B \to X_s\gamma$ branching ratio. The parameter scan was performed using `SSP` [12], with the SISM implemented in `SARAH` [13], and the sparticle spectrum was generated using `SPheno` [14], while DM relic density was calculated using `micrOMEGAs` [15].

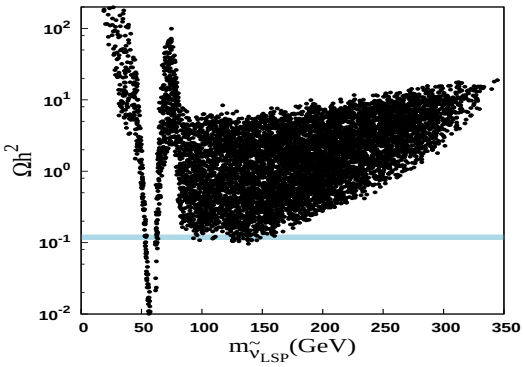

Figure 4.1: Sneutrino relic density as a function of the sneutrino LSP mass for our SISM input parameter scan. The horizontal shaded band shows the Planck 3σ preferred range.

All the points shown in Fig. 4.1 are required to have the lightest CP-even Higgs boson mass in the range 125 ± 2 GeV to be consistent with the latest LHC Higgs data [16, 17]. The horizontal blue band indicates the 3σ preferred range from Planck data: $\Omega h^2 = 0.1199 \pm 0.0081$ [18]. It is clear that for the sneutrino LSP mass below W-boson mass, the observed DM relic density is obtained only near the Higgs-resonance region, thus requiring the sneutrino DM mass in the SISM to be around $m_h/2$. The other possible resonance around $m_Z/2$ is suppressed in this case due to small mixing between the $SU(2)_L$-doublet and singlet neutrinos, as required to satisfy the Z-invisible decay width constraint from LEP [19]. Note that in Fig. 4.1, the observed relic density can also be satisfied for sneutrino LSP in the 80 - 200 GeV mass range due to its large annihilation rate into WW, ZZ and hh final states.

The same interaction that leads to the Higgs-mediated s-channel annihilation of the sneutrino DM in our model also leads to a direct detection signal via t-channel Higgs boson exchange. In Fig. 4.2 we have plotted the spin-independent DM-nucleon scattering cross section predictions as a function of the sneutrino LSP mass for the corresponding points in Fig. 4.1. We also show the subset of points satisfying the relic density constraints.

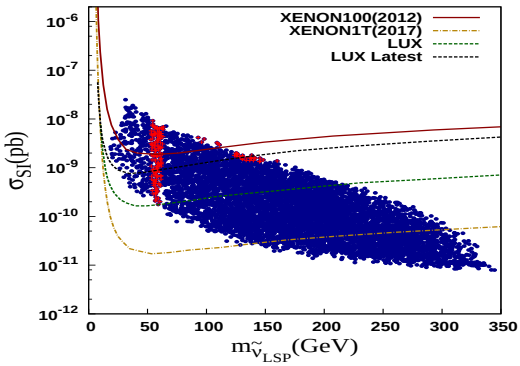

Figure 4.2: Spin-independent direct detection cross section as a function of the sneutrino LSP mass for our SISM parameter scan. The red (+) points satisfy relic density $\lesssim 0.13$. The current experimental limit from XENON100, LUX and the projected limits from LUX and XENON1T are also shown.

The solid line indicates the current limit from XENON100 [20] and LUX data [21]. We also show the projected limits from XENON1T [22] and LUX [23] experiments. As evident from the plot, a few of the allowed points are already ruled out by the XENON100 data, while *all* of the low-mass points satisfying the relic density constraints can be ruled out by LUX and XENON1T projected limits in case of a null result.

From Fig. 4.1 and 4.2 we infer that it is indeed possible to have the lightest Higgs

boson decaying into two sneutrino LSPs, while satisfying the DM relic density and direct detection constraints. We have also checked that all the points shown in Fig. 4.1 and 4.2 are well below the current indirect detection cross section limits from Fermi-LAT [24, 25].

4.2 Some Benchmark Points

Our goal in this section is to find a sparticle spectrum with light sneutrino LSP in the cMSSM scenario with 5 parameters ($m_0, m_{1/2}, \tan\beta, A_0, \text{sgn}\ \mu$) and the additional inverse seesaw parameters $\mu_S, M_R, M_D, B_{\mu_S}$ and B_{M_R}. Once we find a light sneutrino LSP, we require it to satisfy the relic density and direct detection constraints in order be the DM candidate. We also require all the benchmark points to satisfy various collider and low-energy constraints, summarized in Table 4.1. A few comments:

- For the lightest Higgs mass, we use the CMS suggested value of $125.3 \pm 0.4(\text{stat}) \pm 0.5(\text{syst})$ [26]. The ATLAS suggested central value is around 126.5 GeV [27] with presumably similar experimental uncertainties; for concreteness, we just choose to work with the CMS value which has the errors explicitly stated [1].

- For the spin-independent WIMP-nucleon scattering cross-section, we use the 2σ upper limit of the latest XENON100 results [20][2].

- There also exist some constraints on light sneutrino DM from indirect detection searches, e.g. the searches for high-energy neutrinos from the Sun produced by annihilation of these sneutrinos [37]. However, for small admixtures of the left sneutrino component (allowed by Z-invisible decay width) in a mostly dominant singlet sneutrino LSP eigenstate, these constraints are easily satisfied, and hence, we do not discuss them further.

- The lepton anomalous magnetic moments as shown in Table 4.1 are defined as $\Delta a_\ell = a_\ell^{\text{SM}} - a_\ell^{\text{expt}}$ where $a_\ell = (g-2)_\ell/2$. The most important one is the muon anomalous magnetic moment which persistently shows a 3σ discrepancy [32] over the SM prediction and has to be taken into account in any complete beyond SM scenario. For the electron $(g-2)$, the discrepancy is quite small and is a

[1] The most recently updated Higgs boson mass quoted by CMS is 124.7 ± 0.34 GeV [7]. The updated value provided by ATLAS for the same is 125.4 ± 0.4 GeV [8]. However, these changes in Higgs Boson mass data do not affect our analysis or overall conclusion.

[2] More recent LUX results [21] constrains the scattering cross-section value further. However, our benchmark points are still consistent within their 2σ error bar.

Quantity	Value	Source
G_F	$1.1663787(6) \times 10^{-5}$ GeV^{-2}	[28]
$\alpha_s(m_Z)$	0.1184 ± 0.0007	[29]
m_Z	91.1876(21) GeV	[28]
m_τ	1.77682(16) GeV	[28]
m_b	4.19 ± 0.12 GeV	[28]
m_t	173.2 ± 0.9 GeV	[30]
m_h	125.3 ± 0.7 GeV	[7]
$\Gamma_Z^{\text{invisible}}$	< 3.0 MeV	[19]
$\Omega_{\text{CDM}}h^2$	0.112 ± 0.006	[31]
σ_{SI}	$< 5 \times 10^{-9}$ pb	[20]
Δa_μ	$(26.1 \pm 8.0) \times 10^{-10}$	[32]
Δa_e	$(109 \pm 83) \times 10^{-14}$	[33]
$\text{BR}(B \to X_s\gamma)$	$(3.21 \pm 0.33) \times 10^{-4}$	[34]
$\text{BR}(B_s^0 \to \mu^+\mu^-)$	$< 4.5 \times 10^{-9}$	[35]
$\text{BR}(\mu \to e\gamma)$	$< 2.4 \times 10^{-12}$	
$\text{BR}(\tau \to e\gamma)$	$< 3.3 \times 10^{-8}$	
$\text{BR}(\tau \to \mu\gamma)$	$< 4.4 \times 10^{-8}$	
$\text{BR}(\mu \to 3e)$	$< 1.0 \times 10^{-12}$	[28]
$\text{BR}(\tau \to 3e)$	$< 2.7 \times 10^{-8}$	
$\text{BR}(\tau \to 3\mu)$	$< 2.1 \times 10^{-8}$	
$\text{BR}(\tau \to e\mu\mu)$	$< 1.7 \times 10^{-8}$	
$\text{BR}(\tau \to ee\mu)$	$< 1.5 \times 10^{-8}$	
$\lvert\eta\rvert_{ee}$	0.002 ± 0.005	
$\lvert\eta\rvert_{\mu\mu}$	0.003 ± 0.005	
$\lvert\eta\rvert_{\tau\tau}$	0.003 ± 0.005	
$\lvert\eta\rvert_{e\mu}$	$< 7.2 \times 10^{-5}$	[36]
$\lvert\eta\rvert_{e\tau}$	$< 1.6 \times 10^{-2}$	
$\lvert\eta\rvert_{\mu\tau}$	$< 1.3 \times 10^{-2}$	

Table 4.1: Various experimental constraints used in our analysis to find the benchmark points.

rather loose constraint on the new physics parameter space. We do not consider the tau anomalous magnetic moments here, because its value is not known so precisely [28].

- The non-unitarity of the light neutrino mixing matrix is defined in Eq. (2.11) and the constraints on its elements shown in Table 4.1 are derived from a combination of neutrino oscillation data, precision data from weak gauge boson decays and the LFV decays [36].

There are also strong constraints on the cMSSM parameter space from direct SUSY searches at the LHC [10, 11]. Therefore, we must choose the input points in the $(m_0, m_{1/2})$-plane not already excluded by the LHC SUSY searches which for certain cases extends to $m_{1/2} \lesssim 600$ GeV and $m_0 \lesssim 1$ TeV[3] (e.g. in the jets+missing transverse energy search channel [38]). On the other hand, very large values of m_0 and $m_{1/2}$ (larger than a few TeV) are not desirable from phenomenological perspective as they drive most of the sparticle masses beyond the kinematic reach of the LHC. Therefore, we choose our m_0 value close to 1 TeV and the $m_{1/2}$ value close to 600 GeV. We also choose to work with $\mu > 0$ case, since $\mu < 0$ is strongly disfavored by the muon anomalous magnetic moment as well as by the $B \to X_s\gamma$ branching ratio [39]. Similarly, large $\tan\beta$ values $\gtrsim 50$ are disfavored by the recent LHCb results on $B_s \to \mu^+\mu^-$ [35], and hence, we choose some intermediate values between 25 and 35 for the benchmark points discussed below. For the trilinear term A_0, the recent LHC discovery of a SM Higgs-like particle at 125 GeV [7, 8] implies that we must have a large negative A-term (for $\mu > 0$) in order to have the radiative corrections account for the required enhancement of the lightest Higgs boson mass from its tree level value close to m_Z [40].

In the neutrino sector, for simplicity, we assume the inverse seesaw parameter matrices M_D, M_R as well as the B-terms, B_{μ_S}, B_{M_R}, to be diagonal. Hence we can easily satisfy the LFV constraints for our benchmark points. Allowing non-zero off-diagonal entries in the Dirac Yukawa will induce large LFV effects, and we find that for the benchmark points discussed in the following section, we must have the off-diagonal entries less than $\sim \mathcal{O}(0.01)$ in order to satisfy all the LFV decay modes listed in Table 4.1. Moreover, we assume no CP-violation in the neutrino sector, and choose all the mass matrices to be real[4]. Fixing both M_D and M_R also fixes the lepton-number breaking Majorana mass matrix μ_S by fitting to the neutrino mass and mixing parameters (assuming a normal or inverted hierarchy for the neutrino masses). Also note that since we are assuming a complete unification of the scalar sector, we choose $m_L^2 = m_N^2 = m_S^2 = m_0^2$ at the high scale and similarly for the A-terms.

The input parameters are chosen in such a way that all the experimental constraints listed in Table 4.1 are satisfied for all the benchmark points. Table 4.2 lists all the input

[3]Consequences of the updated cMSSM search results are discussed in the end.

[4]Introducing one or more CP-phases in the neutrino sector will not change the sparticle spectrum and hence our results in the subsequent sections.

parameters for three benchmark points we have chosen to work with.

Input parameter	BP1	BP2	BP3
m_0 (GeV)	993.28	996.45	815.48
$m_{1/2}$ (GeV)	600	650	600
A_0 (GeV)	-2712.11	-2858.42	-2442.11
$\tan\beta$	35	25	30
y_ν	(0.161,0.160,0.180)	(0.100,0.100,0.080)	(0.103,0.100,0.100)
M_R (GeV)	(300,1000,1000)	(200,1000,1000)	(610,1000,1000)
B_{μ_S} (GeV^2)	10	10	10
B_{M_R} (GeV^2)	10^6	10^6	10^6

Table 4.2: The input parameters for three chosen BPs. The mSUGRA parameters are defined at the high scale whereas the singlet neutrino parameters are at the low scale. We assume $\mu > 0$ throughout and the neutrino sector parameters shown here have been chosen to be diagonal.

For the low-energy values of y_ν and M_R given in Table 4.2, the observed neutrino mass and mixing parameters can be fit using appropriate values for the mass matrix μ_S in Eq. (2.8). For example, for a normal hierarchy of neutrino masses, using the latest global fit values provided in Table 1.3, we obtain the following values for μ_S for the three BPs shown above:

$$\mu_S = \begin{cases} \begin{pmatrix} 0.54 & 3.01 & 0.99 \\ 3.01 & 34.89 & 24.94 \\ 0.99 & 24.94 & 29.64 \end{pmatrix} \text{ eV} & \text{(BP1)} \\ \begin{pmatrix} 0.62 & 5.18 & 2.39 \\ 5.18 & 89.42 & 89.91 \\ 2.39 & 89.91 & 150.29 \end{pmatrix} \text{ eV} & \text{(BP2)} \\ \begin{pmatrix} 5.48 & 15.38 & 5.67 \\ 15.38 & 89.38 & 71.89 \\ 5.67 & 71.89 & 96.13 \end{pmatrix} \text{ eV} & \text{(BP3)} \end{cases} \tag{4.3}$$

The low-energy mass spectrum for the superpartners corresponding to the BPs are tabulated in Table 4.3.

Sparticle	Notation	BP1	BP2	BP3
Sneutrino	$(\widetilde{\nu}_1^R, \widetilde{\nu}_1^I)$	(53.2155,53.3030)	(53.4623,53.5529)	(62.6587,62.7365)
	$(\widetilde{\nu}_2^R, \widetilde{\nu}_2^I)$	(834.7887,834.7890)	(953.3586,953.3598)	(743.3109,743.3119)
	$(\widetilde{\nu}_3^R, \widetilde{\nu}_3^I)$	(930.6762,930.6810)	(965.9735,965.9784)	(785.4476,785.4536)
	$(\widetilde{\nu}_4^R, \widetilde{\nu}_4^I)$	(951.2057,951.2105)	(987.8791,987.8829)	(798.8994,798.9046)
	$(\widetilde{\nu}_5^R, \widetilde{\nu}_5^I)$	(1033.8279,1033.8280)	(1065.9683,1065.9683)	(890.1739,890.1739)
	$(\widetilde{\nu}_6^R, \widetilde{\nu}_6^I)$	(1042.0259,1042.0261)	(1068.5116,1068.5118)	(893.2873,893.2875)
	$(\widetilde{\nu}_7^R, \widetilde{\nu}_7^I)$	(1419.8892,1419.8929)	(1415.7879,1415.7916)	(1420.8748,1420.8784)
	$(\widetilde{\nu}_8^R, \widetilde{\nu}_8^I)$	(1715.9050,1715.9081)	(1723.9674,1723.9704)	(1627.6817,1627.6848)
	$(\widetilde{\nu}_9^R, \widetilde{\nu}_9^I)$	(1717.9193,1717.9224)	(1726.3187,1726.3217)	(1627.9388,1627.9419)
Slepton	$\widetilde{e}_1$	1018.4017	1025.3009	846.0540
	$\widetilde{e}_2$	1039.4223	1068.9554	893.5697
	$\widetilde{\mu}_1$	1016.6171	1024.4000	844.8843
	$\widetilde{\mu}_2$	1036.3724	1068.5514	893.2266
	$\widetilde{\tau}_1$	513.3771	769.2830	493.4275
	$\widetilde{\tau}_2$	855.9634	973.0149	768.0038
Squark	$\widetilde{u}_1$	1535.0033	1607.4852	1433.9501
	$\widetilde{u}_2$	1569.3038	1645.7291	1471.1607
	$\widetilde{c}_1$	1534.9761	1607.4576	1433.9246
	$\widetilde{c}_2$	1569.1360	1645.6110	1471.0347
	$\widetilde{t}_1$	634.1909	625.0202	613.7963
	$\widetilde{t}_2$	1151.5795	1247.0666	1125.2610
	$\widetilde{d}_1$	1531.6198	1603.3921	1430.2297
	$\widetilde{d}_2$	1571.0874	1647.4075	1473.0788
	$\widetilde{s}_1$	1531.5088	1603.3235	1430.1499
	$\widetilde{s}_2$	1570.9203	1647.2877	1472.9519
	$\widetilde{b}_1$	1087.7751	1194.3270	1061.8161
	$\widetilde{b}_2$	1304.0222	1459.9815	1265.4400
Gluino	$\widetilde{g}$	1401.3910	1505.3351	1392.6117
Neutralino	$\widetilde{\chi}_1^0$	264.3308	286.2447	261.8328
	$\widetilde{\chi}_2^0$	499.2369	539.7525	495.2370
	$\widetilde{\chi}_3^0$	-1376.4775	-1464.4092	-1295.2559
	$\widetilde{\chi}_4^0$	1379.5117	1467.4517	1298.6826
Chargino	$\widetilde{\chi}_1^\pm$	499.4382	539.9501	495.4381
	$\widetilde{\chi}_2^\pm$	1380.0818	1467.8795	1299.2079

Table 4.3: The sparticle masses (in GeV) for the chosen benchmark points. The values are shown up to four decimal places to illustrate the lifting of degeneracy between the sneutrino mass eigenstate pairs due to the small lepton number breaking.

Note that the sneutrino real scalar fields $(\widetilde{\nu}_i^I, \widetilde{\nu}_i^R)$ are split in their masses with the mass splitting in the range of keV-MeV within each pair which is a characteristic feature of the SUSY inverse seesaw mechanism [41]. In later sections, we denote the lightest mass eigenstate pair $(\widetilde{\nu}_1^I, \widetilde{\nu}_1^R)$ simply by $\widetilde{\nu}_1$.

It is clear from Table 4.3 that all the BPs satisfy the direct search limits on the SUSY particle masses in cMSSM. They also satisfy the other low-energy experimental constraints in Table 4.1, as shown in Table 4.4. These constraints, e.g, LFV decay branching ratios, lepton anomalous magnetic moments and the B-Physics constraints were evaluated using `SPheno`.

Parameter	BP1	BP2	BP3
m_h	123.2	123.4	123.2
$\Omega_{\rm DM}h^2$	0.118	0.108	0.112
$\sigma_{\rm SI}$ (pb)	3.6×10^{-9}	5.1×10^{-10}	1.4×10^{-9}
$< \sigma_A v > (cm^3 s^{-1})$	1.72×10^{-27}	3.33×10^{-28}	3.49×10^{-25}
δa_μ	5.2×10^{-10}	3.4×10^{-10}	5.5×10^{-10}
δa_e	1.2×10^{-14}	7.8×10^{-15}	1.3×10^{-14}
BR$(B \to X_s\gamma)$	2.7×10^{-4}	2.8×10^{-4}	2.7×10^{-4}
BR$(B_s \to \mu^+\mu^-)$	4.3×10^{-9}	3.7×10^{-9}	4.1×10^{-9}
BR$(\mu \to e\gamma)$	5.6×10^{-21}	6.6×10^{-22}	3.3×10^{-21}
BR$(\tau \to e\gamma)$	1.1×10^{-19}	1.2×10^{-20}	6.2×10^{-20}
BR$(\tau \to \mu\gamma)$	1.7×10^{-15}	2.1×10^{-16}	1.0×10^{-15}
BR$(\mu \to 3e)$	4.6×10^{-22}	1.1×10^{-22}	2.6×10^{-23}
BR$(\tau \to 3e)$	3.4×10^{-21}	7.4×10^{-22}	7.3×10^{-22}
BR$(\tau \to 3\mu)$	1.1×10^{-15}	2.9×10^{-16}	7.4×10^{-18}
$\lvert\eta_{ee}\rvert$	4.3×10^{-3}	3.8×10^{-3}	4.3×10^{-4}
$\lvert\eta_{\mu\mu}\rvert$	3.9×10^{-4}	1.5×10^{-4}	1.5×10^{-4}
$\lvert\eta_{\tau\tau}\rvert$	4.9×10^{-4}	9.7×10^{-5}	1.5×10^{-4}

Table 4.4: The low-energy observables for the three chosen BPs. These values are to be compared with the experimental values in Table 4.1.

Here we want to make some comments on these observables:

- It is well known that a 125 GeV mass for the lightest neutral Higgs boson in a cMSSM scenario is not very natural [42]. It becomes even more difficult if one has to satisfy the other low-energy constraints and requires the neutralino LSP to have the observed relic density [9]. The situation is very similar in our case;

however, our chosen benchmark points have the lightest Higgs boson mass close to the recently suggested LHC value around 125 GeV. Since fixing the exact mass of the suspected scalar resonance at the LHC will require more data, we are content with values within 2 GeV of the average of the CMS and ATLAS central values [7, 8]. We believe that any tweaking of parameters to confirm the exact Higgs boson mass, when it is known with greater precision, will not affect the general conclusions of this work.

- The correct relic density is obtained near the resonant enhancement region of the annihilation cross-section in the Higgs-mediated s-channel process: $\widetilde{\nu}_1\widetilde{\nu}_1 \to f\bar{f}$ where f denotes the SM fermion (mostly b and τ final states). Therefore, all our benchmark points have the LSP mass close to $m_h/2$. This is illustrated in Fig. 4.1. We also find that the sneutrino DM spin-independent elastic[5] cross section with nucleons is within the upper bound of the latest XENON100 and LUX result except for BP1 which is slightly above their 2σ limit.

- The SUSY contributions to Δa_μ have been calculated to the two-loop order [43] and it has been shown that for a range of parameter space, it is possible to accommodate the discrepancy. As can be seen from Tables 4.1 and 4.4, we are able to explain the discrepancy within 3σ for all our benchmark points. Also for the electron anomalous magnetic moment, we are consistent with the smaller discrepancy to within 1σ.

- The SM prediction for the branching ratio of the weak radiative B-meson decay is $(3.15 \pm 0.23) \times 10^{-4}$ [44], and comparing with the most recent experimental value from BABAR as given in Table 4.1, we see that there is very little room left for the SUSY contribution in this case [45]. However, for the choice of our mSUGRA parameters, we find the values predicted for all our BPs to be within 2σ of the experimental value. Similarly, for the branching ratio of the FCNC process $B_s^0 \to \mu^+\mu^-$, the SM prediction is $(3.2 \pm 0.2) \times 10^{-9}$ [46]; so comparable SUSY contributions [47] are still allowed by the current experimental limits from LHCb. We estimated that the BRs for our BPs are within this allowed range.

- For the rare lepton flavor violating (LFV) decays, since we are working within an mSUGRA scenario, the SUSY contributions are quite small [48]. However, the contributions from the leptonic sector could be large in seesaw models with large

[5]Note here that the splitting between the lightest sneutrino mass eigenstates for our benchmark points is of order of a few MeVs which is too large for inelastic DM-nucleon scattering to occur. Hence we only consider the elastic scattering.

Yukawas [49], as in our case. However, due to our choice of the diagonal textures for the Dirac Yukawas, the leptonic contributions also vanish altogether. Hence, we have very small LFV BRs for all the BPs.

- The non-unitarity effects could, in principle, be large in low-scale inverse seesaw models with large Dirac Yukawas [50–52]. In our case, again due to the diagonal textures chosen for both M_D and M_R, the non-unitarity parameter defined by Eq. (2.11) is also a diagonal matrix. Hence we only show the values for the diagonal entries in Table 4.4, and it is clear that all our values satisfy the current experimental bounds.

We also note that in our scenario, since the sneutrino LSP is sufficiently light, the lightest neutral Higgs boson can in principle decay into a pair of LSP's thus giving rise to an invisible decay width of the Higgs boson. The LHC signatures of these decays are relatively clean, and very large branching ratios to invisible decay channel are disfavored by the current LHC searches [53]. The branching ratio depends, among other things, on the neutrino Yukawa coupling y_ν. Recent global analyses [54][6] have reported that the present LHC Higgs data can indeed accommodate an invisible branching ratio for the Higgs boson, although the best fit values they obtain for the allowed branching ratio vary a little bit. If such a possibility is more precisely fixed by future data, it may lead to an estimate of the bounds on the neutrino Yukawa couplings in the inverse seesaw models which could be compared with those obtained from direct Higgs search results [56]. This possibility will be explored in the next chapter in some detail.

We have thus demonstrated convincingly that (a) a hybrid scenario for the origin of soft SUSY-breaking masses can be used consistently with the inverse seesaw mechanism, (b) one can have a sneutrino LSP which is light and still consistent with all the existing experimental constraints, and (c) the rest of the SUSY spectrum is phenomenologically viable. The next question to ask is: Is there any distinctive signature of this scenario which can be seen at the LHC? We address this question in the next section.

4.3 Collider Signatures

The most copious collider signals of any SUSY scenario will come from the production of colored superpartners, namely squarks and gluinos, which will have cascade decays through charginos and neutralinos, eventually ending up in the stable LSP in R-parity

[6]For a similar analysis with the earlier LEP/Tevatron/XENON/WMAP data and a 50-60 GeV scalar DM scenario as in our case, see Ref. [55].

conserving SUSY models [57]. Unless the squarks and gluinos are too heavy to be kinematically accessible, they will have substantial production cross sections at a hadron collider due to strong interaction. The production channels are gluino pair production, squark-gluino associated production and squark-squark pair production (see Fig. 4.3). As the direct decay of the squarks and gluinos to the color- and electrically-neutral LSP are either forbidden or occur with only a tiny branching fraction, the dominant decay modes for the gluino always involve quarks (and hence multiple jets in the final states). Gluino can have either the two-body decay via $\widetilde{g} \to q\widetilde{q}$ if kinematically allowed, or the three-body decay modes $\widetilde{g} \to q\bar{q}'\widetilde{\chi}_i^{\pm}$, $q\bar{q}\widetilde{\chi}_j^0$ with virtual squarks. Similarly, squarks decay to two-body modes $\widetilde{q} \to q\widetilde{g}$ if kinematically allowed, or $\widetilde{q}_L \to q'\widetilde{\chi}_i^{\pm}$, $q\widetilde{\chi}_j^0$, while $\widetilde{q}_R \to q\widetilde{\chi}_j^0$ only, since right-handed squarks do not couple to charginos in MSSM. If squarks are degenerate, and Yukawa coupling effects negligible, the three-body decays to the wino-like chargino and neutralino usually have larger branching fractions due to their larger gauge couplings. If $|\mu| < M_2$, gluinos and squarks may thus decay most of the time to the heavier charginos and neutralinos, resulting in lengthier cascade decay chains than those shown in Fig. 4.3.

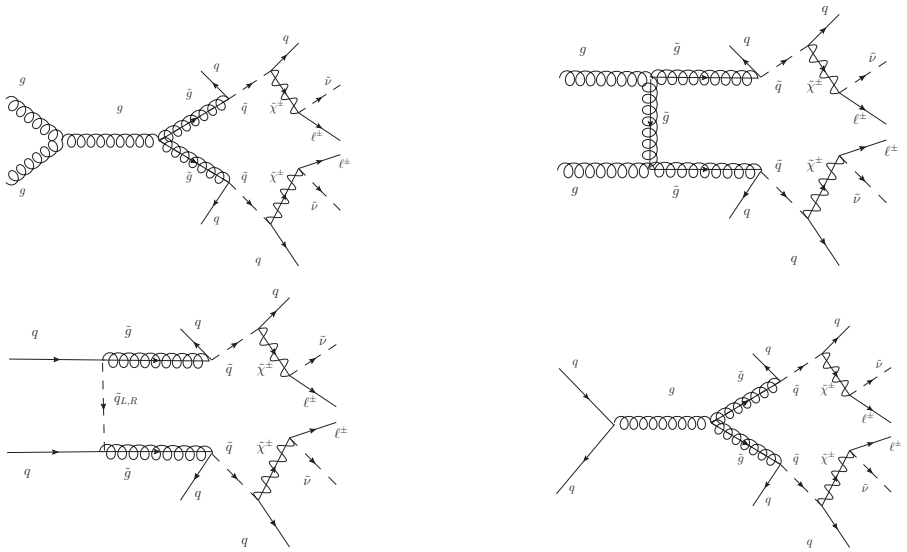

Figure 4.3: The Feynman diagrams for the gluino pair-production and its cascade decays to give the same-sign dilepton+jets+$\not{E}_T$ signal at the LHC. Similar diagrams exist for squark-gluino and squark-squark production and decay which we have not shown here.

The LHC signals of our scenario can differ considerably from those of the pure cMSSM situation. To understand this, let us look at the branching ratios of the two-body decays of the lighter chargino ($\widetilde{\chi}_1^+$) which are listed in Table 4.5 for all of our

benchmark points.

Chargino ($\widetilde{\chi}_1^+$) decay	BP1	BP2	BP3
$W^+\widetilde{\chi}_1^0$	0.23	0.45	0.31
$\ell^+\widetilde{\nu}_1$	0.77	0.55	0.69

Table 4.5: The lighter chargino decay branching ratios for our benchmark points in SISM. On the other hand, in the cMSSM case with neutralino LSP, the branching ratio is close to 100% for the decay $W^+\widetilde{\chi}_1^0$.

While the conventionally expected decay $\widetilde{\chi}_1^+ \to W^+\widetilde{\chi}_1^0$ is there, it is dependent on the $\widetilde{W}_3^0$ components of $\widetilde{\chi}_1^0$ as well as the Higgsino components of both $\widetilde{\chi}_1^+$ and $\widetilde{\chi}_1^0$. On the other hand, here we have another often dominant channel, namely $\widetilde{\chi}_1^+ \to \ell^+\widetilde{\nu}_1$ (where $\widetilde{\nu}_1$ is the sneutrino LSP and $\ell = e, \mu$) triggered by the large mixing in the sneutrino sector[7]. Consequently, the leptonic branching ratio of the $\widetilde{\chi}_1^+$ is remarkably enhanced[8]. Thus the SUSY cascades lead to a highly boosted rate of dileptons, of which the same-sign dileptons (SSD) are more spectacular being relatively background-free. The scenario outlined by us will therefore exhibit a rise in the SSD rate with respect to that of purely (jets+$\not{E}_T$) events, as compared to a pure cMSSM spectrum of comparable heaviness. We also expect the $\not{E}_T$ distribution to be different for a sneutrino LSP case than in case of neutralino LSP, as noted earlier in Ref. [58]. In particular, in our SISM scenario, the $\not{E}_T$ distribution is expected to be much harder compared to the cMSSM scenario.

To illustrate this SSD-enhancement effect in our case compared to the pure cMSSM scenario, we construct a ratio as follows:

$$r = \frac{\sigma(\ell^\pm\ell^\pm + \geq 2j + \not{E}_T)}{\sigma(0\ell + \geq 3j + \not{E}_T)} \tag{4.4}$$

which is expected to be more in our case. As shown in the next section, this variable could be used to distinguish our scenario with sneutrino LSP from a pure cMSSM scenario with neutralino LSP.

Here we want to emphasize that the SSD signal in inverse seesaw is purely supersymmetric in nature. In other words, if one leaves aside the SUSY processes, the SSD

[7] ℓ is mostly electron for our choice of benchmark points, though cases with muons do not make any difference in our analysis. We discuss more about this at the end of this chapter. Since the tau-lepton detection efficiency is not as good as electron and muons, we will not analyze the tau-lepton final states.

[8] Note that all charged sleptons are heavier than the lighter chargino in our case.

signal is suppressed due to the small lepton number violation and pseudo-Dirac nature of the singlet neutrinos. In that case, however, one can look for tri-lepton signals with $\not{E}_T$ for its LHC discovery potential [59].

4.4 Event Generation, Background Simulation and Results

In this section, we give a detailed description of the SSD+jets+$\not{E}_T$ signal in our SISM case with light sneutrino LSP and a comparison of the signal strength with a canonical MSSM scenario with neutralino LSP having similar squark-gluino spectrum for a possible distinction of the two cases at the $\sqrt{s} = 14$ TeV LHC. The SUSY spectrum and the various decay branching fractions were calculated using `SPheno` [14]. The input files are then fed to `PYTHIA` (version 6.409) for event generation. Initial and final state quark and gluon radiation, multiple interaction, decay, hadronization, fragmentation and jet formation are implemented following the standard procedures in `PYTHIA`. Factorization and renormalization scales are set at $\sqrt{\hat{s}}$ (i.e $\mu_R = \mu_F = \sqrt{\hat{s}}$), where $\sqrt{\hat{s}}$ is the parton level center of mass energy. We have used the leading order `CTEQ5L` parton distribution functions for the colliding protons. The jets are constructed using cone algorithm in `PYCELL`. Only those jets are constructed which have $p_T > 20$ GeV and $|\eta| < 2.5$. To simulate detector effects we have taken into account the smearing of jet energies by a Gaussian probability density function [61].

In order to find same-sign di-leptons+n jets+$\not{E}_T$ (with $n \geq 2$) in the final states, we impose the following selection criteria:

- $p_T^\ell > 10$ GeV and $|\eta^\ell| < 2.4$ for both leptons. For same-flavor dilepton final states, we raise it to $p_T^\ell > 15$ GeV.
- Lepton-lepton separation $\Delta R_{\ell\ell} > 0.2$, where $\Delta R = \sqrt{(\Delta\eta)^2 + (\Delta\phi)^2}$.
- Lepton-jet separation $\Delta R_{\ell j} > 0.4$.
- The sum of E_T deposits of the hadrons which fall within a cone of $\Delta R \leq 0.2$ around a lepton, must be less than $0.2 p_T^\ell$.
- Jet-jet separation $\Delta R_{jj} > 0.4$.

Since our goal is to distinguish the SUSY inverse seesaw scenario from the conventional cMSSM case, we need to consider similar squark-gluino spectrum for both the cases. In order to do so, we generated similar benchmark points for the cMSSM case using

the same mSUGRA input parameters given in Table 4.2 and also checked that the effective mass distributions, defined as the scalar sums of the lepton, jet and missing transverse energy:

$$M_{\rm eff} = \sum |p_T^{\ell}| + \sum |p_T^{j}| + \not{E}_T \ , \tag{4.5}$$

are similar for both the scenarios, as shown in Fig. 4.4 for all the benchmark points.

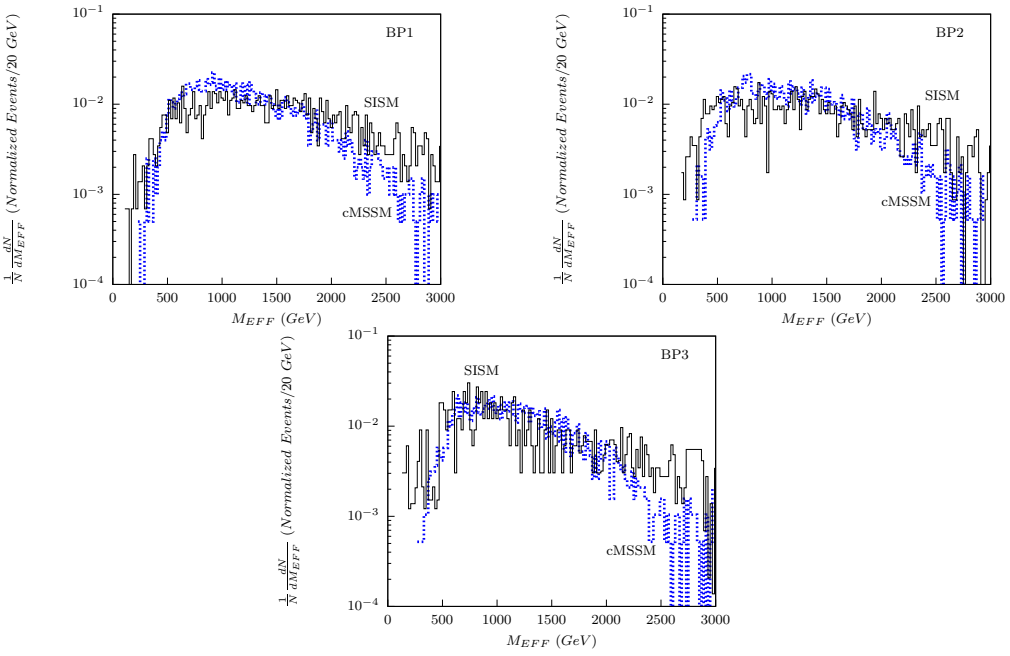

Figure 4.4: The effective mass distribution of the final states as defined in Eq. (5.1) for the SISM and pure cMSSM scenarios to illustrate that the squark-gluino spectrum considered in both cases are similar.

Now in order to distinguish the two scenarios, we compute the ratio r defined in Eq. (4.4) for both SISM and cMSSM cases which are tabulated in Table 4.6.

r	BP1	BP2	BP3
SISM	0.19	0.15	0.11
cMSSM	0.04	0.03	0.03

Table 4.6: The r values for all the benchmark points in both SISM and cMSSM cases.

We find that the value of r in the SISM case is roughly 4-5 times than in case of cMSSM for all the benchmark points. Apart from this clear distinction, we also expect more $\not{E}_T$ in the chargino decay in case of SISM, as mentioned earlier. In order to

illustrate this, we need to analyze the $\not{E}_T$ distribution for the SSD+$\geq 2j + \not{E}_T$ signal for both SISM and cMSSM cases. We also need to analyze the SM backgrounds in detail.

The dominant SM background for SSD events come from $t\bar{t}$, $Wt\bar{t}$, WWW, $WWnj$, $WZnj$, ZZ, $Wb\bar{b}$, $Zb\bar{b}$ final states at the LHC [60]. All SM backgrounds except the $t\bar{t}$ were generated at the parton level using `ALPGEN` (version 2.14) with default factorization and renormalization scales, and then fed to `PYTHIA` for showering, hadronization, fragmentation, decay, etc. The $t\bar{t}$ background was directly generated and analyzed in `PYTHIA`.

The $\not{E}_T$ distributions for both SISM and cMSSM cases are shown in Fig. 4.5 for all the benchmark points. It is clear that the SISM case has a much harder $\not{E}_T$ tail compared to the cMSSM case, which can be used as a distinguishing feature. The combined SM background is also shown which falls rapidly for $\not{E}_T > 300$ GeV.

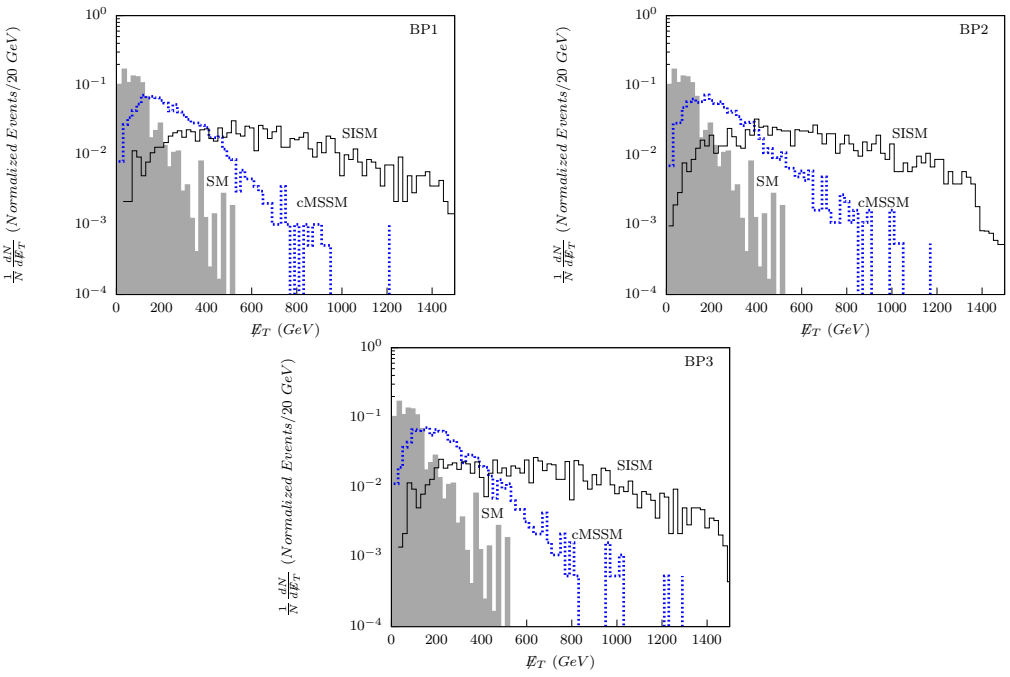

Figure 4.5: The $\not{E}_T$ distribution for the SISM case with sneutrino LSP and pure cMSSM case with neutralino LSP with a similar squark-gluino spectrum. The SM background is also shown.

The number of events obtained after the selection criteria for $\sqrt{s} = 14$ TeV LHC and normalized to 30 fb^{-1} luminosity are shown in Table 4.7. Note that at this stage, some of the SM backgrounds are much larger than the SSD signal, and we need to devise further cuts to reduce the background without affecting the signal much. As shown in Table 4.7, we found two relevant cuts, namely (a) $p_T^j > 50$ GeV for all jets and

$p_T^j > 100$ GeV for the leading jet, and (b) $\not{E}_T > 300$ GeV which reduce the background significantly.

Channel	After basic selection criteria			After jet p_T cut			After $\not{E}_T$ cut		
	$\mu\mu$	$e\mu$	ee	$\mu\mu$	$e\mu$	ee	$\mu\mu$	$e\mu$	ee
BP1	33.24	125.18	144.01	30.73	112.66	127.45	24.30	90.13	114.69
BP2	39.95	32.44	97.26	34.38	26.86	84.34	28.54	23.35	64.87
BP3	35.94	88.94	102.84	34.15	80.05	91.49	32.44	78.48	86.76
WWW	16.86	12.36	29.64	3.18	2.49	6.00	0.39	0.24	0.24
$WWjj$	140.01	75.39	193.86	75.39	43.08	96.93	0.00	0.00	0.00
WZ	84.60	16.92	186.06	33.84	0.00	51.00	0.00	0.00	0.00
ZZ	0.33	0.33	0.66	0.000	0.000	0.03	0.00	0.00	0.00
$Wb\bar{b}$	29.25	5.85	29.25	0.00	0.00	0.00	0.00	0.00	0.00
$Wt\bar{t}$	81.33	66.84	147.54	38.70	31.89	69.75	1.83	1.59	3.18
$t\bar{t}$	2109.00	754.80	2331.00	710.4	222.00	466.2	0.00	0.00	0.00
$Zb\bar{b}$	0.00	6.99	19.38	0.00	0.00	1.62	0.000	0.000	0.000

Table 4.7: Number of events for 30 fb^{-1} luminosity at $\sqrt{s} = 14$ TeV LHC for the SSD+$nj+\not{E}_T$ signal (with $n \geq 2$) and the dominant SM backgrounds. We have shown the numbers after the basic selection criteria (but before applying any additional cuts) as well as after applying the following additional cuts: (i) $p_T^{\text{all jets}} > 50$ GeV with $p_T^{\text{leading jet}} > 100$ GeV, and (ii) $\not{E}_T > 300$ GeV.

Note the boosted rate in SSD+n-jets+$\not{E}_T$ signal particularly with electrons in the final state. Since we consider all SUSY process, the electron and muon abundance should have been similar in the signal. However, the boost in the electron associated final states is a result of the SISM scenario. The same sign leptons are always generated from the lighter chargino for the gluino pair production channel which has the most dominant contribution to the final state we consider. This coupling of the lighter chargino to the singlet sneutrino and a charged lepton is induced by the term $\epsilon_{ab} y_\nu^{ij} \widehat{L}_i^a \widehat{H}_u^b \widehat{N}_j^c$ in the superpotential in Eq. 2.1. Now if y_ν^{ij} is chosen to be diagonal, that means only the same generation scalar and fermionic states from $\widehat{L}$ and $\widehat{N}^c$ couple among themselves. We have chosen our parameters in such a way that the lightest sneutrino eigenstate is essentially singlet-like with a small admixture of the left-handed component. Note that the $M_{R_{11}}$ element from the mixing term $M_{R_{ij}} \widehat{N}_i^c \widehat{S}_j$, which governs the mixing between the fields of $\widehat{N}_1^c$ and $\widehat{S}_1$ is smaller compared to $M_{R_{22}}$ and $M_{R_{33}}$. Besides, we have pushed the left sneutrino soft masses ($m_{\tilde{L}}$) and the soft masses of the singlet states (m_N^2 and m_S^2) above TeV range. Consequently, the LSP sneutrino state

is mainly composed of $\widetilde{N}_1^c$ and $\widetilde{S}_1$. Now since $\widetilde{N}_1^c$ always couples to the first generation scalar and fermionic states in $\widehat{L}_1$, the chargino couples to the LSP mostly alongwith an electron.

4.5 Summary

We have studied SISM in the context of a light scalar DM. We show that this model can not only account for neutrino masses and mixing, but it also leads to an LSP dominated by right chiral sneutrino states. For phenomenologically consistent input parameters, taken as a hybrid of the top-down and bottom-up choices, the sneutrino LSP can act as a DM candidate of mass around 50 GeV while satisfying all the existing collider, cosmological as well as low-energy constraints. We also suggest that such a scenario can be distinguished from one based on pure top-down mSUGRA scenario with a neutralino LSP, through a study of the same-sign dilepton signals at the LHC, and also from the $\not{E}_T$ spectra in the two cases.

Since the publication of this paper, lack of evidence of any SUSY particles at the LHC has resulted in a more stringent constraint on the cMSSM parameter space [62]. The high scale inputs m_0 and $m_{1/2}$ taken in this work to construct the benchmark points are ruled out in the light of these results. However, that does not change our analysis or the conclusion of this work, since we can always find a suitable parameter space for this study with increased sparticle masses and higher luminosity. Since there are still no bounds on the singlet-like sneutrino mass within the cMSSM framework, our DM mass range remains unchanged.

We might also be able to put useful bounds on the Dirac Yukawa coupling in such scenarios from the invisible decay width of the lightest neutral Higgs boson if this gets confirmed with more data at the LHC in near future. This issue will be discussed in more detail in the next chapter.

Bibliography

[1] C. Arina, F. Bazzocchi, N. Fornengo, J. C. Romao, J. W. F. Valle, Phys. Rev. Lett. **101**, 161802 (2008) [arXiv:0806.3225 [hep-ph]].

[2] For global fits of the cMSSM, see e.g., O. Buchmueller *et al.*, Eur. Phys. J. C **72**, 2020 (2012) arXiv:1112.3564 [hep-ph]; L. Roszkowski, E. M. Sessolo and Y. -L. S. Tsai, Phys. Rev. D **86**, 095005 (2012) arXiv:1202.1503 [hep-ph]; C. Strege, G. Bertone, D. G. Cerdeno, M. Fornasa, R. R. de Austri and R. Trotta, JCAP **1203**, 030 (2012) [arXiv:1112.4192 [hep-ph]]; J. Ellis and K. A. Olive, Eur. Phys. J. C **72**, 2005 (2012) [arXiv:1202.3262 [hep-ph]]; A. Fowlie *et al.*, Phys. Rev. D **86**, 075010 (2012) arXiv:1206.0264 [hep-ph]; S. Akula, P. Nath and G. Peim, Phys. Lett. B **717**, 188 (2012) arXiv:1207.1839 [hep-ph]; C. Beskidt, W. de Boer, D.I. Kazakov, F. Ratnikov, Eur. Phys. J. C **72**, 2166 (2012) arXiv:1207.3185 [hep-ph].

[3] P. S. Bhupal Dev, S. Mondal, B. Mukhopadhyaya and S. Roy, JHEP **1209**, 110 (2012) [Erratum-ibid. **1311**, 169 (2013)] [arXiv:1207.6542 [hep-ph]].

[4] C. E. Aalseth *et al.* [CoGeNT Collaboration], Phys. Rev. Lett. **106**, 131301 (2011) [arXiv:1002.4703 [astro-ph.CO]]; *ibid*, Phys. Rev. Lett. **107**, 141301 (2011) [arXiv:1106.0650 [astro-ph.CO]].

[5] G. Angloher *et al.* [CRESST-II Collaboration], Eur. Phys. J. **C72**, 1971 (2012) [arXiv:1109.0702[astro-ph.CO]].

[6] R. Bernabei *et al.* [DAMA Collaboration], Eur. Phys. J. **C56**, 333 (2008) [arXiv:0804.2741 [astro-ph]]; *ibid*, Eur. Phys. J. **C67**, 39 (2010) [arXiv:1002.1028 [astro-ph.GA]].

[7] V. Khachatryan *et al.* [CMS Collaboration], arXiv:1407.0558 [hep-ex].

[8] G. Aad *et al.* [ATLAS Collaboration], arXiv:1408.7084 [hep-ex].

[9] H. Baer, V. Barger and A. Mustafayev, Phys. Rev. D **85**, 075010 (2012) [arXiv:1112.3017 [hep-ph]]; *ibid.*, JHEP **1205**, 091 (2012) [arXiv:1202.4038 [hep-ph]]; J. L. Feng, K. T. Matchev and D. Sanford, Phys. Rev. D **85**, 075007 (2012) [arXiv:1112.3021 [hep-ph]]; A. Arbey, M. Battaglia, A. Djouadi, F. Mahmoudi and J. Quevillon, Phys. Lett. B **708**, 162 (2012) [arXiv:1112.3028 [hep-ph]]; S. Akula, B. Altunkaynak, D. Feldman, P. Nath and G. Peim, Phys. Rev. D **85**, 075001 (2012) [arXiv:1112.3645 [hep-ph]]; L. Aparicio, D. G. Cerdeno and L. E. Ibanez, JHEP **1204**, 126 (2012) [arXiv:1202.0822 [hep-ph]]; M. Kadastik, K. Kannike, A. Racioppi and M. Raidal, JHEP **1205**, 061 (2012) [arXiv:1112.3647 [hep-ph]]. J. Cao, Z. Heng, D. Li and J. M. Yang, Phys. Lett. B **710**, 665 (2012) [arXiv:1112.4391 [hep-ph]]; N. Karagiannakis, G. Lazarides and C. Pallis, J. Phys. Conf. Ser. **384**, 012012 (2012) arXiv:1201.2111 [hep-ph]; J. Cao, Z. Heng, J. M. Yang and J. Zhu, JHEP **1210**, 079 (2012) arXiv:1207.3698 [hep-ph].

[10] `https://twiki.cern.ch/twiki/bin/view/CMSPublic/PhysicsResultsSUS`

[11] `https://twiki.cern.ch/twiki/bin/view/AtlasPublic/SupersymmetryPublicResults`

[12] F. Staub, T. Ohl, W. Porod and C. Speckner, Comput. Phys. Commun. **183**, 2165 (2012) [arXiv:1109.5147 [hep-ph]].

[13] F. Staub, arXiv:0806.0538 [hep-ph]; Comput. Phys. Commun. **181**, 1077 (2010) [arXiv:0909.2863 [hep-ph]]; Comput. Phys. Commun. **182**, 808 (2011) [arXiv:1002.0840 [hep-ph]].

[14] W. Porod, Comput. Phys. Commun. **153**, 275 (2003) [hep-ph/0301101]; W. Porod and F. Staub, arXiv:1104.1573 [hep-ph].

[15] G. Belanger, F. Boudjema, A. Pukhov and A. Semenov, Comput. Phys. Commun. **176**, 367 (2007) [hep-ph/0607059]; Comput. Phys. Commun. **180**, 747 (2009) [arXiv:0803.2360 [hep-ph]].

[16] ATLAS Collaboration, ATLAS-CONF-2013-034.

[17] CMS Collaboration, CMS-PAS-HIG-13-005.

[18] P. A. R. Ade *et al.* [Planck Collaboration], Astron. Astrophys. (2014) arXiv:1303.5076 [astro-ph.CO].

[19] The LEP Electroweak Working Group, `http://lepewwg.web.cern.ch/LEPEWWG`.

[20] E. Aprile *et al.* [XENON100 Collaboration], Phys. Rev. Lett. **109**, 181301 (2012) [arXiv:1207.5988 [astro-ph.CO]].

[21] D. S. Akerib *et al.* [LUX Collaboration], Phys. Rev. Lett. **112**, 091303 (2014) [arXiv:1310.8214 [astro-ph.CO]].

[22] E. Aprile [XENON1T Collaboration], Springer Proc. Phys. **148**, 93 (2013) arXiv:1206.6288 [astro-ph.IM].

[23] D. S. Akerib *et al.* [LUX Collaboration], Nucl. Instrum. Meth. A **704**, 111 (2013) [arXiv:1211.3788 [physics.ins-det]].

[24] M. Ackermann *et al.* [Fermi-LAT Collaboration], Phys. Rev. Lett. **107**, 241302 (2011) [arXiv:1108.3546 [astro-ph.HE]].

[25] M. Ackermann *et al.* [LAT Collaboration], Phys. Rev. D **86**, 022002 (2012) [arXiv:1205.2739 [astro-ph.HE]].

[26] The CMS Collaboration, CMS-PAS-HIG-12-020 (2012).

[27] The ATLAS Collaboration, ATLAS-CONF-2012-093 (2012).

[28] J. Beringer *et al.* (Particle Data Group), Phys. Rev. **D86**, 010001 (2012).

[29] S. Bethke, Eur. Phys. J. C **64**, 689 (2009) [arXiv:0908.1135 [hep-ph]].

[30] The Tevatron Electroweak Working Group and CDF and D0 Collaborations, arXiv:1107.5255 [hep-ex].

[31] E. Komatsu *et al.* [WMAP Collaboration], Astrophys. J. Suppl. **192**, 18 (2011) [arXiv:1001.4538 [astro-ph.CO]]; D. Larson *et al.*, Astrophys. J. Suppl. **192**, 16 (2011) [arXiv:1001.4635 [astro-ph.CO]].

[32] G. Venanzoni, J. Phys. Conf. Ser. **349**, 012008 (2012) [arXiv:1203.1501 [hep-ex]].

[33] T. Aoyama, M. Hayakawa, T. Kinoshita and M. Nio, Phys. Rev. Lett. **109**, 111807 (2012) arXiv:1205.5368 [hep-ph].

[34] J. P. Lees *et al.* [BaBar Collaboration], Phys. Rev. Lett. **109**, 191801 (2012) arXiv:1207.2690 [hep-ex].

[35] R. Aaij *et al.* [LHCb Collaboration], Phys. Rev. Lett. **108**, 231801 (2012) [arXiv:1203.4493 [hep-ex]].

[36] A. Abada, C. Biggio, F. Bonnet, M. B. Gavela and T. Hambye, JHEP **0712**, 061 (2007) [arXiv:0707.4058 [hep-ph]]; S. Antusch, J. P. Baumann and E. Fernandez-Martinez, Nucl. Phys. B **810**, 369 (2009) [arXiv:0807.1003 [hep-ph]].

[37] N. Sato *et al.* (Kamiokande Collaboration), Phys. Rev. D **44**, 2220 (1991).

[38] S. Chatrchyan *et al.* [CMS Collaboration], Phys. Rev. Lett. **109**, 171803 (2012) arXiv:1207.1898 [hep-ex].

[39] U. Chattopadhyay and P. Nath, Phys. Rev. Lett. **86**, 5854 (2001) [hep-ph/0102157]; *ibid.*, Phys. Rev. D **66**, 093001 (2002) [hep-ph/0208012]; W. de Boer, M. Huber, C. Sander and D. I. Kazakov, Phys. Lett. B **515**, 283 (2001).

[40] See e.g., S. Martin, In "Perspectives on supersymmetry II", G. L. Kane (ed.), p. 1-153 [hep-ph/9709356].

[41] H. An, P. S. Bhupal Dev, Y. Cai and R. N. Mohapatra, Phys. Rev. Lett. **108**, 081806 (2012) [arXiv:1110.1366 [hep-ph]].

[42] L. J. Hall, D. Pinner and J. T. Ruderman, JHEP **1204**, 131 (2012) [arXiv:1112.2703 [hep-ph]]; H. Baer, V. Barger, P. Huang, A. Mustafayev and X. Tata, Phys. Rev. Lett. **109** (2012) 161802 arXiv:1207.3343 [hep-ph].

[43] S. Heinemeyer, D. Stockinger and G. Weiglein, Nucl. Phys. B **690**, 62 (2004) [hep-ph/0312264].

[44] M. Misiak *et al.*, Phys. Rev. Lett. **98**, 022002 (2007) [hep-ph/0609232].

[45] S. Bertolini, F. Borzumati, A. Masiero and G. Ridolfi, Nucl. Phys. **B 353**, 591 (1991); P. Nath and R. L. Arnowitt, Phys. Lett. **B 336**, 395 (1994); F. Borzumati, M. Drees and M. M. Nojiri, Phys. Rev. **D 51**, 341 (1995); H. Baer, M. Brhlik, D. Castano and X. Tata, Phys. Rev. **D58**, 015007 (1998) [hep-ph/9712305].

[46] A. J. Buras, Acta Phys. Polon. B **41**, 2487 (2010) [arXiv:1012.1447 [hep-ph]].

[47] S. R. Choudhury and N. Gaur, Phys. Lett. B **451**, 86 (1999) [hep-ph/9810307]; K. S. Babu and C. F. Kolda, Phys. Rev. Lett. **84**, 228 (2000) [hep-ph/9909476]; J. K. Mizukoshi, X. Tata and Y. Wang, Phys. Rev. D **66**, 115003 (2002) [hep-ph/0208078].

[48] F. Gabbiani, E. Gabrielli, A. Masiero and L. Silvestrini, Nucl. Phys. B **477**, 321 (1996) [hep-ph/9604387].

[49] A. Ilakovac and A. Pilaftsis, Nucl. Phys. **B 437**, 491 (1995) [hep-ph/9403398]; F. Deppisch and J. W. F. Valle, Phys. Rev. D **72**, 036001 (2005) [hep-ph/0406040]; *ibid.*, Nucl. Phys. B **752**, 80 (2006) [hep-ph/0512360]; A. Ibarra, E. Molinaro and S. T. Petcov, Phys. Rev. D **84**, 013005 (2011) [arXiv:1103.6217 [hep-ph]]; W. Abdallah, A. Awad, S. Khalil and H. Okada, Eur. Phys. J. C **72**, 2108 (2012) arXiv:1105.1047 [hep-ph]; A. Abada, D. Das and C. Weiland, JHEP **1203**, 100 (2012) [arXiv:1111.5836 [hep-ph]]; A. Abada, D. Das, A. Vicente and C. Weiland, JHEP **1209**, 015 (2012) arXiv:1206.6497 [hep-ph].

[50] P. S. Bhupal Dev, R. N. Mohapatra, Phys. Rev. D **81**, 013001 (2010) [arXiv:0910.3924 [hep-ph]]; Phys. Rev. D. **82**, 035014 (2010) [arXiv:1003.6102 [hep-ph]].

[51] M. Hirsch, T. Kernreiter, J. C. Romao and A. Villanova del Moral, JHEP **1001**, 103 (2010) [arXiv:0910.2435 [hep-ph]].

[52] M. Malinsky, T. Ohlsson and H. Zhang, Phys. Rev. D **79**, 073009 (2009) [arXiv:0903.1961 [hep-ph]]; M. Malinsky, T. Ohlsson, Z. -z. Xing and H. Zhang, Phys. Lett. B **679**, 242 (2009) [arXiv:0905.2889 [hep-ph]]; R. Lal Awasthi and M. K. Parida, Phys. Rev. D **86**, 093004 (2012) arXiv:1112.1826 [hep-ph].

[53] K. Ghosh, B. Mukhopadhyaya and U. Sarkar, Phys. Rev. D **84**, 015017 (2011) [arXiv:1105.5837 [hep-ph]]; Y. Bai, P. Draper and J. Shelton, JHEP **1207**, 192 (2012) arXiv:1112.4496 [hep-ph].

[54] P. P. Giardino, K. Kannike, M. Raidal and A. Strumia, JHEP **1206**, 117 (2012) [arXiv:1203.4254 [hep-ph]]; J. R. Espinosa, C. Grojean, M. Muhlleitner and M. Trott, JHEP **1209**, 126 (2012) arXiv:1205.6790 [hep-ph]; *ibid.*, JHEP **1212**, 045 (2012) arXiv:1207.1717 [hep-ph]; S. Banerjee, S. Mukhopadhyay and B. Mukhopadhyaya, JHEP **1210**, 062 (2012) arXiv:1207.3588 [hep-ph].

[55] Y. Mambrini, J. Phys. Conf. Ser. **375**, 012045 (2012) arXiv:1112.0011 [hep-ph].

[56] P. S. Bhupal Dev, Roberto Franceschini, R. N. Mohapatra, Phys. Rev. D **86**, 093010 (2012) arXiv:1207.2756 [hep-ph].

[57] See e.g., H. Baer and X. Tata, arXiv:0805.1905 [hep-ph].

[58] G. Belanger, S. Kraml and A. Lessa, JHEP **1107**, 083 (2011) [arXiv:1105.4878 [hep-ph]].

[59] A. Das and N. Okada, Phys. Rev. D **88**, no. 11, 113001 (2013) [arXiv:1207.3734 [hep-ph]].

[60] F. del Aguila and J. A. Aguilar-Saavedra, Nucl. Phys. B **813**, 22 (2009) [arXiv:0808.2468 [hep-ph]].

[61] A. J. Barr and C. Gwenlan, *The Race for supersymmetry: Using m(T2) for discovery*, *Phys.Rev.* **D80** (2009) 074007, [0907.2713].

[62] https://atlas.web.cern.ch/Atlas/GROUPS/PHYSICS/CombinedSummaryPlots/SUSY/index.html

Chapter 5

Invisible Higgs Decay in SISM

After the recent discovery [1, 2] of a Higgs boson with mass (m_h) around 125 GeV, a major goal is to establish whether it is "the" Standard Model (SM) Higgs boson or a first glimpse of some Beyond Standard Model (BSM) physics at the LHC. A precise determination of the discovered Higgs boson characteristics will be crucial in resolving some of the outstanding issues of the SM, and in particular, understanding the mechanism of electroweak symmetry breaking and its relationship to the BSM. The experimental results so far [3–6] show no significant deviation from the SM Higgs sector expectations, and already put severe constraints on various new physics models (see, for instance, [7–14]). However, they still do not exclude the possibility of a non-standard Higgs boson.

A precise measurement of the total decay width (Γ_h) of the Higgs boson (h) through its line shape is very difficult at the LHC due to its tiny value: for the SM with $m_h = 125$ GeV, $\Gamma_h = 4.07$ MeV [15]. Hence, a better way to identify a non-standard Higgs boson is by studying its non-standard decay modes (for a review, see e.g., [16]). This is also crucial in case of a statistically significant discrepancy between the measured and SM expected Higgs signal strengths which could be due to either suppression or enhancement of the Higgs production cross section as well as its partial decay widths.

A particularly interesting non-standard Higgs decay which is very sensitive to large BSM contributions is its invisible decay mode [17], since the SM invisible Higgs branching ratio (BR) is very small: BR($h \to ZZ^* \to 4\nu$) $\simeq 0.001$ [18]. Dedicated searches for the Higgs decay into invisible final states were performed at the LEP [19], and no signal was found for Higgs mass up to 114.4 GeV. The LHC prospects of determining the invisible Higgs BR have been analyzed in Refs. [20–29]. ATLAS and CMS have been separately searching for non-standard decay modes of the Higgs boson in different production channels. The combined CMS limit on the invisible Higgs BR derived from vector boson fusion (VBF) and associated Zh production modes is 58% [30], while

the same limit derived from associated Zh production mode by ATLAS is 75% [31]. ATLAS puts a more stringent limit of 68% on the Higgs invisible BR from coupling measurements of the Higgs boson [32]. Global fits to the existing LHC data provide a stronger constraint on $\mathrm{BR}_{\mathrm{inv}} < 0.28$ at 95% CL [12] (for other recent global fits, see [33, 34]).

As was discussed in the previous chapter, in contrast with the pure cMSSM scenario, SISM allows a light DM in the form of a mixed sneutrino with mass around $m_h/2$ and that it requires to have a large annihilation rate via s-channel Higgs resonance to produce correct relic abundance. Due to the large Yukawa couplings allowed in the model, which are responsible for an efficient annihilation of the sneutrino DM, the lightest CP-even Higgs boson can have a large invisible branching ratio to sneutrino final states. This in turn leads to novel missing energy signatures at the LHC. In this chapter, we analyze this possibility in detail by performing a two-parameter global fit with the latest LHC Higgs data to determine the optimal invisible Higgs branching ratio allowed in this model, and find a 2σ (1σ) upper limit of 0.25 (0.15) [35]. This in turn puts an upper limit of $\mathcal{O}(0.1)$ on the Dirac Yukawa coupling in the model. We further show that the model parameter space allowed by the invisible Higgs decay constraints can be completely ruled out in case of null results at the next generation DM direct detection experiments such as LUX and XENON1T. We also select a few benchmark points satisfying all the experimental constraints, and carry out a detailed cut-based analysis, demonstrating the viability of our proposed signal in two Higgs production channels, namely, vector boson fusion (VBF) and associated production with Z, vis-a-vis SM backgrounds at $\sqrt{s}$=14 TeV LHC. We find that a signal significance of 3σ can be achieved in the VBF channel with a relatively smaller integrated luminosity than in the Zh channel for our chosen benchmark points [35].

5.1 Invisible Higgs Decay Width and Current Data

Our goal in this section is to find the prospects of the lightest CP-even Higgs boson decaying into two light DM particles in the form of sneutrino LSP, thereby leading to a missing energy signal at the LHC. In the SISM being discussed here, we have 5 cMSSM parameters $m_0, m_{1/2}, \tan\beta, A_0, \mathrm{sign}(\mu)$ at high scale and the additional inverse seesaw parameters $M_D, M_R, \mu_S, B_{\mu_S}$ and B_{M_R} whose input values are chosen at the low scale. For simplicity, we have assumed these low-energy neutrino sector parameters to be diagonal (apart from μ_s whose structure is fixed by neutrino oscillation data) so that we can easily satisfy the LFV constraints. Also, the trilinear A_ν term in the soft SUSY-breaking Lagrangian, which controls the Higgs BR to sneutrinos is taken

to be $(A_\nu)_{ij} = A_0(y_\nu)_{ij}$. Note that we require a large A_0 in order to have a large radiative correction to the lightest CP-even Higgs boson mass as required by the LHC observation, whereas the Dirac Yukawa coupling y_ν is also required to be large in order to provide an efficient annihilation channel for the sneutrino LSP. These two seemingly uncorrelated effects inevitably lead to a large invisible BR for the Higgs in the SISM.

In order to ascertain how much invisible BR of the Higgs boson is allowed in our model, we perform a two parameter global analysis with all the LHC Higgs data available so far as listed in Table 5.1 Here we list the latest Higgs data sets available from the combined $\sqrt{s} = 7$ and 8 TeV LHC run in five visible Higgs decay channels: $\gamma\gamma$, $ZZ^* \to 4\ell$, $WW^* \to 2\ell 2\nu$, $b\bar{b}$ and $\tau\bar{\tau}$. For each channel, we show the experimental values of the signal strengths $\hat{\mu}_i$ together with its 1σ uncertainty, as reported by the ATLAS and CMS collaborations [36–43][1].

Channel	$\hat{\mu}$	Experiment
$h \to \gamma\gamma$	$1.55^{+0.33}_{-0.28}$	ATLAS [36]
	$0.78^{+0.28}_{-0.26}$	CMS [37]
$h \to ZZ^* \to 4l$	$1.43^{+0.40}_{-0.35}$	ATLAS [36]
	$0.9^{+0.30}_{-0.20}$	CMS [38]
$h \to WW^* \to 2l2\nu$	$0.99^{+0.31}_{-0.28}$	ATLAS [36]
	$0.80^{+0.20}_{-0.20}$	CMS [39]
$h \to b\bar{b}$	$0.20^{+0.70}_{-0.60}$	ATLAS (VH) [40]
	$1.00^{+0.50}_{-0.50}$	CMS (VH) [41]
$h \to \tau\bar{\tau}$	$0.7^{+0.7}_{-0.6}$	ATLAS [42]
	$1.10^{+0.4}_{-0.4}$	CMS [43]

Table 5.1: Data set used in our analysis, with the values of $\hat{\mu}_i$ in various channels and their 1σ uncertainties as reported by the ATLAS and CMS collaborations.

Since the neutrino sector parameters of the SISM do not affect the Higgs production or decay rates into the SM final states, and only affect its invisible decay into sneutrino final states, we can parametrize their effect in terms of a single free parameter, namely, the invisible BR, ε which relates the visible and invisible partial widths of the Higgs boson as

$$\Gamma_{\rm inv} = \frac{\varepsilon}{1-\varepsilon} \sum \Gamma_{\rm vis} \,. \tag{5.1}$$

For the MSSM sector of the SISM, we choose a few benchmark points (BPs) by fixing $m_0, m_{1/2}$ and A_0 as shown in Table 5.2, and vary the remaining parameter, namely,

[1]The signal strength values in different Higgs boson channels were updated recently. We discuss about the implications at the end of this chapter.

$\tan\beta$. The benchmark points[2] given in Table 5.2 were selected from the sample scan ranged over the values given in Eq. 4.2 by requiring them to satisfy the constraints coming from Higgs boson and squark-gluino mass bounds. Note that all the benchmark

Input parameter	BP1	BP2	BP3
m_0 (GeV)	996.45	745.48	614.00
$m_{1/2}$ (GeV)	750.00	1014.17	1083.00
A_0 (GeV)	-2858.00	-2775.09	-2600.00

Table 5.2: The cMSSM input parameters for three chosen benchmark points.

points shown in Table 5.2 require an electroweak fine-tuning at the percent level, which is mandatory given the current LHC data (see e.g., [45]). For the trilinear term A_0, a large negative value is required to obtain the correct Higgs mass ($m_h = 125 \pm 2$ GeV) for our choices of m_0 and $m_{1/2}$ (which are consistent with the general results from other cMSSM parameter scans, e.g. [45]). We have checked that all our benchmark points lead to a stable electroweak vacuum and do not lead to charge- and/or color-breaking minima. For each combination of the high-scale parameters given in Table 5.2, we perform a global analysis in the ε-$\tan\beta$ plane using 10 data points in various Higgs decay channels from the published results of CMS and ATLAS, as listed in Table 5.1.

For each of the variables, with the other one marginalized, we compute the χ^2 function, defined as

$$\chi^2 = \sum_i \frac{(\mu_i - \hat{\mu}_i)^2}{(\delta\hat{\mu}_i)^2}, \tag{5.2}$$

where μ_i's are the Higgs signal strengths calculated from the model and are functions of the model parameters:

$$\mu_i = R_i^{\rm prod} \times \frac{R_i^{\rm decay}}{R^{\rm width}}\,. \tag{5.3}$$

Here R_i's are the ratios of the model predictions for the Higgs production cross sections and partial decay rates for various channels, and similarly R is the ratio of the total width, with the corresponding SM expectations:

$$R_i^{\rm prod} = \frac{\left(\sigma_i^{\rm prod}\right)_{\rm SISM}}{\left(\sigma_i^{\rm prod}\right)_{\rm SM}}\,,\ R_i^{\rm decay} = \frac{\left(\Gamma_i^{\rm decay}\right)_{\rm SISM}}{\left(\Gamma_i^{\rm decay}\right)_{\rm SM}}\,,\ R^{\rm width} = \frac{\left(\Gamma^{\rm width}\right)_{\rm SISM}}{\left(\Gamma^{\rm width}\right)_{\rm SM}}\,, \tag{5.4}$$

[2]Note that the high scale inputs for these three BPs are different from the ones considered in the previous chapter. This is because of the fact that while working on this project the cMSSM search results were updated and the high scale input parameters of the benchmark points presented in the previous chapter were already ruled out [44].

and $\hat{\mu}_i$'s are the experimental best fit values of the signal strengths as listed in Table 5.1, $\delta\hat{\mu}_i$'s being their reported 1σ uncertainty. When the reported uncertainties are asymmetric in nature, we consider the positive uncertainty for $(\mu_i - \hat{\mu}_i) > 0$ and the negative one for $(\mu_i - \hat{\mu}_i) < 0$.

We have varied $\tan\beta$ between 2 and 50, and ε between 0 and 0.7. Note that large $\tan\beta \gtrsim 50$ is disfavored by the recent LHCb results on $B_s \to \mu^+\mu^-$, and very low $\tan\beta \lesssim 2$ are usually not considered due to radiative electroweak symmetry breaking arguments. The 1σ and 2σ contours for $\tan\beta$ and ε for various "snapshot" values of the high-scale parameters are presented in Fig. 5.1, 5.2 and 5.3. We have chosen the benchmark points for signal prediction, ensuring that we stay within 2σ for both of the fitted parameters (ε and $\tan\beta$).

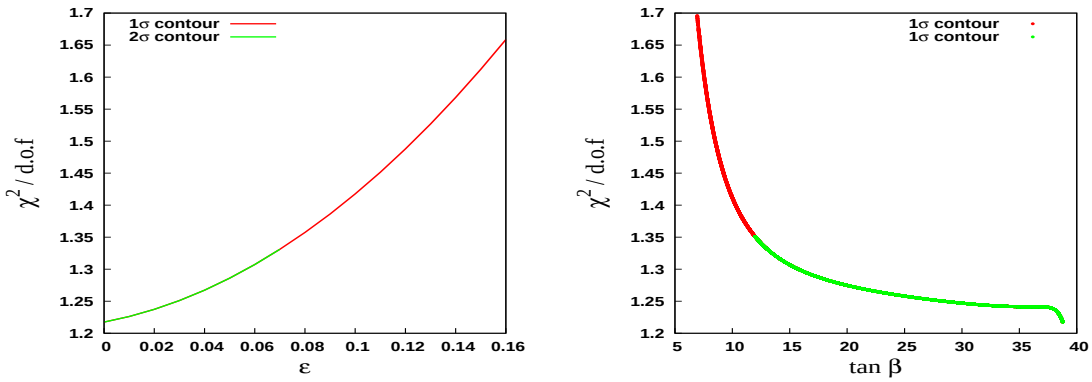

Figure 5.1: 1σ and 2σ contours for ε and $\tan\beta$ from χ^2 minimization obtained for BP1. The green line indicates 1σ reach and the red line indicates 2σ reach of the parameters.

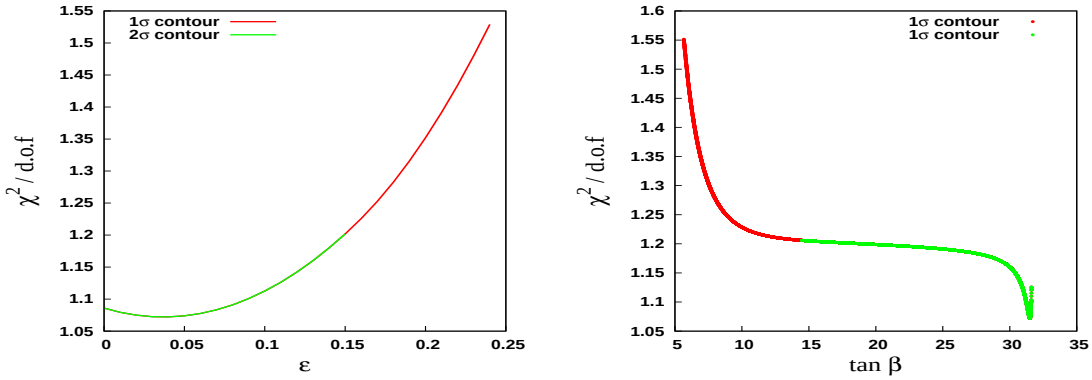

Figure 5.2: 1σ and 2σ contours for ε and $\tan\beta$ from χ^2 minimization obtained for BP2. The green line indicates 1σ reach and the red line indicates 2σ reach of the parameters.

As manifested in these contour plots, the minimum χ^2-value is obtained for $\varepsilon = 0, 0.037$ and 0.04 for BP1, BP2 and BP3 respectively and intermediate values of $\tan\beta$

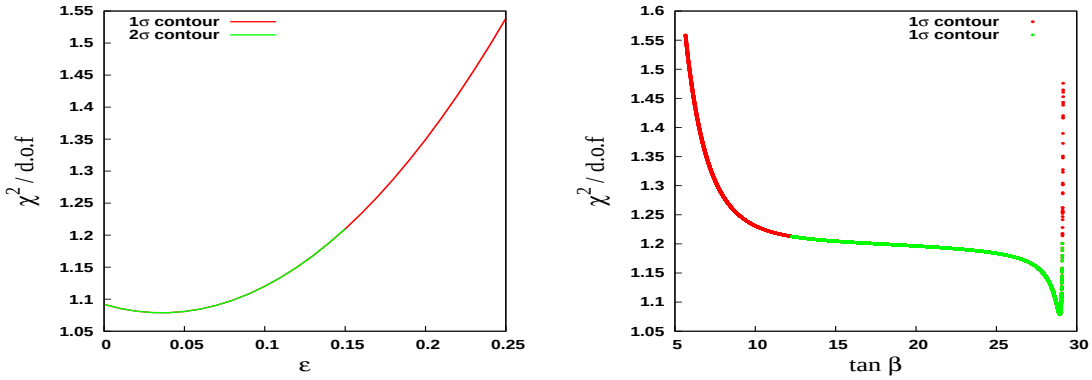

Figure 5.3: 1σ and 2σ contours for ε and $\tan\beta$ from χ^2 minimization obtained for BP3. The green line indicates 1σ reach and the red line indicates 2σ reach of the parameters.

around 30-40 for all the benchmark points. Also, there exists an upper limit on ε to be consistent with the LHC Higgs data. The 68.27% ($\Delta\chi^2 = 1$) and 95.45% ($\Delta\chi^2 = 4$) CL limits derived from Fig. 5.1-5.3 are summarized in Table 5.3, and also shown in Fig. 5.4. These limits are comparable to those obtained in a recent model-independent global fit [12], and much stronger than the direct search limits from associated production of Higgs with Z [30, 31] as well as those derived from monojet searches [28].

Parameter	BP1		BP2		BP3	
	1σ	2σ	1σ	2σ	1σ	2σ
ε	< 0.07	< 0.16	< 0.15	< 0.24	< 0.15	< 0.25
$\tan\beta$	12.0-38.8	6.9-38.8	14.5-31.6	5.7-31.6	12.3-29.1	5.6-29.2

Table 5.3: The 1σ and 2σ limits on the invisible Higgs BR and the MSSM $\tan\beta$ parameter obtained from the marginalized plots (Fig. 5.1-5.3) for the chosen benchmark points in SISM.

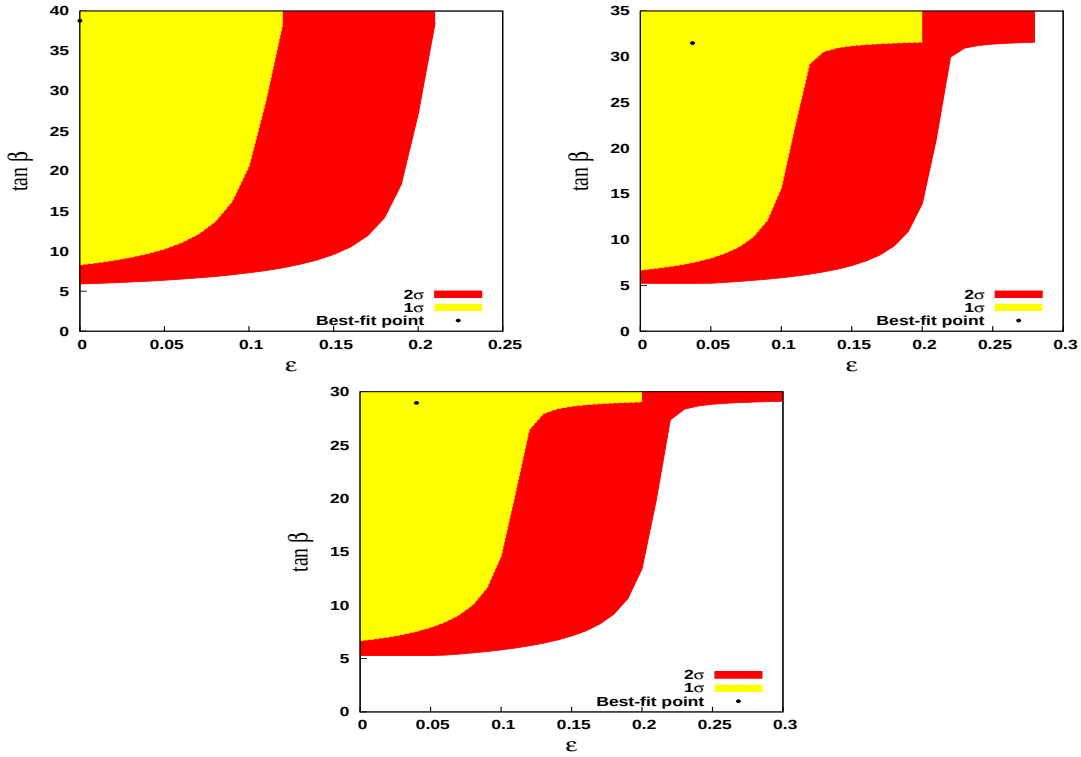

Figure 5.4: 1σ and 2σ allowed contours in the ε - $\tan\beta$ plane from global analysis of the Higgs data for the three benchmark points in our model. The black dots indicate the best fit values of $\tan\beta$ and ε obtained from our analysis.

5.1.1 Constraining model parameters

An upper limit on the invisible Higgs branching ratio, as derived in Table 5.3 from a global analysis of the LHC Higgs data, can put an upper limit on the magnitude of the Dirac Yukawa coupling in the model. To illustrate this, we show in Fig. 5.5 the variation of the invisible Higgs branching fraction as a function of the Yukawa parameter, $(y_\nu)_{11}$. This plot is obtained for a fixed $A_0(\sim -2.8$ TeV) and fixed B_{M_R} and B_{μ_S} as given below Eq. 4.2. However, other parameters are varied in the ranges mentioned in Eq. 4.2. Note that, the invisible Higgs BR is insensitive to other entries of y_ν. We obtain a spread of the points as during the scan the Higgs mass fluctuates a little bit around its central value. Also the M_R parameters vary which means that the LSP mass is not fixed at a particular value. It roughly varies between 20 - 62 GeV, and for most of the points, lie in the 30 - 62 GeV range. As can be seen from the plot, the invisible Higgs branching fraction roughly grows with the Yukawa coupling in the kinematically allowed region. Thus an upper limit on the Dirac Yukawa coupling in

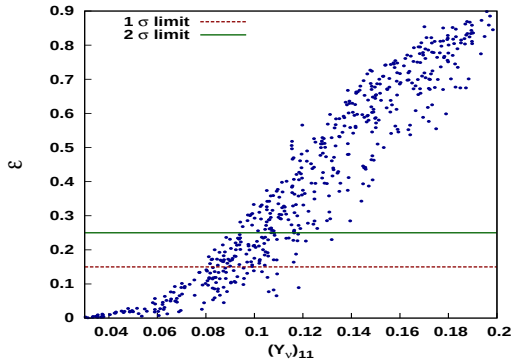

Figure 5.5: The invisible Higgs branching fraction as a function of the Dirac Yukawa coupling. The 1σ and 2σ upper limits on the invisible branching fraction derived earlier are also shown.

the model follows from the upper limit on ε, as can be read off from the 1σ and 2σ lines in Fig. 5.5. Note that the upper limit of order of 0.10 on y_ν derived from this analysis is stronger than those derived from the Higgs visible decay [46] for a heavy neutrino mass larger than the Higgs mass. Comparable limits on y_ν in similar TeV scale seesaw models are obtained from charged-lepton flavor violating decays for the range of heavy neutrino masses we have considered here [47, 48].

The bound on ε also constrains the allowed parameter space for the DM-nucleon elastic scattering cross section in this model. This is shown in Fig. 5.6 which is basically a zoomed-in version of Fig. 4.2 focusing on the light DM region and with only those points obeying the $2\sigma(< 25\%)$ limit on ε.

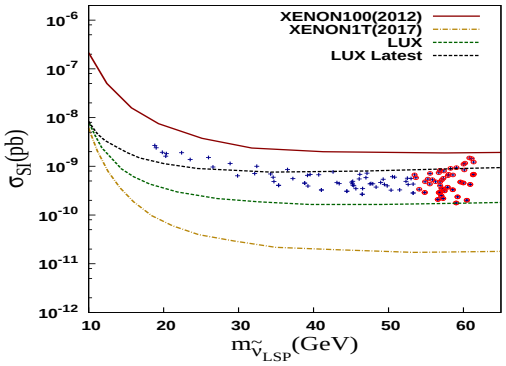

Figure 5.6: Spin-independent cross section as a function of the sneutrino LSP mass for the points satisfying the 2σ upper limit on the invisible Higgs BR. The circled points also satisfy the relic density constraint.

As can be seen from the plot, all these points are just below the current sensitivity

of XENON100 experiment, but can be *completely* probed by the future experiments such as LUX and XENON1T.

5.1.2 Some benchmark points

Input parameter	BP1	BP2	BP3
$\tan\beta$	25	20	25
y_ν	(0.095,0.090,0.090)	(0.074,0.064,0.064)	(0.0701,0.010,0.010)
M_R (GeV)	(192.7,1000,1000)	(679.16,1000,1000)	(798,1000,1000)
B_{μ_S} (GeV^2)	10^{-4}	10^{-4}	10^{-4}
B_{M_R} (GeV^2)	10^6	10^6	10^6
μ_S (eV)	$\begin{pmatrix} 0.55 & 6.06 & 1.92 \\ 6.06 & 107.86 & 87.97 \\ 1.92 & 87.97 & 116.73 \end{pmatrix}$	$\begin{pmatrix} 11.25 & 38.73 & 12.29 \\ 38.73 & 213.51 & 174.15 \\ 12.29 & 174.15 & 231.08 \end{pmatrix}$	$\begin{pmatrix} 17.30 & 307.19 & 97.46 \\ 307.19 & 8738.55 & 7127.59 \\ 97.46 & 7127.59 & 9457.73 \end{pmatrix}$

Table 5.4: Benchmark values of $\tan\beta$ and the low scale neutrino sector parameters for the chosen benchmark points in Table 5.2.

In Table 5.4 we present some benchmark values of the remaining model parameters not shown in Table 5.2 as allowed by the invisible Higgs decay constraints. We have chosen the neutrino sector parameters to be diagonal, except for μ_S which was fixed by fitting the central global fit values of the neutrino oscillation parameters given in Table 1.3. For illustration, we have assumed a normal hierarchy of neutrino masses with $m_1 = 10^{-5}$ eV and the Dirac CP phase $\delta = 0$ in the PMNS matrix. It is clear from the choice of mSUGRA parameters in Table 5.2 that our low-energy MSSM particle spectrum is consistent with the current limits from direct SUSY searches [49, 50]. We also calculate the other low-energy observables in the flavor sector using `SPheno` and in the DM sector using `micrOMEGAs` for the particle spectrum generated from `SPheno` using the input values shown in Tables 5.2 and 5.4. These results, summarized in Table 5.5, ensure that the chosen benchmark points are consistent with all the existing collider, cosmological and low energy constraints listed in Table 4.1 (within their 3σ allowed range, where applicable):

Parameter	BP1	BP2	BP3
m_h (GeV)	124.69	125.79	125.78
$\Omega_{\rm DM}h^2$	0.114	0.122	0.112
$\sigma_{\rm SI}$ (pb)	3.38×10^{-10}	5.26×10^{-10}	5.56×10^{-10}
δa_μ	3.1×10^{-10}	2.5×10^{-10}	3.4×10^{-10}
δa_e	7.0×10^{-15}	5.7×10^{-15}	7.8×10^{-15}
BR($B \to X_s\gamma$)	2.9×10^{-4}	3.1×10^{-4}	3.1×10^{-4}
BR($B_s \to \mu^+\mu^-$)	3.7×10^{-9}	3.5×10^{-9}	3.6×10^{-9}
BR($\mu \to e\gamma$)	5.2×10^{-22}	1.1×10^{-22}	3.5×10^{-22}
BR($\tau \to e\gamma$)	9.8×10^{-21}	2.1×10^{-21}	6.6×10^{-21}
BR($\tau \to \mu\gamma$)	1.6×10^{-16}	3.5×10^{-17}	1.1×10^{-16}
BR($\mu \to 3e$)	1.1×10^{-22}	8.9×10^{-25}	2.7×10^{-24}
BR($\tau \to 3e$)	6.8×10^{-22}	2.5×10^{-23}	7.7×10^{-23}
BR($\tau \to 3\mu$)	2.8×10^{-16}	3.0×10^{-19}	7.9×10^{-19}
$\lvert\eta_{ee}\rvert$	3.67×10^{-3}	1.79×10^{-4}	1.16×10^{-4}
$\lvert\eta_{\mu\mu}\rvert$	1.22×10^{-4}	6.18×10^{-5}	1.51×10^{-6}
$\lvert\eta_{\tau\tau}\rvert$	1.22×10^{-4}	6.18×10^{-5}	1.51×10^{-6}

Table 5.5: The Higgs boson mass, relic density, spin-independent cross section, anomalous magnetic moments and the relevant low-energy flavor sector observables in the SISM for the three chosen BPs.

5.2 Collider Analysis

The possibility of an invisible Higgs signature at the LHC has been explored both theoretically [21–29] and experimentally [30, 31, 51]. These studies show that the most promising Higgs production channel for detecting an invisibly decaying Higgs is the vector boson fusion (VBF), and the next promising channel is its associated production with Z. In the VBF channel, Higgs is produced from vector bosons originated by radiation off two initial state quarks along with two jets, and subsequently decays into invisible final states: $pp \to qqh \to qq + \not{E}_T$. Thus the final state consists of two jets widely separated in rapidity together with large missing transverse energy. In the Zh associated production channel, the Z decays into two oppositely charged leptons and the Higgs decays invisibly: $q\bar{q} \to Z + h \to \ell^+\ell^- + \not{E}_T$. Note that the leptonic decay channel of Z is known to be cleaner than its hadronic counterpart with b-jets. One can also look for an associated Wh production where W decays leptonically to give rise to

a $\ell + \not{E}_T$ final state. However, the signal acceptance efficiency in this channel is found to be very small, and hence, the corresponding exclusion limit is much worse than that from the Zh channel [52].

In addition to these channels, the dominant Higgs production channel at the LHC, namely, gluon-gluon fusion (ggF), can give rise to a monojet+large $\not{E}_T$ signal with the jet coming from initial state radiation and Higgs decaying invisibly. But the QCD background for this process is too large, and moreover, it is hard to isolate the new physics effects only for the Higgs invisible decay since these effects could also show up in loops to modify the ggF production cross section. The $\sqrt{s} = 7$ TeV search results in this channel [53,54] were translated to a weak upper limit on $\varepsilon < 0.4$ - 0.6 [28] depending on the jet p_T threshold selection. Finally, the other relevant Higgs production channel, namely in association with top pairs, has a much smaller cross section [15], and involves complex final states which require a very sophisticated analysis. Therefore, we will focus on the VBF channel with 2 jets+$\not{E}_T$ final states and the Zh channel with $\ell^+\ell^- + \not{E}_T$ final states for the collider analysis of invisible Higgs signature in our model. We show our analysis results for $\sqrt{s} = 14$ TeV LHC.

5.2.1 Event generation

The SUSY particle spectrum is generated using `SPheno`. The `SLHA` files are then fed to `PYTHIA` (version 6.409) for event generation. The initial and final state radiation of quarks and gluons, multiple interactions, decay, hadronization, fragmentation and jet formation are implemented following the standard procedures in `PYTHIA`. The factorization and renormalization scales μ_R and μ_F respectively are both set at the parton-level center of mass energy $\sqrt{\hat{s}}$. We have used the `CTEQ6L` parton distribution functions in our analysis. The jets with $p_T > 20$ GeV and $|\eta| < 4.5$ have been constructed using the cone algorithm via `PYCELL`. To simulate detector effects, we take into account the smearing of jet energies by a Gaussian probability density function [55].

Following are the selection cuts that we have used to find the final state leptons and jets:

- For final state electrons and muons we use $p_T > 15$ GeV and $p_T > 10$ GeV respectively. For both, we take $|\eta| < 2.4$.
- Lepton-lepton separation $\Delta R_{\ell\ell} > 0.2$, where $\Delta R = \sqrt{(\Delta\eta)^2 + (\Delta\phi)^2}$.
- Lepton-jet separation $\Delta R_{\ell j} > 0.4$.
- Scalar sum of E_T deposits by hadrons within a cone of $\Delta R \leq 0.2$ around a lepton must be less than $0.2 p_T^\ell$ to ensure lepton isolation.

- Jet-jet separation $\Delta R_{jj} > 0.4$.

Depending on the hadronic or leptonic signal final states for different Higgs boson production channels, we use specialized selection criteria, as discussed below.

5.2.2 The VBF channel

In this case, the two leading high p_T jets in the final state are produced in forward and backward directions with rapidities opposite in sign and widely separated. Also due to the invisible decay of the Higgs, one expects a large amount of missing energy. These features largely help to reduce the SM background. The dominant SM background for this signal can come from:
(i) $W+$ jets, where W decays leptonically and the lepton escapes detection.
(ii) Z + jets, where Z decays into two neutrinos.
(iii) mismeasured QCD events giving fake missing energy.
The contributions from non-VBF processes, for instance, from hard QCD production of a single Higgs or a Higgs with associated quarks and gluons, must also be taken into account for the signal. Despite its poor efficiency to pass the background reducing cuts, due to its large production cross section the ggF channel can contribute 4-5% of the VBF signal [56, 57]. The following cuts have been used to reduce the background:

- Absolute rapidity difference between the two leading jets, $|\eta_{j_1} - \eta_{j_2}| > 4.0$. To ensure that the two jets are produced in forward and backward directions, we require $\eta_{j_1} \cdot \eta_{j_2} < 0$.

- A jet veto with $p_T > 40$ GeV in the central region since we do not expect any jets in the rapidity gap of the two jets for a pure VBF process. We discard jets with $|\eta| < 2.5$

- Invariant mass of the two leading jets, $M_{jj} > 1.8$ TeV .

- A $\not{E}_T$ cut of 100 GeV.

The $\not{E}_T$ and M_{jj} cuts reduce the background efficiently, and also reduce the QCD contributions significantly. We note here that two additional cuts have been occasionally used in the literature for isolating events with invisible final states. These are $\Delta\phi(j, \not{E}_T)$ and $\Delta\phi(j_1, j_2)$. We have checked that these cuts reduce the signal cross section too much in our case. Therefore, we have dropped them and used the optimal set of event selection criteria mentioned above.

The cross sections for the signal corresponding to the benchmark points chosen earlier as well as dominant backgrounds coming from W + n-jets and Z + n-jets

($n = 0, 1, 2, 3$) are shown in Table 5.6. The background events were generated using `Alpgen` at the partonic level and then passed to `PYTHIA` for showering. While interfacing, we have incorporated the `MLM` [58] prescription to match between the hard jets generated by `Alpgen` and the soft radiation jets generated by `PYTHIA` in order to avoid double counting. Since the background channels have huge inclusive cross sections, we generated at least $\sim 10^7$ unweighted events for all the channels in `Alpgen` in order to get proper convergence. For the signal cross section, we show the values obtained for VBF as well as for other hard processes $gg \to h$, $q\bar{q} \to gh$, $qg \to qh$ and $gg \to gh$. It is clear that, despite the large production cross section, contributions to

Channel	Production cross section (pb)	Cross section after cuts (fb)
BP1 (VBF)	3.76	0.99
BP1 (others)	125.9	0.16
BP2 (VBF)	3.72	1.55
BP2 (others)	125.4	0.25
BP3 (VBF)	3.73	1.72
BP3 (others)	125.7	0.25
W + n-jets	56848.54	46.57
Z + n-jet	10198.72	24.90

Table 5.6: Final cross sections obtained for all the signal and SM background channels for a 14 TeV LHC run. For the background channels, the cross sections in the 2nd column are those of the final states, i.e, W and Z decays into lepton-neutrino and two neutrino channels respectively. The cross sections in the 3rd column are the ones obtained after all the selection and background reduction cuts. n-jets corresponds to 0, 1, 2, 3 jets combined result.

the signal coming from channels other than VBF channel are very small after applying all the cuts. Also the SM backgrounds are hugely suppressed after all the cuts, optimized for a good signal significance, $\frac{S}{\sqrt{S+B}}$, where S and B stand for the signal and background strengths respectively. From Table 5.6, we find that for BP1 with the maximum (2σ allowed) invisible branching ratio $\varepsilon_{\rm max} = 0.16$ for the Higgs, we obtain a 3σ signal significance at 500 fb^{-1} whereas for BP2 and BP3 with $\varepsilon_{\rm max} = 0.24$ and 0.25 respectively, we can obtain a 3σ significance at 200 fb^{-1}.

5.2.3 The Zh channel

In this channel, we are interested in the leptonic decay of Z leading to a same-flavor, opposite-sign dilepton plus large missing energy from the invisible decay of the Higgs boson. The dominant SM background in this case comes from:
(i) WW production, where both the W's decay leptonically.
(ii)WZ production, where Z decays into two charged leptons and W into a charged lepton and neutrino, and one charged lepton misses detection.
(iii)ZZ, where one Z decays into two charged leptons and the other into two neutrinos.
(iv)$t\bar{t}$ production followed by $t \to Wb$, where both the W's decay leptonically and the b-jets escape detection.

We use the following cuts to reduce the SM background:

- A jet veto with $p_T > 20$ GeV and $|\eta| < 4.5$ since the signal consists of no jets.
- Dilepton invariant mass $|M_Z - M_{\ell\bar{\ell}}| < 10$ GeV since the two charged leptons in the final state come from Z-boson decay.
- Di-lepton transverse mass $M_T^{\ell\ell} \geq 150$ GeV, where $M_T^{\ell\ell} = \sqrt{p_T^{\ell\ell} \not{E}_T [1 - cos\phi(p_T^{\ell\ell}, \not{E}_T)]}$. This is because the Z-boson and the Higgs are more likely produced back-to-back for the signal, thus leading to a harder transverse mass distribution for the di-lepton system, as can be seen from Fig. 5.7.

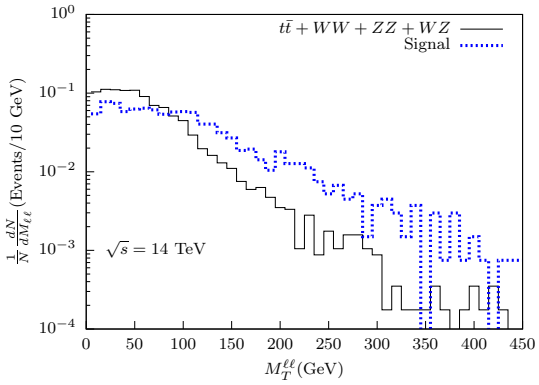

Figure 5.7: Normalized transverse mass distribution for the di-lepton system in the Zh signal and combined SM background events at 14 TeV LHC.

- $\not{E}_T > 100$ GeV since the signal is expected to have a harder $\not{E}_T$ distribution, as verified by Fig. 5.8.

Table 5.7 shows the production cross sections and final cross sections after all the cuts for the signal corresponding to the chosen benchmark point as well as for the SM

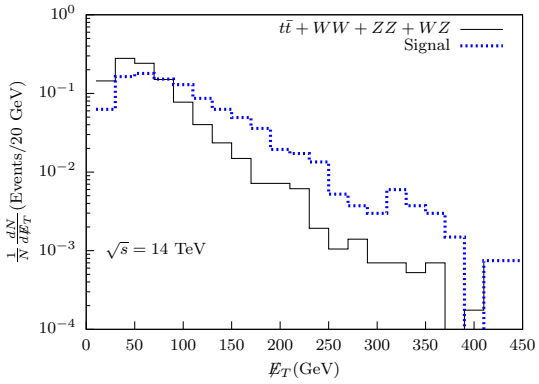

Figure 5.8: Missing transverse momentum distribution of the Zh signal and combined SM background events at 14 TeV LHC.

Channel	Production cross section (pb)	Cross section after cuts (fb)
BP1	0.53	0.35
BP2	0.51	0.51
BP3	0.51	0.52
WW	76.51	0.38
ZZ	10.58	7.77
WZ	28.95	8.83
$t\bar{t}$	370.20	0.92

Table 5.7: Cross sections obtained for all the signal and SM background channels for 14 TeV LHC. The 2nd column shows the production cross sections for various channels and the 3rd column after all the selection and background reduction cuts.

background. As can be seen from Table 5.7, this channel has a huge SM background which can easily dominate over the signal events. The signal significance factor is quite low in this case for all the benchmark points. For BP2 and BP3 with a maximum invisible BR of Higgs $\varepsilon \sim 0.25$, the signal can achieve a significance of 3σ only at 600 fb^{-1} luminosity, whereas for BP1, to get such significance, we need to go beyond 1300 fb^{-1} at 14 TeV center of mass energy.

The reason for better LHC detection prospects for BP2 and BP3 compared to BP1 can be understood by comparing their corresponding particle spectra. The invisible Higgs branching ratio ε depends on the masses of the Higgs, LSP sneutrino and the Higgs-sneutrino-sneutrino coupling. Since the masses of the parent and daughter particles are almost identical for all the three cases, what makes the difference in the invisible decay width is the coupling which depends on the amount of mixing of the

singlet sneutrinos with the left-handed ones. The singlet components dominate the lightest sneutrino mass eigenstates for all the three benchmarks because of the large B_{M_R} term in the off-diagonal of the sneutrino mass matrix given by Eq. 2.13. This parameter does not change for the three benchmark points and as a result, the right-handed components are not expected to vary much from BP1 to BP3. However, these components also depend on the matrices m_N^2, m_S^2 and M_R. Here m_N^2 and m_S^2 scale as m_0^2. Now from BP1 to BP3, m_0 keeps decreasing and M_R keeps increasing. Hence the diagonal terms in Eq. 2.13, although comparable, keep increasing slightly. This brings down the right-handed contribution in the lightest state by a very small amount from BP1 to BP3 (to be precise, the component comes down from 0.716 to 0.710). On the other hand, as the absolute value of the trilinear term A_ν in Eq. 2.13 decreases from BP1 to BP3, it brings down the left-component and increases the right-handed component. As a result of these competing effects, the left-component of the sneutrino LSP, and hence, the Higgs invisible decay width increases from BP1 to BP3, thus enhancing the LHC detection prospects.

Let us emphasize on an important distinction of our scenario from similar signals in the MSSM with a neutralino LSP which could otherwise obliterate the distinct collider signals of our model. As already pointed out in the previous chapter, the pure cMSSM case can be distinguished from the SISM case by studying the same-sign dilepton+jets+$\not{E}_T$ signal which is enhanced in the SISM case. Also the SISM case has a much harder $\not{E}_T$ tail compared to the cMSSM case which can be used as another distinguishing feature of our model. Finally, the "residual MSSM backgrounds" can be reduced/removed by studying the effective mass distribution of the events, defined as the scalar sum of the lepton and jet transverse momenta and missing transverse energy:

$$M_{\rm eff} = \sum |p_T^\ell| + \sum |p_T^j| + \not{E}_T. \tag{5.5}$$

Taking into account the current limits on the sparticle masses, the $M_{\rm eff}$ distribution of events arising from sparticle production will be considerably harder in the pure MSSM case than in our case. Note that the cascade decays involving chargions can also be used to measure the mass of the sneutrino LSP at the LHC applying the m_{T_2} endpoint technique [59].

5.3 Results in the light of updated LHC data

The signal strength($\hat{\mu}$) values used in this analysis in different Higgs boson decay channels have been updated both by ATLAS [60, 61] and CMS [62–65] collaborations.

The $\hat{\mu}$ values have changed particularly for $\gamma\gamma$ and $\tau\bar{\tau}$ final states. The numbers are closer to 1 which is their SM value and the error bars on them have also reduced. This new data set indicates increase in the branching fractions of the SM decay modes and decrease in any non-standard decay BR of the Higgs boson. Naturally, a χ^2 analysis with this new data set may put more stringent limit on ϵ which would rule out our benchmark points. However, even with a smaller ϵ our analysis is still valid. The coupling of the sneutrino DM with the Higgs boson should be reduced to lower the invisible decay BR. As a result, we need to get closer to the s-channel resonance to produce correct relic density. With a smaller ϵ, the limit on $(Y_\nu)_{11}$ will be more stringent. Therefore, the cross-sections of both the final states originating from VBF and Zh production channels are expected to be reduced. Consequently, we require increased luminosity at the LHC to probe the scenario. Rest of our conclusions remain unchanged.

5.4 Summary

A light scalar DM in SISM leads to the possibility of the lightest CP even Higgs boson in the MSSM decaying invisibly into two such DM particles induced by a soft trilinear coupling. We have explored this possibility in details by performing a global χ^2-analysis of all the available LHC Higgs data so far, and derive 2σ (1σ) upper limits of 0.25 (0.15) on the invisible Higgs decay branching ratio in this scenario. These in turn put upper limits of order 0.1 on the Dirac Yukawa coupling in this model. We further show that the model parameter space allowed by the invisible Higgs decay branching ratio limits is fully accessible in the near future DM direct detection experiments such as LUX and XENON1T, and can be ruled out *completely* in case of a null result from these experiments. Finally, we have explored the prospects of the invisible Higgs decay signature at the $\sqrt{s} = 14$ TeV LHC for a chosen set of benchmark points. We find that a signal significance of 3σ can be achieved in the VBF channel with an integrated luminosity as low as 200 fb^{-1}, whereas in the Zh channel, it requires a luminosity of at least 600 fb^{-1} for our chosen benchmark points.

Bibliography

[1] G. Aad *et al.* [ATLAS Collaboration], Phys. Lett. B **716**, 1 (2012) [arXiv:1207.7214 [hep-ex]].

[2] S. Chatrchyan *et al.* [CMS Collaboration], Phys. Lett. B **716**, 30 (2012) [arXiv:1207.7235 [hep-ex]].

[3] ATLAS Collaboration, ATLAS-CONF-2013-034.

[4] ATLAS Collaboration, ATLAS-CONF-2013-040.

[5] CMS Collaboration, CMS-PAS-HIG-13-005.

[6] ATLAS Collaboration, ATLAS-CONF-2013-014.

[7] T. Corbett, O. J. P. Eboli, J. Gonzalez-Fraile and M. C. Gonzalez-Garcia, Phys. Rev. D **86**, 075013 (2012) [arXiv:1207.1344 [hep-ph]]; Phys. Rev. D **87**, 015022 (2013) [arXiv:1211.4580 [hep-ph]].

[8] S. Banerjee, S. Mukhopadhyay and B. Mukhopadhyaya, JHEP **1210**, 062 (2012) [arXiv:1207.3588 [hep-ph]].

[9] G. Belanger, B. Dumont, U. Ellwanger, J. F. Gunion and S. Kraml, JHEP **1302**, 053 (2013) [arXiv:1212.5244 [hep-ph]].

[10] K. Cheung, J. S. Lee and P. -Y. Tseng, JHEP **1305**, 134 (2013) arXiv:1302.3794 [hep-ph].

[11] A. Falkowski, F. Riva and A. Urbano, JHEP **1311**, 111 (2013) arXiv:1303.1812 [hep-ph].

[12] P. P. Giardino, K. Kannike, I. Masina, M. Raidal and A. Strumia, JHEP **1405**, 046 (2014) arXiv:1303.3570 [hep-ph].

[13] J. Ellis and T. You, JHEP **1306**, 103 (2013) arXiv:1303.3879 [hep-ph].

[14] A. Djouadi and G. Moreau, Eur. Phys. J. C **73**, 2512 (2013) arXiv:1303.6591 [hep-ph].

[15] S. Dittmaier *et al.* [LHC Higgs Cross Section Working Group Collaboration], arXiv:1101.0593 [hep-ph].

[16] S. Chang, R. Dermisek, J. F. Gunion and N. Weiner, Ann. Rev. Nucl. Part. Sci. **58**, 75 (2008) [arXiv:0801.4554 [hep-ph]].

[17] R. E. Shrock and M. Suzuki, Phys. Lett. B **110**, 250 (1982).

[18] A. Denner, S. Heinemeyer, I. Puljak, D. Rebuzzi and M. Spira, Eur. Phys. J. C **71**, 1753 (2011) [arXiv:1107.5909 [hep-ph]].

[19] J. Abdallah *et al.* [DELPHI Collaboration], Eur. Phys. J. C **32**, 475 (2004) [hep-ex/0401022].

[20] J. F. Gunion, Phys. Rev. Lett. **72**, 199 (1994) [hep-ph/9309216].

[21] S. G. Frederiksen, N. Johnson, G. L. Kane and J. Reid, Phys. Rev. D **50**, 4244 (1994).

[22] O. J. P. Eboli and D. Zeppenfeld, Phys. Lett. B **495**, 147 (2000) [hep-ph/0009158].

[23] B. P. Kersevan, M. Malawski and E. Richter-Was, Eur. Phys. J. C **29**, 541 (2003) [hep-ph/0207014].

[24] K. Belotsky, D. Fargion, M. Khlopov, R. Konoplich and K. Shibaev, Phys. Rev. D **68** (2003) 054027 [hep-ph/0210153].

[25] R. M. Godbole, M. Guchait, K. Mazumdar, S. Moretti and D. P. Roy, Phys. Lett. B **571**, 184 (2003) [hep-ph/0304137].

[26] H. Davoudiasl, T. Han and H. E. Logan, Phys. Rev. D **71**, 115007 (2005) [hep-ph/0412269].

[27] S. -h. Zhu, Eur. Phys. J. C **47**, 833 (2006) [hep-ph/0512055].

[28] Y. Bai, P. Draper and J. Shelton, JHEP **1207**, 192 (2012) [arXiv:1112.4496 [hep-ph]].

[29] D. Ghosh, R. Godbole, M. Guchait, K. Mohan and D. Sengupta, Phys. Lett. B **725**, 344 (2013) arXiv:1211.7015 [hep-ph].

[30] S. Chatrchyan *et al.* [CMS Collaboration], Eur. Phys. J. C **74**, 2980 (2014) arXiv:1404.1344 [hep-ex].

[31] G. Aad *et al.* [ATLAS Collaboration], Phys. Rev. Lett. **112**, 201802 (2014) [arXiv:1402.3244 [hep-ex]].

[32] ATLAS Collaboration, ATLAS-CONF-2014-010.

[33] J. R. Espinosa, M. Muhlleitner, C. Grojean and M. Trott, JHEP **1209**, 126 (2012) [arXiv:1205.6790 [hep-ph]].

[34] G. Belanger, B. Dumont, U. Ellwanger, J. F. Gunion and S. Kraml, Phys. Lett. B **723**, 340 (2013) arXiv:1302.5694 [hep-ph].

[35] S. Banerjee, P. S. B. Dev, S. Mondal, B. Mukhopadhyaya and S. Roy, JHEP **1310**, 221 (2013) [arXiv:1306.2143 [hep-ph]].

[36] G. Aad *et al.* [ATLAS Collaboration], Phys. Lett. B **726**, 88 (2013) arXiv:1307.1427 [hep-ex].

[37] CMS Collaboration, CMS-PAS-HIG-13-001.

[38] CMS Collaboration, CMS-PAS-HIG-13-002.

[39] CMS Collaboration, CMS-PAS-HIG-13-003.

[40] ATLAS Collaboration, ATLAS-CONF-2013-079.

[41] CMS Collaboration, CMS-PAS-HIG-13-012.

[42] ATLAS Collaboration, ATLAS-CONF-2012-160.

[43] CMS Collaboration, CMS-PAS-HIG-13-004.

[44] ATLAS Collaboration, ATLAS-CONF-2012-109.

[45] H. Baer, V. Barger, P. Huang, D. Mickelson, A. Mustafayev and X. Tata, Phys. Rev. D **87** (2013) 3, 035017 arXiv:1210.3019 [hep-ph].

[46] P. S. B. Dev, R. Franceschini and R. N. Mohapatra, Phys. Rev. D **86**, 093010 (2012) [arXiv:1207.2756 [hep-ph]].

[47] A. Ibarra, E. Molinaro and S. T. Petcov, Phys. Rev. D **84**, 013005 (2011) [arXiv:1103.6217 [hep-ph]].

[48] D. N. Dinh, A. Ibarra, E. Molinaro and S. T. Petcov, JHEP **1208**, 125 (2012) [arXiv:1205.4671 [hep-ph]].

[49] `https://twiki.cern.ch/twiki/bin/view/AtlasPublic/SupersymmetryPublicResults`

[50] `https://twiki.cern.ch/twiki/bin/view/CMSPublic/PhysicsResultsSUS`

[51] S. Bansal, K. Mazumdar and J. B. Singh, Pramana **74**, 231 (2010).

[52] P. Gagnon, ATL-PHYS-PUB-2005-011.

[53] ATLAS Collaboration, ATLAS-CONF-2011-096.

[54] CMS Collaboration, CMS-PAS-EXO-11-059.

[55] A. J. Barr and C. Gwenlan, Phys. Rev. D **80**, 074007 (2009) [arXiv:0907.2713 [hep-ph]].

[56] V. Del Duca, W. Kilgore, C. Oleari, C. Schmidt and D. Zeppenfeld, Nucl. Phys. B **616**, 367 (2001) [hep-ph/0108030].

[57] A. Nikitenko and M. L. Vazquez Acosta, arXiv:0705.3585 [hep-ph].

[58] M. L. Mangano, talk at Lund University, http://cern.ch/ mlm/talks/lund-alpgen.pdf

[59] G. Belanger, S. Kraml and A. Lessa, JHEP **1107**, 083 (2011) [arXiv:1105.4878 [hep-ph]].

[60] G. Aad *et al.* [ATLAS Collaboration], arXiv:1406.3827 [hep-ex].

[61] ATLAS Collaboration, ATLAS-CONF-2014-009.

[62] V. Khachatryan *et al.* [CMS Collaboration], arXiv:1407.0558 [hep-ex].

[63] S. Chatrchyan *et al.* [CMS Collaboration], Phys. Rev. D **89**, 092007 (2014) [arXiv:1312.5353 [hep-ex]].

[64] S. Chatrchyan *et al.* [CMS Collaboration], JHEP **1401**, 096 (2014) [arXiv:1312.1129 [hep-ex]].

[65] S. Chatrchyan *et al.* [CMS Collaboration], Nature Phys. **10** (2014) [arXiv:1401.6527 [hep-ex]].

Chapter 6

Conclusion

In Chapter 1, we discussed in brief about the foundations of the Standard model of particle physics and its immense success rate in describing the particle phenomena experimentally observed so far. Recent discovery of its last missing piece, the Higgs boson, makes it a complete theory. However, there still remain some very serious issues which need the introduction of some beyond the SM physics. We have considered Supersymmetry as the best possible new physics model because over the years, among all the BSM candidates, SUSY has remained phenomenologically the most interesting one. In Section 1.2, we give a brief introduction to supersymmetry and discuss briefly about the minimal supersymmetric extension of the SM, known as the MSSM which answers some major issues unanswered in SM. Among all the unresolved issues in the SM, in this thesis we mainly concentrate on the neutrino mass and mixing phenomena and the existence of DM. However, even the MSSM in itself is not the complete theory as under R-parity conserving scenario, the neutrinos still remain massless. Therefore, such a scenario requires further inclusion of neutrino mass generation mechanisms to account for neutrino oscillation data. In Section 1.3, we discuss about the neutrino oscillation data and various neutrino mass generation mechanisms. We also give a brief introduction to the DM, its experimental detection techniques and the present search status in Chapter 1.4. R-parity conservation is preferred from the DM point of view as this symmetry prevents the LSP to decay further making this a natural choice DM candidate. However, present experimental bounds suggest that within the cMSSM scenario neither a neutralino nor a left sneutrino are good light DM candidates. Hence we consider a singlet sneutrino as the DM candidate in the supersymmetric inverse seesaw mechanism in order to address both the neutrino oscillation and DM issues. This seesaw mechanism introduces at least one pair of singlet superfields in the model with opposite sign lepton numbers assigned to them. The minimal version of the model, referred to as MSISM in this text, contains just one pair of such singlet superfields which

can induce a tiny non-zero mass to one of the active neutrinos by means of a small ($\sim$ keV) lepton number violating parameter, μ_s. Another neutrino gains a non-zero mass at one loop level to take into account the neutrino oscillation data acquired so far. We have also considered a not so minimal account of the model, referred to as SISM, where one adds three pairs of singlet superfields, one for each generation, instead of just one. The advantage of this scenario is that the neutrino oscillation data can be explained at the tree level itself as one can now accommodate two non-zero neutrino masses in the model without going to the one loop level. Of course, the neutrino masses will receive finite correction terms from the loop contributions. However, these contributions can be rendered negligible by keeping relevant neutrino sector parameters ($B^{ii}_{\mu_S}$) small, which do not affect the DM or collider aspects of the model.

Since the small μ_s parameter is responsible for the smallness of the neutrino masses in both the scenarios, one can have a ~ 0.1 Yukawa coupling and also keep the seesaw scale at TeV range. These features of the model make it phenomenologically rich. It can provide enhancement over the MSSM case in certain signals being studied presently at the LHC. The lightest sneutrino state which is mostly singlet with a small admixture of the doublet components, can be made the lightest supersymmetric particle (LSP) that contributes to the missing energy in a collider search. We have studied different possible signatures of the model that can be seen at the LHC. Also as a consequence of considering R-parity conserving scenario, the sneutrino LSP state can serve as a good DM candidate. A mixed sneutrino state which is dominantly singlet proves to be a very good light scalar DM.

In Chapter 3, we consider the MSISM scenario and explore the feasibility of searching such a model at the LHC in the trilepton channel associated with missing energy. Charginos, in addition to their MSSM decay modes, can also decay into a charged lepton and a dominantly singlet sneutrino. We have let the lighter chargino state to decay into a charged lepton and the sneutrino LSP. The decay patterns of the chargino into this mode are controlled by the parameters which also generate the neutrino mixing angles. As a result, the ratio of these new decay branching fractions into different charged lepton flavors correlate with the neutrino mixing angles. We have considered the ratio of the branching ratios of $\widetilde{\chi}_1^{\pm}$ decaying into μ and τ channels and observe that this ratio shows a sharp correlation with $\tan^2\theta_{23}$, θ_{23} being the atmospheric neutrino mixing angle. A correlation like this can connect neutrino oscillation data to the collider search for the correct neutrino mass generation model. We have explored this situation in the context of LHC in gaugino pair production channel. We have considered pair production of $\widetilde{\chi}_2^0$ and $\widetilde{\chi}_1^{\pm}$ and subsequent generation of a trilepton signal from their cascade decays at the LHC. The SUSY mass spectrum was generated accordingly

to suit our purpose. We have made $\widetilde{\chi}_2^0$ decay into a charged lepton-slepton pair, the slepton further decaying into a charged lepton and the lightest neutralino which then decays into a neutrino and the LSP sneutrino. The $\widetilde{\chi}_1^\pm$ on the other hand decays into a charged lepton and sneutrino LSP. Hence an opposite sign same flavor charged lepton pair is always originated from the $\widetilde{\chi}_2^0$ decay whereas the other charged lepton comes from the $\widetilde{\chi}_1^\pm$ decay. Since we have considered $\widetilde{\chi}_1^\pm$ decaying into μ and τ channels, the cascade decays always yield a $3\ell + \not{E}_T$ or a $2\ell + \tau-\text{jet} + \not{E}_T$ final state, where $\ell = e, \mu$.

We have carried out detailed collider analyses of the above mentioned signals at the LHC for both 7 TeV and 14 TeV center of mass energies in specific benchmark scenarios. The signal and background event cross-sections obtained after applying suitable cuts indicate that the parameter space of the model will be severely constrained if such a trilepton signal is not found at the LHC. We also observe that the correlation $\frac{\sigma(pp\to\mu\sum\ell\ell+\not{E}_T\ )}{\sigma(pp\to\tau\sum\ell\ell+\not{E}_T\ )}$ vs. $\tan^2\theta_{23}$ persists even after all the selection and background reduction cuts are applied. We obtain different slopes of the correlation plots corresponding to the different benchmark points as a result of choosing a non-uniform τ detection efficiency which varies with transverse momentum, p_T of the $\tau-$jet. Different slopes for different benchmark points reduce the predictability of the model. However, once we take an uniform τ detection efficiency, the correlation plot appears to provide a unique slope and thus making this a general feature of the model. Value of the slope might change if one takes a different set of cuts but non-observation of any such correlations at the LHC can rule out such scenarios.

As discussed in section 1.4, a left-handed sneutrino in MSSM is not a good light DM candidate. Hence we look out for a mixed sneutrino state which is dominantly singlet with a small admixture of the left-handed component as a DM candidate. In Chapter 4, we consider SISM within the cMSSM framework to explore this possibility. We observe that, the LSP sneutrino in the model can be as light as ~ 50 GeV serving as a perfect DM candidate. The state is mostly singlet as a significant contribution coming from the left-handed component can enhance the direct detection cross-section alarmingly. We have carried out a detailed scan in the cMSSM as well as the neutrino sector parameter space to examine the general feature of the DM observables in this scenario. The DM pair annihilates mostly into a fermion pair mediated by the Higgs bosons. Our choice of the parameter space pushes all the Higgs boson masses close to the TeV range apart from the CP-even state at 125 GeV. Hence the Higgs boson mediated s-channel process is the all important annihilation channel for the DM pair in this scenario. We observe that it is not possible to achieve enough annihilation to produce right relic density in this model in the mass region below 50 GeV. The DM with mass lying close to the value $m_h/2$ produces enough pair annihilation through

s-channel resonance process to yield correct relic density. On the other hand, there is also another DM mass zone, around 100-150 GeV, where the relic density constraint is satisfied due to new annihilation channels with WW, ZZ or hh final states opening up. Whereas the direct detection cross-section in the 100-150 GeV mass region is a bit too large and is partially ruled out by the latest LUX result, there is still a sizable parameter space left in the 50-60 GeV mass region that will be probed by the future run of the LUX and XENON1T experiments.

We choose some suitable benchmark points from our scan satisfying various collider and low energy experimental constraints and perform a detailed collider analysis in the same-sign dilepton + n-jets $+\not{E}_T$ channel, where n$\geq$ 2. The dominating contribution to this signal comes from gluino pair production channel, where the gluinos decay into a quark-squark pair, the squarks subsequently decaying into a quark and the lighter chargino. As a consequence of having a gluino pair, it is possible to produce same-sign charginos on both the branches. The charginos then decay into a charged lepton and the LSP sneutrino to boost the same-sign dilepton signal rate associated with large missing energy and a number of jets. A similar signal can arise within the MSSM scenario with the usual neutralino LSP. The charginos in that case decay dominantly into a charged lepton and a left-handed sneutrino. Hence it is necessary to differentiate between the two scenarios. We, therefore, generated similar cMSSM spectrum with the same high scale inputs as our benchmark points and looked for the same signal. We observe that the SISM case has a much harder $\not{E}_T$ spectrum compared to the cMSSM case. This feature helps to differentiate between the two scenarios and also to reduce the SM background largely. To manifest our result we have constructed a variable 'r' which is a ratio between the cross sections $\sigma(\ell^\pm\ell^\pm + \geq 2j + \not{E}_T)$ and $\sigma(0\ell + \geq 3j + \not{E}_T)$. This ratio is enhanced in the SISM case as due to the presence a large Dirac neutrino Yukawa coupling, the chargino dominantly decays into a charged lepton and a LSP sneutrino, which is bound to produce two leptons in the final state, whereas in cMSSM, there are other dominant decay modes as well for the chargino that may not produce same-sign dilepton in the final state. We observe that the ratio is indeed 4-5 times larger than the same obtained in cMSSM case.

In Chapter 5, we probe the 50-60 GeV DM mass region of SISM further in invisible Higgs decay channel. Since the discovery of the 125 GeV scalar at the LHC, different measurements of its couplings and decay modes have been going on to confirm if this indeed is the SM Higgs boson. Although the recent results are pointing towards a SM Higgs boson, there still remain some discrepancy in the measurement of its couplings, making room for non-standard Higgs boson decay modes like an invisible one. The direct search limits on the invisible Higgs decay branching ratio obtained by both

ATLAS and CMS collaborations are much relaxed. On the other hand, a global χ^2 minimization with the Higgs boson signal strength measurements in different decay modes produces far more stringent constraint on the branching ratio of the invisible decay mode. Hence we performed a 2-parameter global χ^2 minimization to ascertain how much invisible Higgs decay width is allowed after taking into account all the signal strength values provided by ATLAS and CMS collaborations. We observe that although the best-fit value of the invisible BR lies very close to zero, allowing a 2σ range puts an upper limit of 25% on this non-standard decay mode. The 2σ bound on the invisible BR is taken more seriously than the best-fit value obtained from the χ^2 analysis because there are uncertainties involved in calculating the Higgs production cross-section and its various decay widths. We take this bound as another constraint to study the SISM parameter space. We notice that the parameter space is further reduced by a significant amount by this constraint. Nevertheless, one can still have a sneutrino DM candidate with a mass just below $m_h/2$ satisfying all the DM and collider constraints simultaneously giving rise to a new invisible decay mode for the SM-like higgs boson with a non-negligible BR. We find a few benchmark points to explore the scenario at the LHC.

The Direct search for invisible Higgs boson decay have been carried out mainly in two Higgs boson production channels: VBF and Z-boson associated production channels. Another associated production channel Wh has irreducible SM background. In VBF Higgs boson production channel, the final state consists of two jets associated with missing energy. For the Zh production channel, we only study the leptonic channel where the Z-boson decays into opposite sign dilepton pair and the Higgs boson decays invisibly. In VBF channel, the two jets are produced in forward and backward directions with a large rapidity gap. Also the invariant mass of the two jets is large. These factors help to reduce the SM background more efficiently than in the Zh production channel. We observe that in VBF production channel, the scenario can be probed at the LHC with 14 TeV center of mass energy at 200 fb^{-1} luminosity whereas for the Zh production channel one needs a luminosity of 600 fb^{-1}.

In a nutshell, inverse seesaw, like other seesaw mechanisms, is a very efficient way to generate tiny non-zero masses for the neutrinos as well as producing appropriate mixing between the neutrino states to account for neutrino oscillation data. Inverse seesaw model is also phenomenologically very rich mainly because in this scenario, one can have a large (~ 0.1) Dirac neutrino Yukawa coupling and a sub-TeV seesaw scale simultaneously. The SUSY implementation of inverse seesaw, called MSISM/SISM not only takes into account the neutrino oscillation data, but also has a DM candidate which is light (50 GeV) and satisfies all the DM, collider and low energy experimental

constraints existing so far. The model can have some unique signatures at the LHC that we have explored. We have also proposed ways to differentiate this scenario from similar signatures that can be obtained in cMSSM/mSUGRA scenario without inverse seesaw. Although some of the benchmark points we present in this thesis have been ruled out due to non observation of SUSY at the collider to date, but the search strategies for SUSY scenarios with heavier sparticles remain unchanged. In addition, there are also some predictions based on the model for a 14 TeV LHC run, which are to be probed in the coming years.

ABSTRACT

Title of the Thesis: Some Studies on the Prospect of Finding New Physics Beyond the Standard Model at the LHC

Submitted by: Subhadeep Mondal

After the discovery of a $\sim$ 125 GeV Higgs boson at the Large Hadron Collider (LHC), now the Standard Model (SM) of particle physics is complete although there are still some doubts over the fact that this can be a beyond the Standard Model (BSM) Higgs boson. More updated data on Higgs boson coupling measurements will reveal its true identity. Meanwhile, we need to go beyond the SM to address some vital experimental findings. One of them is the neutrino oscillation data that indicates at least two neutrinos have tiny but non-zero masses. The other one is the existence of Dark Matter (DM) revealed from cosmological data. Weak scale supersymmetry (SUSY) is the most popular choice for explaining these new physics phenomena beyond the SM. However, even Minimal Supersymmetric Standard Model (MSSM) itself is not sufficient to explain the neutrino oscillation data under R-parity conserving scenario. In this thesis, we, therefore, attempt to explore a SUSY model with added singlets that can account for small neutrino masses by means of inverse seesaw mechanism. As a consequence, we can have a mixed sneutrino lightest SUSY particle (LSP) that may be as light as $\sim$ 50 GeV. Within R-parity conserving scenario, this LSP can serve as a very good DM candidate satisfying all existing constraints arising from collider, DM and low energy experiments. This model can have enhanced same-sign dilepton final states with large missing energy coming from gluino and squark pair as well as squark-gluino associated productions and their cascade decays through charginos. The two body decays of the lighter chargino into a charged lepton and a singlet sneutrino has a characteristic decay pattern which is correlated with the observed large atmospheric neutrino mixing angle. This feature can be probed at the LHC through trilepton channel. Moreover, the $\sim$ 125 GeV Higgs boson now have a new decay channel into a pair of LSP sneutrinos that is completely invisible. Most recent data published by ATLAS and CMS collaborations at the LHC in different Higgs boson decay channels constrain this sort of non-standard decays. We perform a two parameter global analysis of the available experimental data to date to determine the optimal invisible Higgs boson branching fraction in this scenario. This new decay provides us a new missing energy channel that can be probed at the LHC. We present detailed cut-based analyses for these different proposed signals at the LHC to test the viability of such a scenario.

Subhadeep Mondal
25.9.14